An *IPRF* Research Report

Innovative Pavement Research Foundation

Airport Concrete Pavement Technology Program

Report IPRF-01-G-002-05-2

JOINT LOAD TRANSFER IN CONCRETE AIRFIELD PAVEMENTS:

APPENDIX B: LITERATURE REVIEW SUMMARY

Programs Management Office
9450 Bryn Mawr Road
Rosemont, IL 60018

August, 2011

An *IPRF* Research Report

Innovative Pavement Research Foundation

Airport Concrete Pavement Technology Program

Report IPRF-01-G-002-05-2

JOINT LOAD TRANSFER IN CONCRETE AIRFIELD PAVEMENTS:

APPENDIX B: LITERATURE REVIEW SUMMARY

Lead Investigator and Author

Christopher R. Byrum, PhD, PE

Principal Investigators

Starr D. Kohn, PhD, PE (decd)
Chuck A. Gemayel, PE
Shiraz Tayabji, PhD, PE

Contributing Authors
Rohan W. Perera, PhD, PE
Ray Rollings, PhD, PE

Programs Management Office
9450 Bryn Mawr Road
Rosemont, IL 60018

PREFACE

This report has been prepared by the Innovative Pavement Research Foundation (IPRF) under the Airport Concrete Pavement Technology Program. Funding is provided by the Federal Aviation Administration (FAA) under Cooperative Agreement Number 01-G-002. Dr. Satish Agrawal is the Manager of the FAA Airport Technology R&D Branch and the Technical Manager of the Cooperative Agreement. Mr. Jim Lafrenz is the IPRF Cooperative Agreement Program Manager.

The IPRF and the FAA thank the Technical Panel that willingly gave of their expertise and time for the development of this report. They were responsible for the oversight and the technical direction. The names of those individuals on the Technical Panel follow.

Mr. Stan Herrin, P.E.	**Crawford, Murphy, and Tilly, Inc.**
Dr. Wayne Seiler, P.E.	**All About Pavements, Inc.**
Mr. Gary Harvey, P.E.	**Othon, Inc.**
Dr. David Brill, P.E.	**FAA Technical Advisor**

The contents of this report reflect the views of the authors who are responsible for the facts and the accuracy of the data presented within. The contents do not necessarily reflect the official views and policies of the FAA.

ACKNOWLEDGEMENTS

The project team would like to acknowledge the contributions by the staff of the following:

- Federal Aviation Administration
- Airport Authorities that supported the field testing

The contents of this report reflect the views of the authors, who are responsible for the facts and the accuracy of the data presented. The contents do not necessarily reflect the official views and policies of the FAA. This report does not constitute a standard, specification, or regulation.

TABLE OF CONTENTS

ACRONYMS

AC	Advisory Circular
BPR	Bureau of Public Roads
DIA	Denver International Airport
FAA	Federal Aviation Administration
CDF	Cumulative Damage Factor
COE	Corps of Engineers
FE	Finite Element
FEM	Finite Element Method
FWD	Falling Weight Deflectometer
LED	Layered Elastic Design
MDOT	Michigan Department of Transportation
PCC	Portland Cement Concrete
LT	Percent of "Free-Edge Stress" Transferred
LTE_{δ}	Load Transfer Efficiency for Deflection
LTE_{σ}	Load Transfer Efficiency for Stress
LTPP	Long-Term Pavement Performance
MDOT	Michigan Department of Transportation
NAPTF	National Airport Pavement Test Facility
NDT	Nondestructive Testing
USAF	United States Air Force
WES	Waterways Experiment Station

CHAPTER 1: INTRODUCTION

1.1 OVERVIEW

This document presents key findings from the literature review that was performed for the IPRF Project 01-G-002-05-2, Joint Load Transfer in Concrete Airfield Pavements. This information was compiled over the first year of the project and circulated among the team members. The findings from the extensive literature review were also the focus of the first and second year progress meetings for the project, including the IPRF panel members, FAA representatives and project team members. This information guided the research and it was decided to compile key literature data into an informal and separate "Appendix B" to the Full Report for the project. Only a small portion of this data was included in the final reports for the project.

1.2 JOINT LOAD TRANSFER EFFICIENCY

Many studies have been conducted to investigate the load transfer across joints in portland cement concrete (PCC) pavements, with a large body of literature available on this subject. There are many different measures of joint load transfer that have been used in the past. However, in airfield applications, the following three primary definitions for load transfer at a joint or crack have been most commonly used:

$$\text{Load Transfer Efficiency for Deflection } (LTE_{\delta}) = 100\left(\delta_U / \delta_L \right)$$

$$\text{Load Transfer Efficiency for Stress } (LTE_{\sigma}) = 100\left(\sigma_U / \sigma_L \right)$$

$$\text{Percent of "Free-Edge Stress" Transferred (LT)} = 100\left(\varepsilon_U / \varepsilon_F \right)$$

Where,

δ_L = Deflection of the loaded side of the joint
δ_U = Deflection of the unloaded side of the joint
σ_L = Bending stress at the joint in the loaded slab
σ_U = Bending stress at the joint in the unloaded slab
ε_U = Bending strain at the joint in the unloaded slab
ε_F = Bending strain at the joint for "free-edge" loading conditions

When describing load transfer in this document, the appropriate acronyms for load transfer described above (LTE_{δ}, LTE_{σ}, LT) are used.

The parameter LT is defined above in terms of strain and not stress. This is because in field tests that have been performed, strains have been measured at joints in the loaded and unloaded slabs and used to define load transfer and slab bending stress.

There has been some inter-mixing of these definitions in the past literature that can cause some confusion to readers not aware of the differences between these definitions. It is relatively easy to measure deflection LTE_{δ}. It is quite difficult to accurately measure the stress or strain ratios in PCC panels. Theoretical slab models, or real slabs instrumented with strain gages can be used to get estimates of stress, or change in stress, which is directly related to strain.

The LT concept evolved in direct support of airfield pavement design and is related to testing of instrumented slabs using embedded strain gages, with a focus on measuring slab bending strain. It is this load transfer concept that is the primary focus of this research. Reported values for LT typically range from 0 to 50%. The LT value and its 50% upper limit evolved to simplify airfield pavement designs and allowed the use of the well-known slab on grade structural analysis equations by Westergaard (1948). The Westergaard equation for free edge stress was used as the basis of analysis and design for pavement systems, without directly modeling joint behavior as part of pavement design in civil airports until recently. The most recent Federal Aviation Advisory (FAA) Advisory Circular (AC) related to airfield pavement design that was released in 2009 (FAA 2009) uses stress computed using a finite element method for PCC airfield pavement design, and superseded the earlier AC Version 6D for airfield pavement design (FAA 1995) that used stress computed from the Westergaard equation.

The LTE_{δ} concept is different than LT, and has evolved more with a focus on measuring joint deflections, which is easy to accomplish with equipment such as the Falling Weight Deflectometer (FWD). Reported values for LTE_{δ} as well as LTE_{σ} typically range from 0 to 100%.

Joint deflections have also been used in recent research efforts involving Finite Element Method (FEM) type theoretical modeling of pavements, where joints are actually being modeled within the slab structural analysis and design process. It is necessary to quantify and understand real joint load transfer behavior if joints are directly being modeled in a multi-slab structural analysis.

Perhaps the first attempt to define load transfer was by Teller and Sutherland (1936) and they proposed two methods to define load transfer:

$$\text{Load Transfer (Method 1)} = 2\delta_u / (\delta_L + \delta_u)$$

$$\text{Load Transfer (Method 2)} = 2(\delta_F - \delta_L) / \delta_F$$

These load transfer index values were not used much in later research. However, they may have been the first to attempt to measure and quantify load transfer at joints in this detailed way. This philosophy may have led to the LT concept, which was the first widely used load transfer concept.

The LT value has been assumed to be related to the LTE_{σ} value by the following equation.

$$\text{Percent of “Free-Edge Stress” Transferred (LT)} = LTE_{\sigma}/(1+LTE_{\sigma})$$

The above relation is based on the two following simplifying approximations:

$$\delta_L + \delta_U = \delta_F$$
$$\sigma_L + \sigma_U = \sigma_F$$

Past research has shown that the above two relations are generally valid for slab structural analysis when using the dense liquid (springs) foundation model and assuming that the slab remains in direct contact with its ideal spring foundation support (i.e. for relatively soft subgrade, flat slabs, and small loads).

Westergaard (1927) clearly stated that the equations for the slab on grade model developed by him become invalid as slab lift-off from curling and warping curvatures develop. Westergaard noted that large up-warp, similar to a 5°F/inch thermal gradient could develop in slabs, and this slab warping was capable of lifting joints off of the subgrade.

In reality, it is very difficult to correlate what we call slab stress to measured deflection or strain. Calculated stresses from analytical models for load and environmental effects can only capture part of the problem, as there are effects such as pumping or drying shrinkage that are typically not considered in such models. The models are simplifications of complex real field conditions. Consequently, comparison of physical field-measured deflections or strains will always include effects not addressed in analytical calculations for stress. When joints lift off the foundation due to factors such as upward warp or due to foundation erosion along slab edges, the above sum-of-deflection and sum-of-stress relations have been shown to be false.

1.3 AIRFIELD PAVEMENT THICKNESS DESIGN

In FAA pavement thickness design methods, the magnitude of load transfer across pavement joints has been accounted for using indirect or simplified design approaches. These approaches were based on a series of field studies, described in Chapter 2 of this document, where slab bending strain was measured using strain gages. Based on these studies, in FAA PCC thickness design procedures the interior joints were assumed on average to be capable of developing an LT value of 25%, meaning the maximum stress level in the loaded slab used for thickness design is assumed to be 75% of the free edge stress.

This simplifying qualitative assumption for all interior joints allowed joint considerations to be eliminated from within the thickness design process, and allowed the entire basis of thickness design for airfield PCC pavements to be based on 75% of the free edge stress at a joint. This 75% concept is still used as the basis of design today for FAA airfield PCC pavements. In FAA thickness design procedures this free edge stress was computed using the Westergaard equation until recently. In the most recent FAA AC on airfield pavement design (150/5320-6E), the stress computations are based on a finite element method (FAA 2009). Seasonal or daily thermal effects on slab stress or joint behavior were not considered in the FAA airfield pavement thickness design procedures. PCC fatigue models were calibrated to this generalized analysis approach using field test sites. Recent detailed slab structural analysis studies such as those conducted at the National Airport Pavement Test Facility (NAPTF) have put this simplified assumption of 75% free edge stress used in design procedures into question, leading to this study.

CHAPTER 2: AIRFIELD PAVEMENT DESIGN

2.1 OVERVIEW

AC No. 150/5320-6D (FAA 1995) that was issued on July 7, 1995 was used until recently to design civil airfield pavements. AC 150/5320-6D presented nomographs for performing pavement designs. The pavement design methods presented in this AC were those adopted in 1978.

On October 22, 1995, the FAA issued AC 150/5320-16, which implemented LEDFAA, which is a computer program developed by the FAA, as the new standard for design of airport pavements intended to serve Boeing 777 aircraft. The program LEDFAA is based on layered elastic analysis.

During the period that AC No. 150/5320-6D was effective, FAA issued four changes to this AC called change 1, change 2, change 3, and change 4 that were issued on 11/30/96, 6/3/02, 4/30/04, and 6/23/06, respectively. Change 3 made some significant changes to the pavement design procedures. Change 3 announced the release of two Microsoft Excel spreadsheets for pavement design, which were based on the pavement design procedures described in chapter 3 and 4 of AC No. 150/5320-6D. The spreadsheet F805FAA.XLS was for determining pavement thickness requirements for flexible pavements and bituminous overlays of existing flexible pavements The spreadsheet R805FAA.XLS was for determining pavement thickness requirements for rigid pavements and bituminous or PCC overlays for rigid pavements. These spreadsheets could be used instead of the nomographs presented in AC No. 150/5320-6D for pavement design. Change 3 cancelled AC 150/5320-16, and incorporated the contents of this AC as a new Chapter 7 to AC No. 150/5320-6D. This change also allowed the layered elastic design method that was earlier used to design airports that were subjected to Boeing 777 aircraft be used as an alternate design method to the pavement design procedures described in chapter 3 and 4 of AC No. 150/5320-6D. Therefore, this change allowed LEDFAA to be used for pavement design of any airport, including those that were not expected to be subjected to Boeing 777 aircraft.

On September 30, 2009, FAA released AC No. 150/5320-6E (FAA 2009) that outlined procedures for airfield pavement designs for civil airfields and cancelled AC No. 150/5320-6D. The pavement design procedures presented in AC No. 150/5320-6E are based on layered elastic theory for flexible pavements and three-dimensional finite element theory for PCC pavements. The FAA adopted these methodologies to address the impact of new landing gear configurations and increased pavement load conditions. The FAA has released a computer program called FAARFIELD to perform pavement designs in accordance with the procedures described in AC 150/5320-6E.

This chapter presents an overview of military airfield design procedures in the United States that laid the foundation for the current FAA pavement design procedures, a description of layered elastic analysis procedures that have been used for pavement design, a description of PCC fatigue models used for pavement design, an overview of the pavement design procedures described in the current FAA AC on pavement design (AC No. 150/5320-6E), variations from pavement design assumptions that affect pavement performance, and the effect of curling and warping of PCC pavements on pavement performance.

2.2 MILITARY PAVEMENT DESIGN PROCEDURES

2.2.1 General History

The unprecedented size of military aircraft used during the Second World War forced the United States military to become actively involved in development of appropriate design and construction criteria for airfields. The FAA design procedures have evolved along the same philosophy pathway as the military procedures. From November 1940 to today, the military plays an active role in the airfield pavement arena as military aircraft continue to evolve (Rollings 2003, Ahlvin 1991, Fine and Remington 1972). In a series of tests during the Second World War, Corps of Engineers investigators established the framework for military airfield rigid pavement design that included the following aspects:

- The ability of the Westergaard models to reasonably predict strains and stresses in airfield pavements.
- Critical stresses were developed by edge-loading adjacent to the joints rather than center-of-slab loading.
- Slow moving or stationary aircraft cause higher stresses than landing aircraft.
- Importance of controlling non-load related curling stresses.
- Repetitions of load were an important design factor.
- Properly designed joints could transfer load from one slab to another.
- Expansion joints were a source of weakness unless proper load transfer was designed for the joint.

Following the second world war through the cold war and into the current war on terrorism, military airfield pavement design continued to evolve to meet changing needs and used theoretical development, small scale model tests, full-scale accelerated traffic tests, instrumented in-service pavements, and observation of airfield performance to support the evolution of design concepts (Rollings 1981, Rollings 1989, Rollings 2003, Rollings and Pittman 1992, Ahlvin 1991, Hutchinson and Vedros 1977, Ahlvin et al. 1971, Hutchinson 1966, Sale and Hutchinson 1959, Mellinger and Carlton 1955).

2.2.2 Load Transfer

Throughout the development of the military rigid airfield design procedure, the ability of properly constructed joints in the pavement to transfer loads between slabs has been recognized and has been a fundamental part of the military rigid airfield pavement design criteria. Initial tests at Lockbourne during the Second World War suggested that 25 percent was an appropriate design value for load transfer for properly designed joints (US Army Corps of Engineers 1946). The performance of various joint designs during the Lockbourne No. 2 full-scale accelerated traffic tests in the 1940s were assessed from strongest to weakest as: (1) doweled contraction joint, (2) doweled construction joint, (3) keyed construction joint with tie bar, (4) contraction joint, (5) keyed construction joint, (6) doweled expansion joint, and (7) free edge expansion joint

(Ahlvin 1991, Sale and Hutchinson 1959, US Army Corps of Engineers 1950a and 1950b). These studies found there was no advantage in using structural shapes in joints in lieu of conventional round dowel bars

The experience gained at the Lockbourne tests and the follow-on full-scale accelerated traffic tests at Sharonville found the 25 percent load transfer to be adequate for design and probably conservative for doweled joints, but details and quality of joint construction were recognized as critical to obtaining high levels of load transfer (unpublished minutes of All-Division Meeting on Doweled Joints, US Army Engineer Ohio River Division Laboratories, September 1958, available at ERDC Technical Library, Vicksburg, MS).

The early Corps of Engineers design policy concerning load transfer that prevailed until the late 1970's was articulated by Hutchinson (1966) as:

From these studies (full-scale test tracks, theoretical studies, model studies, in-service pavement assessments), the decision was made to use three types of load transfer devices: (a) keys and keyways constructed in the joints during construction; (b) dowels, consisting of round smooth steel bars or pipe, one end of which would be bonded in the concrete and the other end left unbonded; and (c) the interlock provided by a natural crack occurring shortly after concrete was placed. ... each demonstrated that it would provide at least 25 percent load transfer and maintain slab alignment. ... In addition, the difference between the maximum stress from edge and interior loading is only about 25 percent; hence any device that reduces the edge stress by more than 25 percent then makes the interior loading condition critical.

In the event that these approved load-transfer capable joint designs were not used, a thickened edge joint 25 percent thicker than the design thickness was required. This thickened edge effectively reduced stresses along the critically loaded slab edge.

In the late1950s, the Sharonville Heavy-Load test tracks were built to assess design criteria for 325,000 lb twin-tandem gears representing a 700,000 lb aircraft. These test tracks received some initial trafficking, but changing priorities led to halting the traffic, and the results were never formally reported (Ahlvin 1991, Rollings 1987). Some of this trafficking suggested that keys might not be adequate under such heavy gear loads, and the Multiple-Wheel Heavy-Gear Load Tests conducted in the 1960s for aircraft exceeding 600,000 lb confirmed that keys were inadequate under heavy aircraft loads (Ahlvin 1991, Ahlvin et al. 1971, Grau 1972). A later assessment of keyed joints in civil airports reached a similar conclusion (Barenberg and Smith 1979). The military initially restricted keys to more lightly loaded pavements on favorable subgrades, but then abandoned them all together for new construction leaving the sawcut contraction joint and doweled construction joint as the default joints for United States Air Force (USAF) airfield pavements (Rollings 1981, Rollings 1989, Department of Defense 2001). Thickened edge, expansion, and doweled contraction joints can be used for special circumstances.

The early Corps of Engineers (COE) investigations collected strain measurements on the loaded and unloaded side of the joint to define load transfer. Their load transfer measurements of in-service airfield pavements are particularly germane. A summary of these measurements is shown in Table 2.1. The key joint measurements are too limited to allow one to draw any conclusions.

TABLE 2.1. SUMMARY OF LOAD TRANSFER FROM STRAIN MEASUREMENTS ON IN-SERVICE USAF AIRFIELDS (ROLLINGS 1981, BASED ON DATA FROM US ARMY CORPS OF ENGINEERS 1959 AND GRAU 1979)

Location	Modulus of Subgrade Reaction, kPa/cm	Pavement Thickness, cm	Number of Measure-ments	Load Transfer, %[a]		
				Range	Mean	Coefficient of Variation,%
Doweled Joints						
Beale AFB, CA	580	58	15	16.7-52.3	32.8	32
Dow AFB, MI	950	48	16	0.0-35.7	10.5	94
Ellsworth AFB, SD	580	58	16	30.4-50.0	40.6	12
Hunter AFB, GA	475	46	15	18.2-42.9	27.4	28
Lincoln AFB, NE	180	53	16	27.8-50.0	36.5	19
Lockbourne AFB, OH	200	30	11	7.4-23.7	15.8	37
March AFB, CA	270	41	15	20.0-47.4	32.0	24
McCoy AFB, FL	610	46	14	14.3-35.7	24.2	25
Tyndall AFB, FL	430	20-25	10	15.6-46.8	30.4	30
		Overall	128	0.0-52.3	28.1	43
Keyed Joints						
Lincoln AFB, NE	180	53	2	35.9-36.1	36.0	-
McCoy AFB, FL	610	46	2	35.9-38.6	37.3	-
		Overall	4	35.9-38.6	36.6	-

Note: 1 kPa/cm = 0.369 lb/in^2/in, 1 cm = 0.3937 in
a. Calculated from measured strains on loaded and unloaded edges of joint.

The doweled construction joint measurements reveal that on the average the measured load transfer exceeded the 25% used in design, but there is much variation in the data. Three of the bases, Dow, Lockbourne and McCoy, fail to average the design allowance, with Lockbourne failing to have a single measurement equal to or greater than 25%.

In contrast, Ellsworth and Lincoln do not have a single measurement below 25% and had average load transfer, values of 40.6 and 36.5% respectively. While the in-service doweled joints appear to generally meet the 25% design allowance, there is much variation. This could easily reflect factors such as variation in construction technique or temperature at the time of the test.

Table 2.2 is a compilation of Corps of Engineers load transfer data based on strain measurements, and estimates based on joint deflections during full-scale traffic tests from in-service pavements. This data emphasizes that although properly designed joints can achieve the 25% design allowance for load transfer, there is much variation, and sometimes this is met, and sometimes it is not. Joints without provision for load transfer consistently fail to meet the design allowance (e.g., the Lockbourne "free" or butt joint). The mean of the keyed joint barely meets the 25% design allowance for load transfer presaging the eventual inadequacy of this joint design under heavy aircraft. The joint designs currently authorized for USAF airfields (doweled construction, doweled expansion, and sawcut contraction joint with aggregate interlock) all have mean load transfer values 5% or more above the design target of 25%.

TABLE 2.2. REPRESENTATIVE CORPS OF ENGINEERS LOAD TRANSFER MEASUREMENTS FOR FULL-SCALE TEST SECTIONS AND IN-SERVICE PAVEMENTS DURING 1942 - 1979 (BASED ON ROLLINGS 1987, 1989)

Type of Joint	Number of Measurements	Load Transfer, %		Coefficient of Variation, %
		Mean	Range	
Doweled Construction Joint	195	30.6	0.0 - 50.0	38.0
Doweled Expansion Joint	15	30.5	15.4 - 42.6	24.4
Contraction Joint with Aggregate Interlock	46	37.2	15.6 - 50.0	19.2
Tied Contraction	6	29.2	23.9 - 34.8	13.4
Doweled Contraction	4	35.1	28.2 - 42.8	17.3
Keyed	61	25.4	5.6 - 49.0	41.4
Tied Key	2	25.8	25.6 - 26.1	-
Butt	8	15.5	5.8 - 24.5	40.9

Notes: Includes load transfer based on direct strain measurements in Table 2.1 plus load transfer estimated from deflections. See Rollings 1987 for methodology of estimating load transfer from measured joint deflection under load.

The Corps of Engineers conducted load transfer measurements with a heavy weight deflectometer at Atlanta, Dallas - Fort Worth, Denver, and Madison airports in 1992-1993 (Hammons et al., 1995). The overall results of these tests are summarized in Table 2.3. This investigation attempted to assess the impact of other variables on load transfer including support below the slab, season, and dowel insertion method. The impact of season and slab support is apparent in this field data. Like Table 2.2, these data show the doweled contraction joint has lower load transfer than the aggregate interlock contraction joint which is counterintuitive and contrary to the performance data from the Corps' Lockbourne tests. The tied keyed joint is superior to the untied key as also suggested in Table 2.2 and in the Lockbourne joint performance rating given earlier. In general, the mean load transfer in Table 2.3 is lower than 25% design value during the winter. These tests in Table 2.3 had negligible impact on military design philosophy as the tested slab lengths were generally much longer than used in the military, which would lower load transfer values from what would be expected with shorter slabs, and the doweled longitudinal construction joints included data for dowel insertion techniques not allowed in the military.

TABLE 2.3. CORPS OF ENGINEERS LOAD TRANSFER MEASUREMENTS AT CIVIL AIRPORTS (BASED ON HAMMONS ET AL. 1995)

Joint Type	Base	Season	Number of Measure-ments	Load Transfer	
				Mean, %	Coefficient of Variation, %
Doweled Transverse Contraction	stab	winter	58	14.7	36.4
		summer	11	28.1	7.1
	nonstab	winter	11	19.9	28.6
Transverse Contraction	stab	winter	14	21.6	21.1
Doweled Longitudinal Construction	stab	winter	31	18.6	24.8
Tied Longitudinal Construction	stab	winter	12	15.9	30.6
Keyed Longitudinal Construction	stab	winter	9	15.5	37.4
	nonstab	winter	6	23.6	9.8
Tied Keyed Longitudinal Construction	stab	winter	23	20.2	20.4

Notes: stab = stabilized base
nonstab = nonstabilized granular base
Slab lengths varied from 20 to 75 ft with most being reinforced slabs with 50 and 75 ft lengths

The military's policy on load transfer for rigid airfield pavement design has evolved over time. The early expectation that, with accumulating knowledge, one might be able to use higher load transfer design values for doweled joints (unpublished minutes of All-Division Meeting on Doweled Joints, US Army Engineer Ohio River Division Laboratories, September 1958, available at ERDC Technical Library, Vicksburg, MS) never came to fruition as the data failed to support this expectation. Keyed joints proved unreliable under increasingly heavy aircraft and were abandoned for new construction. The importance of construction details were recognized early and this is reflected in very exacting construction specifications. A number of dowel construction innovations such as plastic sleeves or machine insertion into plastic slip-formed concrete are not allowed by the military because of a lack of data showing such innovations will not compromise achievable load transfer values. A number of publications make the point clearly that load transfer is a stochastic variable that changes over time and not a constant (e.g., Rollings 2003, Hammon et al. 1995, Rollings 1987, Barenberg and Smith 1977, Hutchinson 1966), so the 25% load transfer value used by the military is best thought of as a "design allowance" rather than a specific single value in the field.

Allowance for load transfer during design and mandatory provisions for achieving load transfer during construction have been fundamental parts of military airfield rigid pavement design since the Second World War, and they continue to be so today. While the 25% load transfer used in design by the military and the FAA is often referred to as an "assumption," the selection of this value represents an engineering estimate based on a variety of measurements during full-scale traffic tests, on model pavements, and on in-service pavements. The military data indicates that on the average, the joint designs used in current military airfields exceed the design allowance or assumption. Military design aids such as design charts and computer programs routinely include the 25% load transfer in the design aid calculations. When such aids have been used incorrectly to design an airfield pavement that actually does not have joints with load transfer provisions, failure is rapid and dramatic illustrating the structural significance of the load transfer provision (e.g., Rollings 2001, Rollings and Rollings 1991). Attempts to judge the adequacy of military design procedures versus actual airfield performance are very difficult, but generally, these design procedures give usable results that meet the user's need for relatively low-cost pavement designs with limited maintenance (Rollings 1987, Hutchinson and Vedros 1977, Kohn 1985). The use of the 25% load transfer design value when coupled with the military's other requirements such as allowable slab length, joint design requirements, and field construction inspection seems to have proven effective over the past 50 years as a design tool.

2.2.3 Design Procedures

The Lockbourne and model tests of the 1940's found Westergaard interior stress was not the critical state but edge stress was. The military funded Westergaard (1948) to help develop his 1948 free-edge equations. These are for a single wheel loads and this is when the first models of the B-36 aircraft came out having a large 75,000 lb single wheel gear load. Practicality eventually led to multiple-wheel gears being used on subsequent models and future large aircraft. The 1948 equations do not handle multiple-wheel loading configurations directly.

Pickett and Ray (1950) published their well-known influence diagram solution to Westergaard's free-edge formulation. The Corps used these influence diagrams to develop their design curves of this era. Military design of this era used the Westergaard edge stress formulation for stress calculation, made adjustments for load transfer, and used available full scale traffic tests to relate the design factor (calculated stress and flexural strength) to coverages (cycles of stress at a point) and was a fatigue analysis. In the 1960's General Dynamics developed the H-51 computer solution to the Pickett and Ray influence diagrams. Starting in about 1979, the FAA changed their design criteria to be based on Westergaard's free-edge stress equation in FAA AC 150/5320-6C (Barenberg and Arntzen 1981).

Airfield pavement design procedures are often presented in nomograph forms. Figure 2.1 shows a design nomograph from Rollings (1981), where the 1979 Army TM 5-824/AFM 88-6 procedure for PCC pavement thickness determination is demonstrated. This design method used the "design aircraft" approach for traffic philosophy, along with the 75% of the Westergaard free edge stress and a model-specific calibrated PCC fatigue model as the basis for pavement life estimates and thickness design.

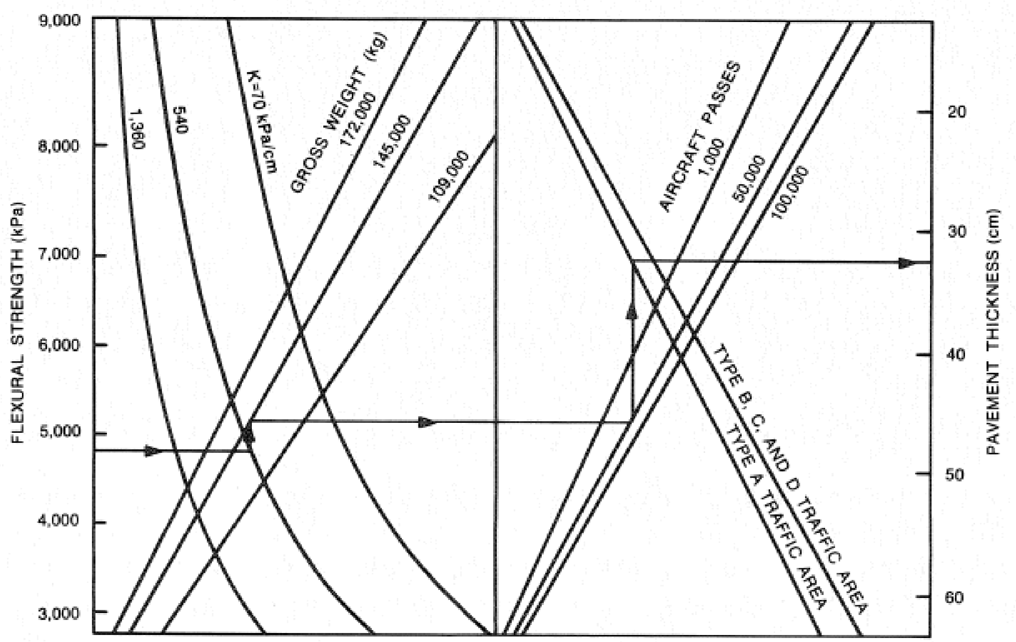

Note: 1 kPa = 0.145 lbf/in.^{2}; 1 cm = 0.397 in.

FIGURE 2.1. THICKNESS DESIGN NOMOGRAPH FROM THE 1979 ARMY TM 5-824 / AFM 88-6 DESIGN PROCEDURES (ROLLINGS, 1981).

The 1979 procedure had adjustments to the design thickness from the nomographs to account for very good subgrade and also for cement treated econocrete base as shown in Table 2.4. The FAA and the military differ in how they treat the effect of stabilized bases in design philosophy. The FAA uses an increased subgrade *k*-value concept, while the military uses a slab thickness reduction concept. The high strength subgrade adjustment factors are based on studies of field performance of sites from the 1940's and 1950's. These reductions were allowed based on recognition that post cracking behavior for slabs was better at sites with good foundation conditions compared to sites with poor foundation conditions.

TABLE 2.4. THICKNESS ADJUSTMENT FACTORS FROM THE 1979 DESIGN PROCEDURE (ROLLINGS 1981).

Subgrade Modulus, k (kPa/cm)	Reduction in Thickness (%)
540	0.0
810	4.6
1090	10.6
1360	19.2

Note: 1 kPa/cm = 0.369 lbf/in.^{3}.

Rollings (1989) describes upgrades to the use of the Westergaard equation in COE airfield designs that occurred in the 1980's. The equation was updated in an attempt to account for multiple wheel loads via the Pickett and Ray influence charts. Figure 2.2 shows the form of the Westergaard equation used in 1989. The table 1 referred to in figure 2.2 is shown in table 2.5, and provides data regarding the adjustment constants to be applied to the Westergaard equation

$$\sigma_e = \frac{P}{h^2}\left[a_0 + a_1 \ln \ell + a_2 (\ln \ell)^2\right]$$

where

σ_e = Westergaard free edge tensile stress (lb/in.^{2})

P = actual gear load, lb

h = slab thickness, in.

a_0, a_1, a_2 = regression constant from Table 1, calculated for a specific gear to match the computerized solutions of Pickett and Ray influence chart solutions

ℓ = radius of relative stiffness, in.

$$= \sqrt[4]{\frac{Eh^3}{12(1-\upsilon^2)k}}$$

E = modulus of elasticity of the slab, lb/in.^{2}

υ = Poisson's ratio of the slab

k = modulus of subgrade reaction, lb/in.^{2}/in.

FIGURE 2.2. THE FORM OF THE WESTERGAARD EQUATION USED FOR COE PCC DESIGNS IN 1988 (ROLLINGS 1989).

TABLE 2.5. AIRPLANE DATA AND CONSTANTS FOR EACH AIRPLANE FOR USE WITH THE WESTERGAARD EQUATIONS AS SHOWN IN FIGURE 2.2 (ROLLINGS 1989).

Aircraft	Typical Main Gear Load lb	Pass to Coverage Ratio		Regression Constants		
		Channelized*	Nonchannelized**	a_0	a_1	a_2
B-52	249,600	1.63	2.00	1.1249	-0.8449	0.1966
B-727	82,250	3.25	6.00	-0.8081	0.1698	0.1165
B-747	187,200	3.48	5.22	1.4096	-1.1067	0.2387
E-3/B-707	157,450	3.25	6.00	1.5490	-1.1773	0.2530
C-5A	361,900	1.62	2.20	1.1904	-0.7615	0.1351
C-130	78,750	4.18	8.10	0.5560	-0.6011	0.1936
C-141	162,150	3.44	6.34	1.4990	-1.1877	0.2634
A-10	22,500	7.82	15.52	-4.0850	2.4409	-0.1650
F-4	27,000	8.58	17.00	-4.0251	2.4894	-0.1775
F-14	34,500	7.14	14.29	-2.4290	1.4950	-0.0413
F-15 C/D	30,600	9.37	14.10	-4.3900	2.9452	-0.2649
F-111	54,000	4.92	9.80	-2.7582	1.4794	0.0322
KC-10-30	224,200	3.42	5.45	2.6351	-1.7184	0.3078
P-3	63,900	3.57	6.67	-1.1908	0.4615	0.0758
T-43/B-737	70,500	3.68	6.91	-1.1567	0.4012	0.0910
Shuttle	119,250	3.60	6.49	-1.0736	0.3180	-0.0986
Concorde	183,600	3.18	5.90	2.1465	-1.5308	0.3074
18 Kip axle	18,000	2.64	2.64	0.2440	-0.2172	0.1263

* 70 in. wander (e.g. taxiways or ends of runways).
** 140 in. wander (e.g. parking areas, runway interiors).

In the 1970's, layered elastic research for airfield pavements was initiated (Parker et al., 1979). Inherent in developing the layered elastic design models is the fundamental basis that the layered elastic fatigue models are only valid for pavements using 25% load-transfer capable joint systems. This is because the field fatigue data upon which relationships were based all used such joints and the relationships cannot be extrapolated to free-edge conditions. The wars of the 2000's led military to realize layered elastic was not robust enough to handle all of the variation encountered in the field, and hence CBR and Westergaard-based designs remain in use along with layered elastic methods.

FAA and military design procedures did not evolve independently, but were intertwined from 1940 through the early 1990's with the military essentially establishing methodology and FAA accepting or modifying it to suit their needs. With the more recent establishment of the NAPTF and a program of three dimensional finite element modeling, the FAA has been going off in an independent direction separate from the military but basing their philosophy to start with on past military research.

2.3 LAYERED ELASTIC DESIGN PROCEDURES

At the First International Conference for Concrete Pavements in 1977, James P. Sale, Chief of the Waterways Experiment Station (WES) Soils and Pavement Laboratory announced that the joint military/FAA design research was beginning to depart from the use of the Westergaard Free Edge stress equation, and was embarking on a mission to develop an Layered Elastic Design (LED) approach for PCC and asphalt airfield pavements (Sale, 1977). The LED approach was assumed to be better at predicting mid-panel deflections for complex layered pavements that included stabilized base layers, which were becoming popular. Some researchers at the time thought that the Westergaard equations were not adequately representing stabilized base effects. It was however, recognized early that the LED method's primary weakness was that it was completely ignoring joints, and corner/edge loading as part of the analysis used as the basis of designs, and was relying on empirical calibrations embedded within the LED method's fatigue model to account for the effects of jointing on slab fatigue and design life. The final LED design method development report is FAA-RD-77-81 (Parker et al. 1979).

At the 2nd International Conference for Concrete Pavements in 1981, Barker (1981) summarized the LED method in detail, and provided some comparisons of the new LED method to the older "75% of Westergaard Free-edge stress" method. Figure 2.3 shows the results from Barker (1981), comparing the 75% of Westergaard free-edge stress magnitudes, to the interior stress magnitudes from layered elastic model. Clearly a general proportionality exists, but there is considerable scatter around the general linear trend in this plot. Most of the scatter is likely due to the effect of the stabilized base on the LED model interior stress magnitude. The actual effect of stabilized bases on joint stiffness and stress load transfer ability is not well understood at this time.

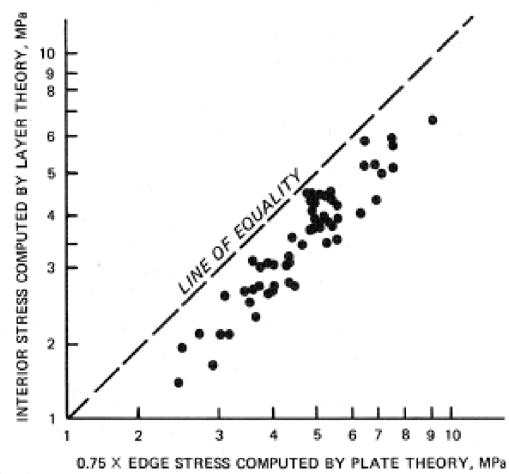

Note: 1 MPa = 145 lbf/in.^{2}.

FIGURE 2.3. PLOT COMPARING STRESS ANALYSIS RESULTS FROM THE LED MODEL TO THE WESTERGAARD FREE-EDGE STRESS EQUATION (BARKER 1981).

A separate fatigue relationship was developed for the LED approach, which allows the direct input of the bottom of infinite slab interior stress value as shown below:

$$DF = 0.58901 + 0.35486 \log(Cov)$$

Where,

DF = Design factor (PCC flexural strength divided by the maximum principal tensile stress at bottom of PCC slab)
COV = Traffic in terms of coverages

The conversion of LED model interior type loading stress to critical fatigue stress, at the slab edge or wherever it may be, is done indirectly within the LED fatigue equation regression coefficients.

In general, as shown in figure 2.4, the LED method fatigue model and stress analysis routine appears to give more allowable coverages for low coverage levels, and less allowable coverages for higher coverage levels when compared to the Westergaard based stress analysis routine and fatigue model. Said in another way, the plot implies that LED method designs will have lower thickness for low coverages and higher thickness for high coverages compared to the older edge stress method. Barker (1981) showed that designs from LED methods for DC-8 and C-141 aircraft were slightly thicker than the Westergaard free edge stress method required thickness values.

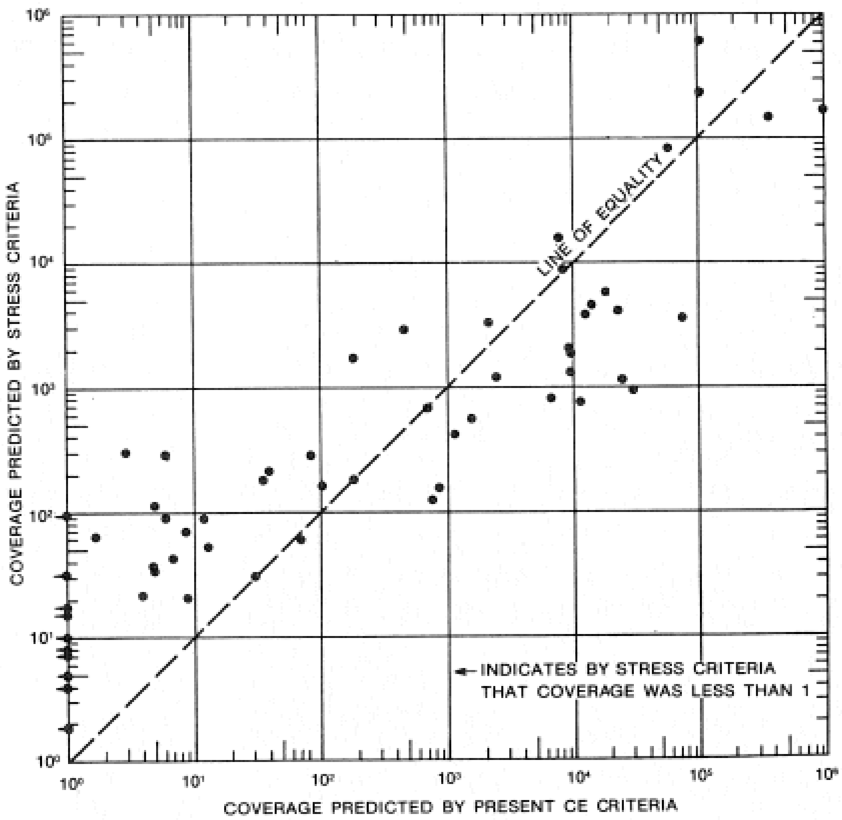

FIGURE 2.4. COMPARISON OF FATIGUE LIFE FOR SEVERAL TEST SITES USING THE LED (STRESS CRITERIA) APPROACH COMPARED TO THE WESTERGAARD EQUATION (VERSION D) APPROACH (BARKER 1981).

On October 22, 1995, the FAA issued AC 150/5320-16, which implemented LEDFAA, which is a computer program developed by the FAA, as the new standard for design of civil airport pavements intended to serve Boeing 777 aircraft. The program LEDFAA is based on layered elastic analysis. Change 3 issued for AC No. 150/5320-6D (that addressed airport pavement designs) cancelled AC 150/5320-16, and incorporated the contents of AC 150/5320-16 as a new Chapter 7 to AC No. 150/5320-6D. This change also allowed the layered elastic design method that was earlier used to design airports that were subjected to Boeing 777 aircraft be used as an alternate design method for both flexible and rigid pavement design procedures (described in chapter 3 and 4 of AC No. 150/5320-6D). Hence, this change allowed LEDFAA to be used for flexible and rigid pavement design of any airport, including those that were not expected to be subjected to Boeing 777 aircraft. AC No. 150/5320-6D was superseded on n September 30, 2009 by AC No. 150/5320-6E (FAA 2009). The pavement design procedures presented in AC No. 150/5320-6E are based on layered elastic theory for flexible pavements and three-dimensional finite element theory for PCC pavements.

2.4 CONCRETE FATIGUE MODELS

Figure 2.5 shows the fatigue models used for PCC pavements in the 1988 military design manual (Rollings, 1988). Figure 2.6 shows a comparison of the COE fatigue models to other fatigue models available in the literature at that time.

$$DF_w = \frac{R}{(1 - \alpha)\ \sigma_w} = 0.50 + 0.25 \text{ Log } C$$

where

DF_w = Westergaard design factor

R = flexural strength of concrete measured by third point flexural beam test

α = load transfer across joints, taken as 0.25 for conventional Corps of Engineers joint construction standards

σ_w = maximum tensile stress calculated with the Westergaard edge model

C = coverages of traffic

$$DF_{EL} = \frac{R}{\sigma_{EL}} = 0.59 + 0.35 \text{ Log } C$$

where

DF_{EL} = layered elastic model design factor

R = flexural strength of concrete measured by third point flexural beam test

σ_{EL} = maximum tensile stress calculated using the layered elastic model

C = coverages of traffic

FIGURE 2.5. FATIGUE MODELS FOR THE WESTERGAARD ANALYSIS METHOD, AND THE LED ANALYSIS METHOD AS USED IN THE 1988 PAVEMENT DESIGN MANUAL FOR THE MILITARY (ROLLINGS 1989).

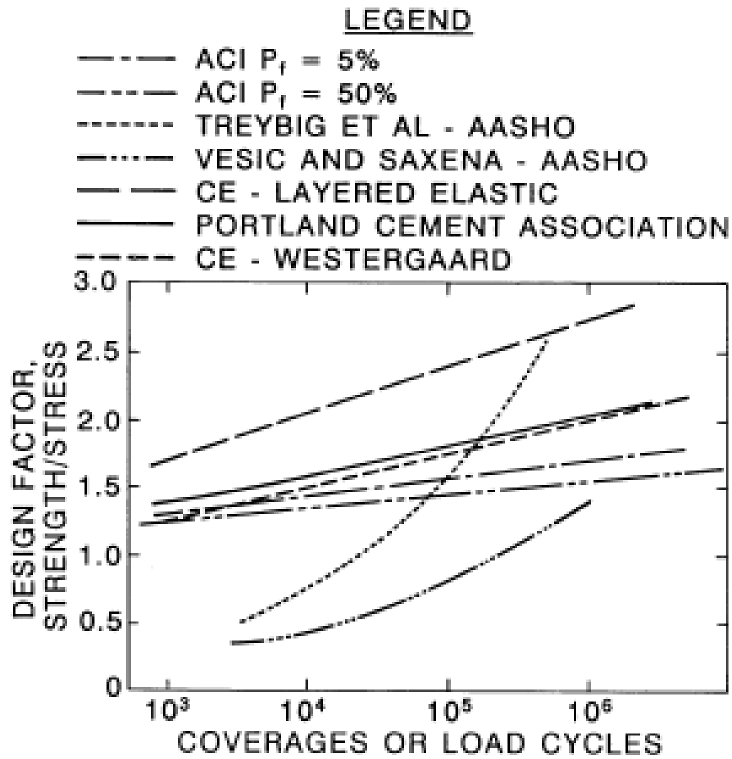

FIGURE 2.6. COMPARISON OF THE 1988 COE PCC FATIGUE MODELS TO OTHER PCC FATIGUE MODELS (ROLLINGS 1989).

The LED fatigue model curve is above the others because the fatigue model is indirectly used to empirically adjust the LED interior load into an apparent controlling tensile stress. The important observation here is that both design models have a structural analysis engine that is directly calibrated to a model specific damage equation. Calibration of the fatigue equation to the analysis engine is a challenging task. Damage functions are model specific. In addition, how PCC flexural strength is measured affects the damage model form. For example, if PCC strength is measured from cut beams, versus cylinders, versus full size slab failure tests, different strength values will be obtained and different damage model forms would results for each different strength measurement technique used. There is a three way loop consisting of field measurement of damage, measurement of system strength, and model predictions of stress/strain that is specific to each PCC fatigue or damage equation developed by various researchers.

Roesler et al. (2005) evaluated the following two fatigue models used by the COE and FAA that were reported by Rollings and Witczak (1990). The first equation is referred to as the "first crack" and the second equation as the "shattered slab."

$$DF = 0.5234 + 0.3920 * \log(C100)$$

$$DF = 0.2967 + 0.3881 * \log(C0)$$

Where,
DF = Design factor = Modulus of Rupture/stress

C100 = Coverages for the SCI to drop below 100.
C0 = Coverages to reduce SCI of the pavement to zero.

Interpolation can be performed for allowable coverages at intermediate SCI values. This team was also looking at scale effects and observed that full size slabs generally had higher bending stress levels at failure when compared to smaller sized beam samples. Figure 2.7 shows comparison of the fatigue models for some gear assemblies they evaluated. In figure 2.7 two lines are shown, noted as first crack and shattered slab conditions, which correlate to SCI values of 100 and zero, respectively. FAA considers an SCI value of 80 as the failure threshold and this is reportedly when about 50 percent of slabs reach a cracked condition.

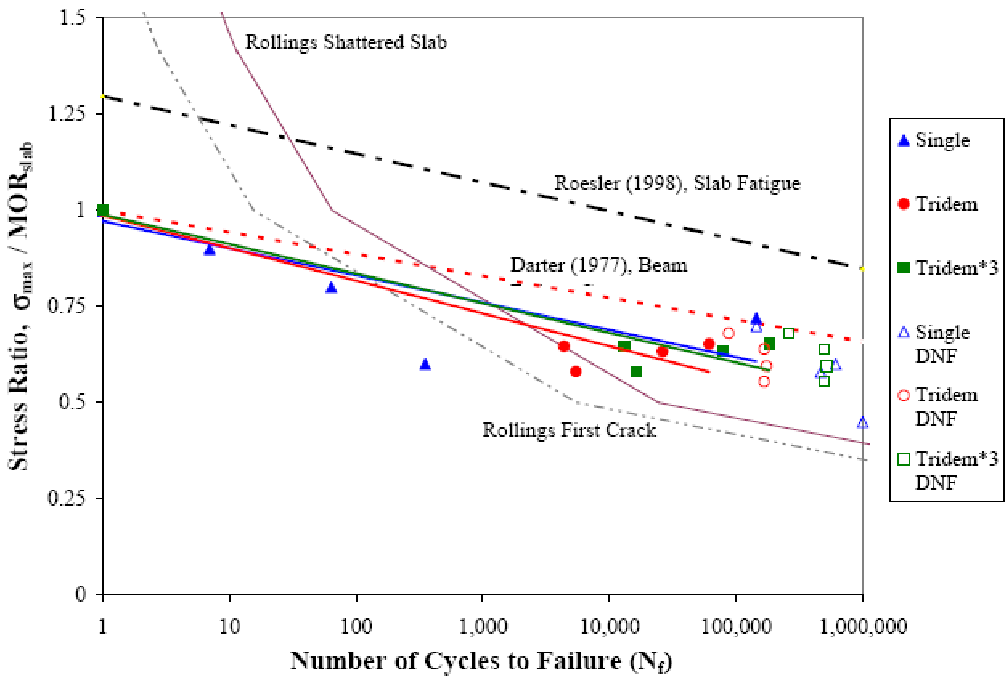

FIGURE 2.7. COMPARISON OF ROLLINGS FATIGUE MODELS TO OTHER MODELS FOR VARIOUS GEAR CONFIGURATIONS (ROESLER ET AL. 2005).

The FAA design procedure outlined in AC 150/5320-6D (FAA 1995), which has now been superseded by AC 150/5320-6E, used the following edge stress based models:

$$COV = 5{,}000(10^{(\sqrt{\frac{R_F}{\sigma(1.3)}})/0.15603}) \quad \text{for coverages} > 5{,}000$$

$$COV = 5{,}000(10^{(\sqrt{\frac{R_F}{\sigma(1.3)}})/0.07058}) \quad \text{for coverages} \leq 5{,}000$$

Where

σ = working stress in the design caused by the load
R = design flexural strength
COV = equivalent coverage for the loading

The latest LED failure model is based on the Structural Condition Index (SCI) values and is as follows:

$$\mathrm{SCI} = \frac{R_F/\sigma - 0.2967 - F_S(0.3881 + F_{SC}(0.000039)SCI(\log_{10}(COV))}{0.002269}$$

Where,
R_F = Flexural strength of concrete
σ = Stress at the bottom of the slab
COV = Coverages

Fs and Fsc are adjustment factors that were more recently applied to the original form of this damage model.

$$F_{SC} = \frac{0.392 - 0.3881F_S}{0.0039F_S}$$

The fatigue failure model used in the current FAA AC on pavement design (150/5320-6E) that is incorporated in FAARFIELD is shown below:

$$\frac{DF}{F_c} = \left[\frac{F_s' bd}{\left(1 - \frac{SCI}{100}\right)(d-b) + F_s' b} \right] \times \log C + \left[\frac{\left(1 - \frac{SCI}{100}\right)(ad - bc) + F_s' bc}{\left(1 - \frac{SCI}{100}\right)(d-b) + F_s' b} \right]$$

DF = design factor, defined as the ratio of concrete strength R to computed stress
C = coverages
SCI = structural condition index, defined as a subset of the pavement condition index (PCI) excluding all non-load related distresses from the computation
a, b, c, d = parameters
F'_s = compensation factor for high quality and stabilized base
F_c = calibration factor

Historically, the Westergaard free edge based design methods have used the "design aircraft" concept (where one aircraft is used to represent the mix of aircraft), while the LED based models have used a Miner's law type damage accumulation that considered all aircraft traffic.

However, the pavement design procedures described in AC 150/5320-6E, which is the current FAA AC on pavement design, use the Critical Damage Factor (CDF) concept, which is based on Miner's principle, for design of both rigid and flexible pavements. The CDF concept is described as:

$$CDF_i = \frac{n_i}{N_i} = \frac{D_a L}{(P/C)C_f} = \frac{C_a}{C_f}$$

Where,

$CDFi$	=	*CDF* for aircraft type *i*
n_i	=	number of passes of aircraft type *i*
N_i	=	number of allowable repetitions to failure for aircraft *i*
D_a	=	annual departures
L	=	pavement life in years
(P/C)	=	pass/coverage ratio
C_f	=	coverages to failure
C_a	=	applied coverages

Then all damages are summed up using Miner's law as follows, where N = total number of aircraft types.

$$CDF = \sum_{i=1}^{N} CDF_i$$

A *CDF* of 1 means that the fatigue life has been used and some of the slabs should reach the point of being fatigue cracked. An iterative routine is used to vary slab thickness values within the analysis engine until the CDF value converges to near 1.0, and the slab thickness corresponding to a CDF value of 1 is the design slab thickness.

2.5 FINITE ELEMENT ANALYSIS

2.5.1 Early Finite Element Modeling

At the same time the new LED method was being introduced, some of the first detailed joint evaluations in the context of the Westergaard free edge stress method were being performed based on newly introduced computer based finite element (FE) modeling (Barenberg and Arntzen 1981, Barenberg and Smith 1979). These teams performed some of the first FE modeling of jointed PCC pavements to evaluate the load transfer efficiency values LTE_σ and LTE_δ in detail. Figures 2.8 to 2.10 show the key plots from this early FE joint load transfer research. Teller and Sutherland (1936) were perhaps the first to measure both LTE_σ and LTE_δ for a test site with strain gages and their trend line is plotted on figure 2.8.

2.5.2 Recent Finite Element Modeling Efforts

In the true spirit of mechanistic pavement modeling, the FAA has been developing tools to perhaps one day replace the indirect empirical estimation of fatigue from free edge stress or from layered elastic analysis basins (Kawa et al 2002).

In general, the overall *CDF* or "design aircraft" design philosophy has been in place for the last several decades, while the bending stress values used in the fatigue calculations have over time evolved from:

1. Methods based on Westergaard interior stress.
2. 75% of the Westergaard free edge stress.
3. Empirically adjusted layered elastic basin stress (LEDFAA).
4. 75% of the free edge stress computed from simplified FE methods (FAARFIELD).

In the future, stress computed from the FE program FEAFAA (described in the next section), perhaps the direct top and bottom of slab edge stress calculations from some sort of highly sophisticated 9-slab FE model using sophisticated joint model algorithms and full combined aircraft gear configurations may be used.

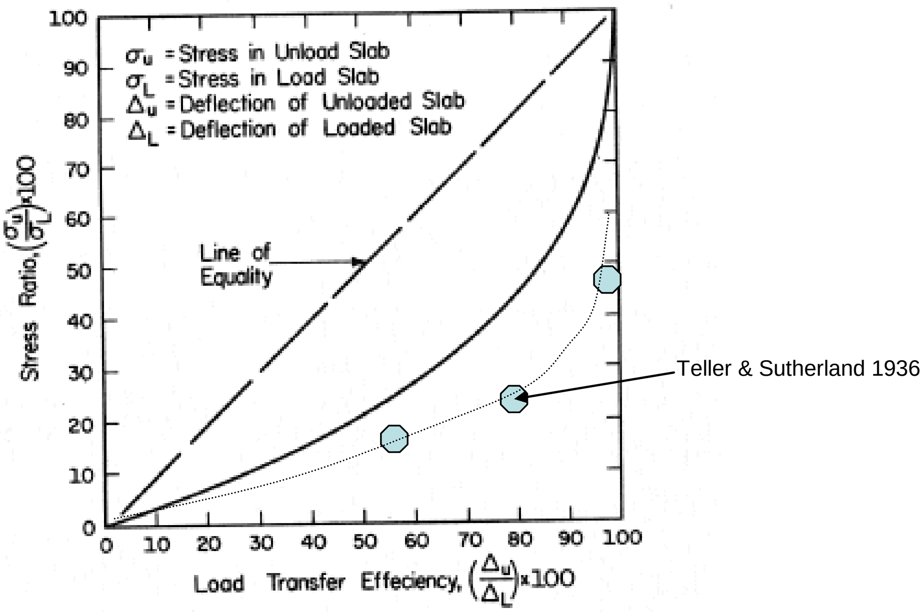

FIGURE 2.8. NON-LINEAR RELATION BETWEEN LTE$_\sigma$ AND LTE$_\delta$ FROM FEM MODELS REPORTED BY BARENBERG AND ARNTZEN, (1981).

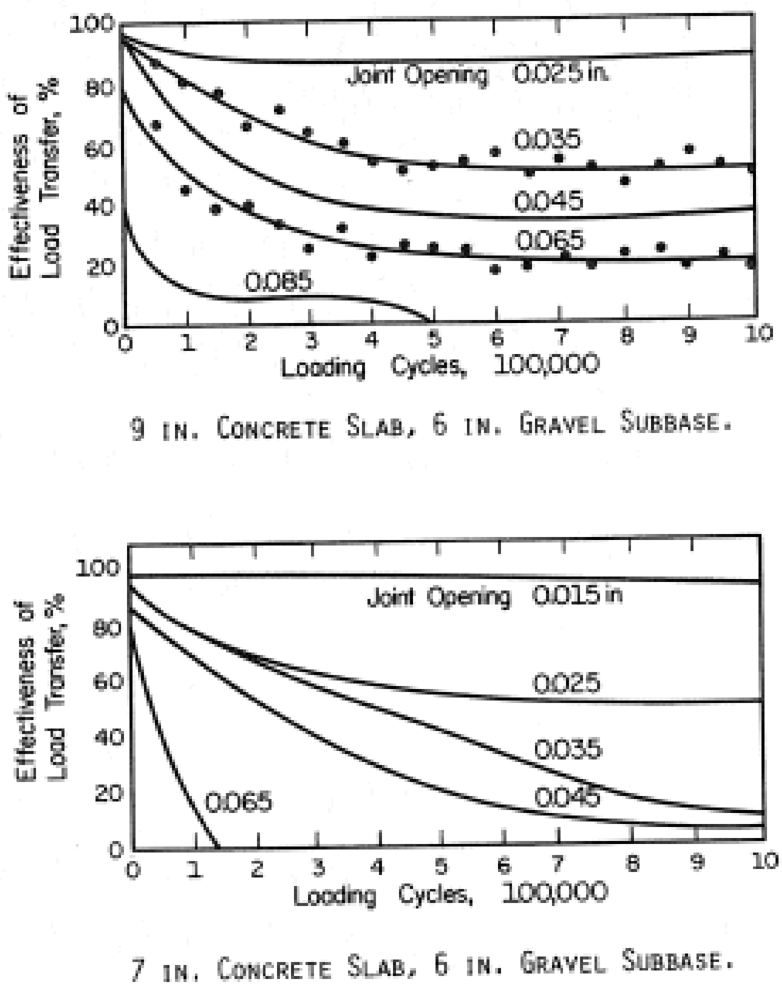

FIGURE 2.9. LOSS OF LOAD TRANSFER ABILITY AS RELATED TO JOINT OPENING AND NUMBER OF LOAD CYCLES REPORTED BY BARENBERG AND ARNTZEN (1981).

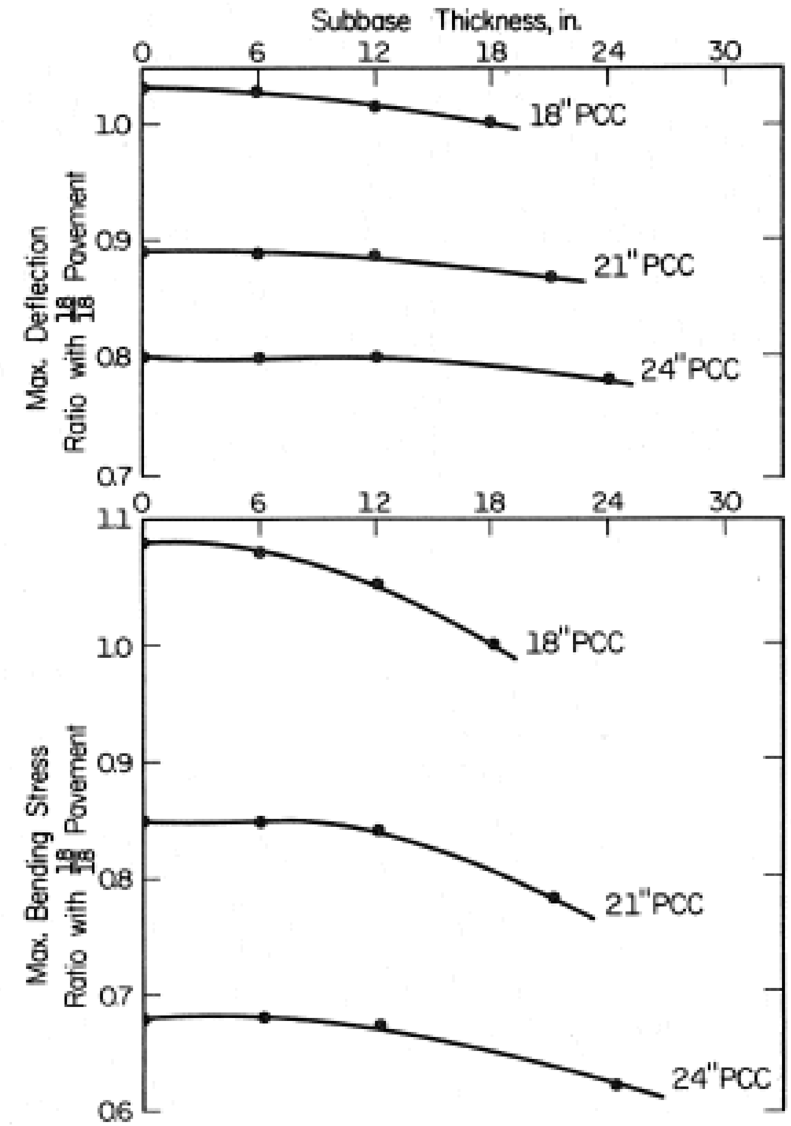

FIGURE 2.10. PLOTS SHOWING A GENERAL TREND OF DECREASING LOAD TRANSFER (LTE_{σ} AND LTE_{δ}) FOR INCREASING SLAB THICKNESS AND FOUNDATION STIFFNESS AS REPORTED BY BARENBERG AND ARNTZEN (1981).

In 1998, the following two FAA research reports in the area of FE model development studies were released: DOT/FAA/AR-97/47 (Brill 1998) and DOT/FAA/AR-97/7 (Hammons 1998).

Brill (1998) introduced a 3-D FE model for jointed PCC slab analysis based on the NIKE3D FEM software. The developed UNIX based 9-slab FE model can simulate cracked and uncracked base, and elastic or spring foundations. A pure free-slip joint is assumed for the cracked base option and no base crack stiffness is assumed to be present, so the base is assumed to be either 100% uncracked, or to have zero shear stiffness at the joint. Brill (1998) shows an example of what is described as slab-base separation that is predicted for the uncracked base assumption. When a combination of a stiff uncracked base is modeled along with a slab joint having low load transfer, the loaded slab will force the base downward and cause it to detach from the unloaded slab creating an air void beneath the unloaded slab. This condition causes theoretically infinite shear stresses in the uncracked base at the edge of the loaded slab. This base cracking concept is a significant phenomenon. When the joint is new, there may be only some localized crushing of base materials along the joint line when heavy loads cross the joints. However, after many heavy load passes and some loss of load transfer at the joint, the base will certainly crack. Brill has in general referred to joint stiffness as the parameter k_{joint} in units of lb/in/in.

Hammons (1998) used a 3-D ABAQUS FE model to simulate the behavior of small scale jointed slab models developed in a laboratory setting. This research focused on two key factors affecting LTE_{δ}, de-bonding of the slab and base bond, and cracking of treated base materials. Cracking of the treated base was considered to be the primary factor affecting load transfer deterioration observed by Hammons (1998). Hammons discusses the different joint models available in ABAQUS and notes the JOINTC model was selected for their study.

Both Hammons (1998) and Brill (1998) predict significant loss of LTE_{δ} for cracked versus uncracked base assumptions.

2.5.3 Current Finite Element Modeling Efforts

FEAFAA (Finite Element Analysis – Federal Aviation Administration) is the current state of the art FE model being developed by the FAA Airport Technology R&D Branch. The computational engine of FEAFAA is a modified version of the finite element program NIKE3D and the meshing is generated by the program INGRID. Both of these programs were originally developed by the U.S. Department of Energy, Lawrence Livermore National Laboratory.

The major features of FEAFAA program are:

- 9-slab jointed rigid pavement model.
- Joint load transfer model.
- Up to 6 structural layers.
- Infinite subgrade model.
- Interior or edge loading capability.
- Overlay modeling capability.
- User-defined slab size.
- Customizable aircraft library.

We understand there are two FE models that have been used recently by FAA, a single 30 ft by 30 ft slab free edge jointless model being used in FAARFIELD, and a nine-slab jointed model being used more as a research and analysis tool. The single slab FEAFAA is the basis for the current FAA design procedure for rigid pavements described in FAA AC 150/5320-6E (FAA 2009). The single-slab FE model uses individual gear configurations on the single slab and calculates free edge stress. The free edge stress is then multiplied by the long standing 75% factor and used for fatigue damage calculations.

The enhanced nine-slab version of FEAFAA consists of nine slabs configured in a 3 by 3 array and the slabs are connected by linear elastic joints, which are modeled by discrete vertical spring elements. The FEFAA program is currently used for analyses only, and the results from this program have not yet been incorporated to any pavement thickness design procedure by the FAA. FEAFAA can use either 3D 8-noded brick elements with incompatible modes formulation or shell elements to model PCC layers. Infinite elements are used to model subgrade and joint elements are used to model elastic joints. The following are some features of FEAFAA

1. 3D 8-Noded Brick Element with Incompatible Modes Formulation: Additional freedoms (a1 through a9) are added into the formulation to improve the bending behavior of conforming 3D 8-Noded brick element. The formulation is presented as below:

$$u = \sum N_i u_i + (1-\xi^2)a1 + (1-\eta^2)a2 + (1-\zeta^2)a7$$
$$v = \sum N_i v_i + (1-\xi^2)a3 + (1-\eta^2)a4 + (1-\zeta^2)a8$$
$$w = \sum N_i w_i + (1-\xi^2)a5 + (1-\eta^2)a6 + (1-\zeta^2)a9$$

   It is stated in the FEAFAA help file that each layer consists of one element through the thickness due to the superior bending behavior of this type of element.

2. 2D/3D Shell Element: When shell elements are used to model PCC layers, conforming 3D 8-noded brick elements are used to model subbases. There are four layers of such elements in each subbase.

3. Infinite Elements: The same mapping functions are used to transform both conforming and incompatible 8-noded brick elements to infinite elements. These types of elements are used to model subgrade.

4. Joint Elements: A unidirectional spring element is used to model linear elastic joints between adjacent slabs in FEAFAA. In general, the amount of force provided by a spring specified to act in the *i*-direction is given by: $F_i = k\Delta_i$, where, F_i is the spring force in the *i*-direction, k is the specified spring stiffness, and Δ_i is the extension of the spring in the *i*-direction. The joints are assumed to act as linear continuous elastic springs, transmitting vertical loads between adjacent slabs in shear through the joint.

The default joint stiffness in FEAFAA, often assigned to aggregate interlock joints with no dowels or tie bars, is 100,000 lb/in/in along the joint length. The joint stiffness can also be estimated to approximately reflect dowel bar conditions and estimated joint opening that may exist, given the following dowel bar parameters as input: bar diameter, dowel spacing, joint opening, and method of placement

The equivalent spring stiffness for a doweled or tied joint in FEAFAA is computed according to the following formula:

$$k = \frac{1}{s\left(\frac{\varpi}{0.9G_d A_d} + \frac{\varpi^3}{12E_d I_d} + \frac{2+\beta\varpi}{2\beta^3 E_d I_d}\right)}$$

Where: s is the dowel bar spacing, ω is the joint opening, A_d is the dowel cross-sectional area, and E_d, G_d, and I_d are the Young's modulus, shear modulus and moment of inertia of the dowel bar, respectively. The variable β is defined as:

$$\beta = \sqrt[4]{\frac{Kd}{4E_d I_d}}$$

where, d is the bar diameter and K is the "Modulus of Dowel Support" between the bar and the PCC. In the above formula, FEAFAA assumes that E_d = 29,000,000 psi for mild steel. The modulus K depends on the method of placement: (1) bar placed in fresh PCC. K = 8,290,000 psi, and (2) bar placed in drilled holes. K = 5,270,000 psi

Dowel bar parameters can be entered in the appropriate text box. Drop-down lists provide typical values for the various parameters. The Equivalent Joint Stiffness (*k)* having units of lb/in/in is automatically calculated using the new parameters. The calculated value appears at the bottom of the frame. The Equivalent Joint Stiffness (*k)* can be also assigned manually in FEAFAA by entering a numerical value in a designated area, which overrides the default or dowel equation value.

2.6 CURRENT FAA DESIGN PROCEDURE (FAARFIELD)

The current FAA AC on airfield pavement design is AC 150/5320-6E, and it incorporates the model developed by Brill (1998) for computing the stress in PCC pavements. This stress computation is based on a single-slab version of the original 9-slab model developed by Brill (1998).

The flexible pavement design procedure in FAARFIELD is based on layered elastic design and is similar to the procedures implemented in the program LEDFAA.

Figures 2.11 to 2.13 show some highlights from the current single slab FE model that is used for the thickness design procedures included in FAA AC 150/5320-6E. These figures were obtained from a FAA on-line training presentation regarding the computer program FAARFIELD that incorporates the design methodology presented in FAA AC 150/5320-6E.

Figure 2.11 shows the general mesh shape for the model and shows one of the key findings, which is the finite slab size causes a reduction in free edge stress compared to Westergaard equations that are based on an infinite slab size. (The legend in the figure indicates FEDFAA, which was the name given to the beta version of FAARFIELD.) Apparently a slab with 30-ft dimensions is used as the basis of design within FAARFIELD, which results in slightly lower edge stress for weak subgrade and no change in edge stress for stiff subgrade, compared to infinite slab assumptions.

Figure 2.12 shows the concept of subbase/base extension used in the FE model. Figure 2.13 shows the aircraft gear alignment positions on the edge of a slab. FAARFIELD either places the gear perpendicular or parallel to the edge of the slab. This determination is made by FAARFIELD.

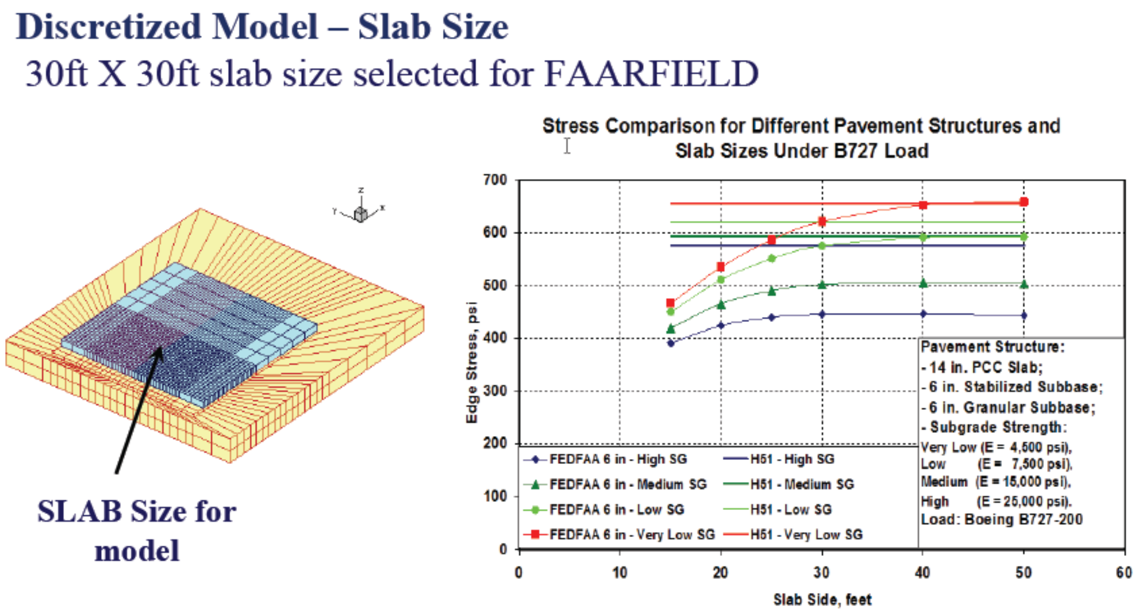

FIGURE 2.11. GENERAL SHAPE OF THE NEW SINGLE SLAB FEM MODEL IN FAARFIELD AND SOME FE ANALYSIS RESULTS.

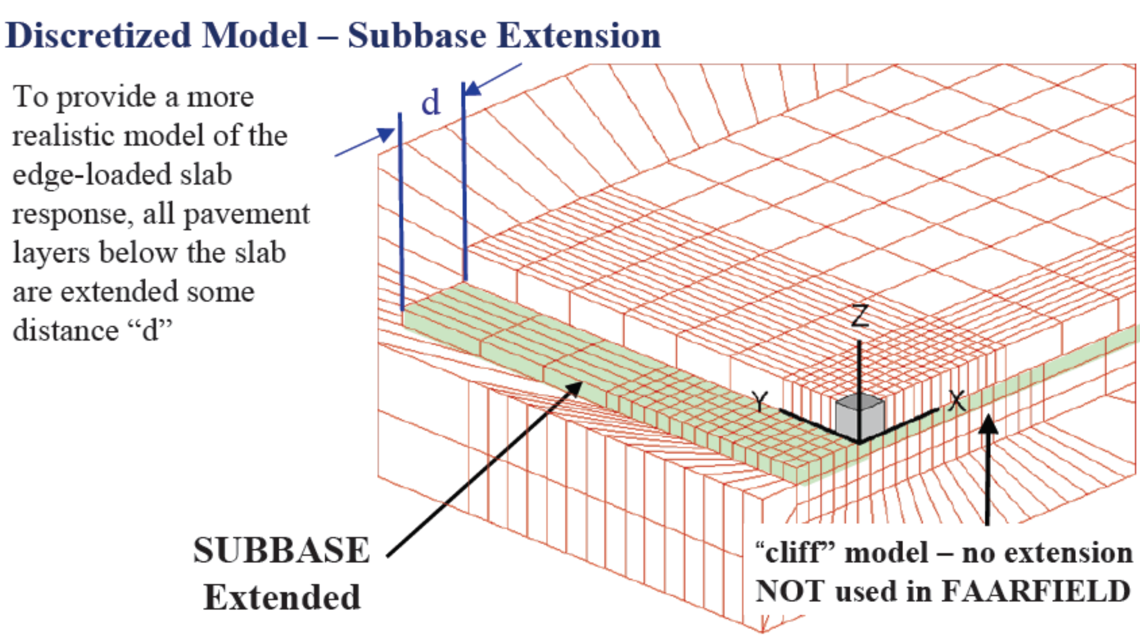

FIGURE 2.12. CONCEPT OF SUBBASE/BASE EXTENSION FOR THE FE MODEL USED IN FAARFIELD.

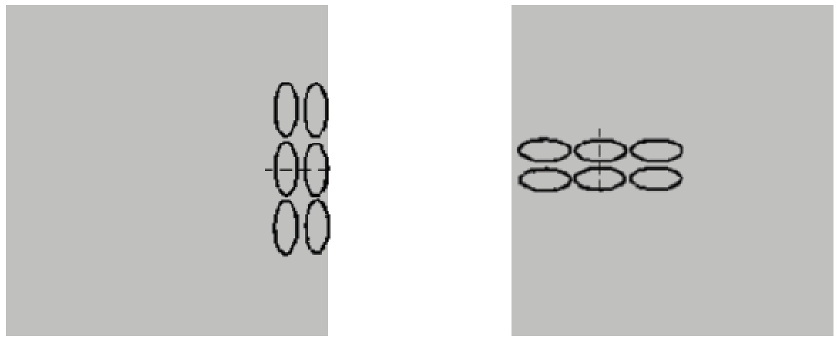

FIGURE 2.13. LOAD POSITIONS USED IN THE FAARFIELD SINGLE-SLAB FE PROCEDURE

2.7 VARIATIONS FROM DESIGN ASUMPTIONS AFFECTING PAVEMENT PERFORMANCE

With any pavement design method, there may be some inherent errors caused by simplifying assumptions, some on the conservative and some on the liberal side of reality. Kohn (1985) showed an example of an error on the conservative side that may be inherent in current FAA thickness design philosophies. Figure 2.14 shows measured aircraft weights as a function of the planned flight distance. The aircraft generally only load as much fuel as they need for their trip and some possible diversions. The true weights of departing aircrafts were in general significantly less than the weights used for design. Kohn (1985) found this as a possible factor why several airfields had not experienced cracking when the design model fatigue equations and design aircraft loading indicated they should be cracked. The estimated fatigue damage differences for 80% versus 100% of the design take-off weights were very significant

Table 2.6 from Kohn (1985) shows how design assumptions for subgrade stiffness and PCC flexural strength compared to values obtained from nondestructive testing (NDT). The in-situ subgrade stiffness estimated by NDT was well below what was assumed for design, while the flexural strength of the PCC on-site was much higher than that assumed for design. Measured thickness was in most cases slightly greater than design, but at one site it was about 2 inches less.

PCC materials often have significantly higher flexural strength in-place than are assumed for design. The fatigue models used in PCC airfield pavement design are empirical. The regression coefficients within these models are indirectly taking into account many conservative versus liberal error sources associated with simplified analysis model assumptions. As aircraft load data and slab structural analysis models used as the basis of pavement design become more precise and accurate, the fatigue models will have to be continually re-calibrated.

2.8 CURLING AND WARPING EFFECTS IN CONCRETE PAVEMENTS

The models currently used in airport pavement thickness designs do not consider curling stresses nor do they analyze stress occurring at the top of slab. Roesler et al. (2007) recently did an analysis showing that when joints have low load transfer, certain aircraft gear configurations, especially the A-380 and MD-11 aircraft, can generate large tensile stresses on the top of the slab, which can control the fatigue crack based design and critical stress location for even flat slab condition (i.e. zero thermal gradient and zero warp). They note that top-down cracking has been observed as the primary cracking mode at test sites that had thick slabs.

Byrum and Hansen (1994) used time of day truck weight data from a weigh in motion scale combined with time of day curling stress estimates to compare top down cracking versus bottom up cracking. Their research showed that highway slabs that develop a common degree of slight locked in up-warp , which is equal to the effects of roughly a 2°F/inch thermal gradient, can have the critical fatigue damage location at the top of the slab. This critical damage location can occur at a significant distance, 10-15 feet, from the transverse joint loading location, due to an unsupported cantilever-end type effect for joint uplift conditions. In highway slabs, either upward slab curvature or downward slab curvature from slab warping (not thermal curling) can be large, typically many times as large as typical curling effects from thermal gradients.

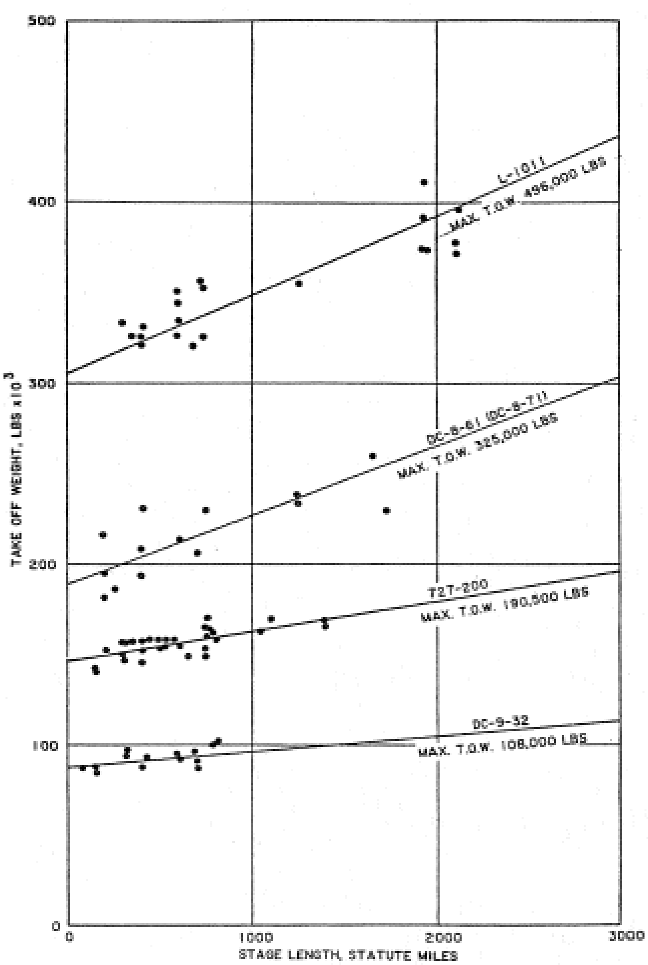

FIGURE 2.14. PLOT SHOWING HOW MEASURED AIRCRAFT WEIGHTS ARE TYPICALLY LESS THAN THE DESIGN AIRCRAFT WEIGHTS USED FOR PAVEMENT DESIGN (KOHN 1985).

TABLE 2.6. COMPARISON OF IN-SITU PARAMETERS FROM NDT TESTING TO THOSE ASSUMED FOR DESIGN (KOHN 1985).

Section Number	Existing T in.	NDT Properties K pci	NDT Properties MR psi	NDT Properties T in.	Design Properties K pci	Design Properties MR psi	Design Properties T in.
DFW 1	15	289	900	12	360	680	14
DFW 2	15	289	900	12	360	680	14
DFW 3	16	292	900	13	360	680	16
DFW 4	16	292	900	13	360	680	16
DFW 5	17	231	900	12	360	680	13
DFW 6	17	231	900	12	360	680	14
DFW 7 & 8	17	274	885	14	360	680	17
DFW 9 & 10	15	246	900	15	360	680	17
DFW 11	16	183	900	15	360	680	17
DFW 12	16	183	900	15	360	680	16
DFW 13	17	273	900	13	360	680	16
DFW 14	17	98	867	16	360	680	17
ATL 1	16	440	900	13	500	715	14
ATL 2 & 3	16	285	884	13	500	715	14
ATL 4 & 5	16	265	876	13	500	715	14
ATL 12 & 13	16	290	840	13	500	715	13
ATL 16 & 17	16	255	802	15	500	715	14
ATL 20	16	205	715	17	500	715	14
JFK 4	13	191	640	17	---	---	---

Up-warp curvatures having magnitudes equivalent to thermal gradient curvature (curling) magnitudes of that caused by a 10°F/inch gradient (roughly 90°F temperature difference through a 9 inch slab) have been measured at long term pavement performance (LTPP) GPS3 highway test sites that performed poorly over time (Byrum 2000, Byrum 2009).

A detailed study of airfield pavement profiles for slab warping has apparently not been performed. In general, a thicker and shorter slab is probably less susceptible to factors that result in locked-in warp than a thin and long slab. However, at the same time, the thicker slabs have far larger flexural rigidity, which is proportional to thickness cubed, and are less capable of relaxing out warp stress.

Nishizawa et al. (2009), showed test site data and a thermal gradient prediction model that clearly show that thick slabs do not develop curling gradients as large as thinner slabs, given the same daily thermal input at the top of slab. The key point is that if significant up-warp or up-curl is present in airfield pavements, the critical design stress may be located on the top of the slab, near mid slab, possibly between wheels or gear assemblies. For example, it is this up-warp effect that is reported to be a primary cause of early top-down cracking in the NAPTF CC-1 PCC test slabs, leading to the controlled wetting of slabs and careful curing methods for the CC-2 project (Guo 2007).

Figure 2.15 shows simulated strain history response from a modified ILLISLAB FE model for top of slab tension at mid-slab, 360 inches, caused by a simulated rolling wheel load on a slab with upward curling having low load transfer at the joints, showing how there can be two tensile fatigue spikes for one passing wheel load for top-down cracking modes (Byrum and Hansen 1994).

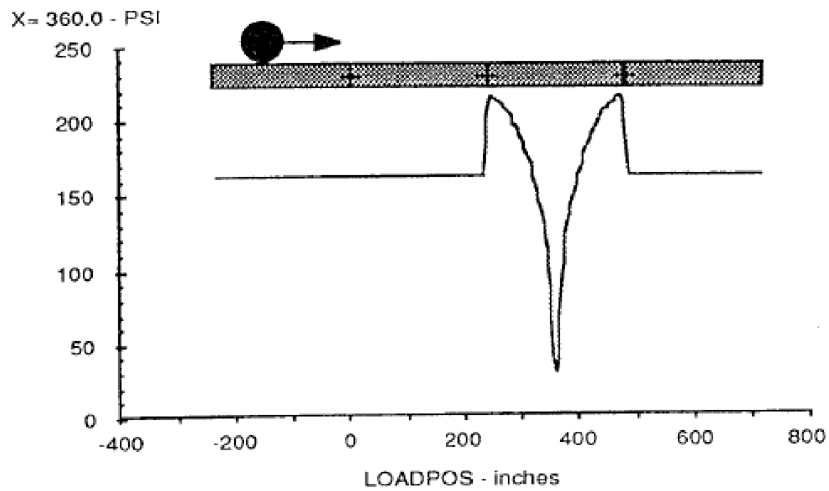

FIGURE 2.15. SIMULATED STRAIN HISTORY RESPONSE FROM A MODIFIED ILLISLAB FE MODEL FOR TOP OF SLAB TENSION AT MID-SLAB CAUSED BY COMBINED UPWARD CURLING AND A SIMULATED ROLLING WHEEL LOAD (BYRUM AND HANSEN 1994).

If the axle spacing is just less than the slab length, the top down crack stress increases additionally when the loads are placed on each end of the slab simultaneously. There is only one bottom of slab tensile spike for each load. For the 11 inch thick slab modeled in figure 2.15, the 9 kip wheel load stress was smaller than the residual curling stress and the bottom of slab at the mid slab location never felt any tensile stress. If load transfer is low and if any up-warp is present, the chance of top of slab stress being critical is higher. The best way to simultaneously look at warping and curling effects, top and bottom slab stress, and the effect of aircraft gear configurations is to use realistic joint structural models that incorporate all of these elements into a sophisticated FE model.

CHAPTER 3: JOINTS IN AIRFIELD CONCRETE PAVEMENTS

3.1 HISTORICAL BACKGROUND ON JOINT SPACING

In the early years of PCC pavement construction, a general philosophy that building fewer joints, spaced further apart in PCC pavements grew over time as it was recognized that joints were the primary area in PCC pavements that experienced distress. As agencies started building slabs with joints that were far apart, increased problems with random cracking between joints occurred over time, and joints deteriorated more rapidly due to increased joint openings. Increased cracking between constructed joints was also somewhat enhanced by industry changes such as the use of slip form pavers, cements that generated more heat, and light membrane curing methods. Older curing and placement methods (i.e. formed placement of higher slump, slower heat generation mixes, and use of wetted burlap and ponded earth curing methods) allowed the use of longer joint spacing with less premature cracking issues.

An interesting jointing philosophy history is that of the Michigan Department of Transportation (MDOT). By around the Second World War, MDOT had evolved into using a 99-ft joint spacing for highway pavements, with reinforcement provided within the slab. Some of these wet cured and non slip form pavements did not develop any significant cracks between the 99-ft joints for many years after initial construction. However, many of these slabs cracked into 10-15 ft segment lengths generally 5 to10 years after initial construction. One such segment of original 99-ft jointed PCC pavement from the 1950’s is still in service under medium interstate traffic levels near Brighton, Michigan and there are some relatively long non-cracked segments still in place, but most of the original joints have been cut out and replaced. As truck weights and traffic volumes increased, and after the introduction of slip formed pavers and membrane curing, MDOT realized that the mid panel random cracks were showing up earlier and was a source of premature spalling and faulting. Over time, MDOT started to reduce the joint spacing. By the mid 1970’s the standard joint spacing dropped to 71 feet, with reinforcement provided within the slab. Problems with poor performance of random cracking between joints still occurred frequently. By the mid 1980’s the standard joint spacing had dropped to 41 feet, with reinforcement provided within the slab. These slabs often developed two significant cracks between the joints, each about 10 to 15 feet from the joint. By the mid 1990’s the standard joint spacing had dropped to 28 feet, with reinforcement provided within the slab. These slabs tended to only develop one major random crack between joints. Today MDOT constructs plain jointed PCC pavements that have joint spacing varying from 12 to 15 ft depending on the slab thickness.

Shortly after the first generation of large PCC slab areas were constructed in the early 1900’s, it was recognized that the slabs had a tendency to crack shortly after placement from forces related to PCC shrinkage and daily temperature changes. Prior to 1920, an early American Concrete Institute paper presented cracking patterns observed in some of the first large area PCC placements, and indicated for a given thickness, the PCC had cracked at shorter intervals when placed on hard subgrades compared to weak subgrade. The weak subgrade encouraged longer initial spacing of cracks. If no joints are used in a PCC placement, initial cracks will form at a somewhat predictable preferred spacing, which will typically be at about 4.2 times the radius of relative stiffness of the slab system (Bradbury 1938, Byrum 2001, Byrum and Hansen 1994).

Radius of relative stiffness values range from about 30 to 45 inches for highway slab thickness, 40 to 60 inches for airfields, and can be higher for some thicker heavy-duty industrial or airfield slab systems. Based on these values, if joints are not formed during the construction process, cracks will eventually form and will be spaced on average at about 10 to 20 feet spacing for typical highway slabs, and about 15 to 40 feet spacing for typical airfield slabs.

Perhaps the worst possible joint spacing that can be used at a site is a joint spacing of about 8.4 times the radius of relative stiffness, known as the critical slab length. This critical slab length develops the maximum thermal bending stress response at the mid slab location, and the maximum joint elevation changes from curling, resulting in more rapid mid slab cracking and joint deterioration. If you build slabs with a joint spacing longer than 8.4 times the radius of relative stiffness, there is actually a slight reduction in thermal stress, but joints will generally develop greater opening magnitudes and suffer accelerated deterioration. Two or more cracks will likely develop in slabs constructed at significantly longer than 8.4 times the radius of relative stiffness. For slabs constructed at joint spacing less than about 8.4 times the radius of relative stiffness, the peak thermal stress level at mid slab decreases from the maximum value.

In general, most highway agencies are using joint spacing in the 12 to 25 feet range. Joint spacing of 20 to 25 feet is common for thicker PCC airfield pavements. The joint spacing used today is slightly shorter than the critical slab length that causes peak thermal responses at the mid-slab position and maximum joint uplift during morning curling. For these shorter slabs, the thermal stresses in the slab interiors are generally less than the fully restrained (i.e. no curling allowed) thermal stress for a given gradient.

Slabs should not be constructed too short or they can be subject to mass instability, or rocking under heavy loads, which can rotate slabs causing displacement and joint faulting that result in poor ride quality and spalling at the joints (Byrum 2007, Pringle 1950). If a slab is short and a heavy load is placed at the edge, significant uplift deflection of the far edge of the slab can occur. This back and forth movement can enhance subgrade pumping and erosion and cracking of stabilized bases. For a given load range, there is an ideal slab length that is not too long or not too short. It is generally accepted philosophy that well constructed joints are significantly less likely to spall than an irregular random crack. Therefore, over the last century, agencies have developed jointing schemes for use with PCC pavements to control cracking and reduce spalling.

A primary task in the PCC pavement design process is the development of a proper jointing pattern. For large area PCC slab placements such as airfield aprons and runways, the design team uses a combination of expansion and contraction joints that allow opening and closing, and fixed (tied) joints to manage the tendency of slabs to spread apart or crush each other due to the thermal contraction and expansion from winter to summer.

3.2. TYPES OF JOINTS IN AIRFIELD CONCRETE PAVEMENTS

3.2.1 Past Practices

Teller and Sutherland (1936) present an interesting discussion on the early history of jointing for PCC pavements. In the early years of PCC pavement construction, various joint load transfer devices and various approaches for constructing joints were employed. As most early PCC pavements did not employ bases or subbases, over time, the joints, especially the smooth-faced butt joints, experienced relatively rapid faulting and deterioration. Another factor that affected joint performance was the rapid increase in wheel load magnitudes over time. Several images of load transfer devices used in the past are shown in figures 3.1 through 3.5 (Van Breemen and Finney 1950, Teller and Sutherland 1936).

Some examples of joints and load transfer devices used at joints in the past that are no longer in general use today are briefly described below:

- Steel Plate Joints: A steel plate was placed on the subgrade below a joint location.

- Steel T Joints: An inverted steel T structure was placed along the joint, with the web of the steel member causing the joint to form over the steel web.

- Patented Joint Devices: Patented devices of various shapes were tried with the intention of getting significant bending moment transfer from one slab to another while allowing relative horizontal movement of the slabs.

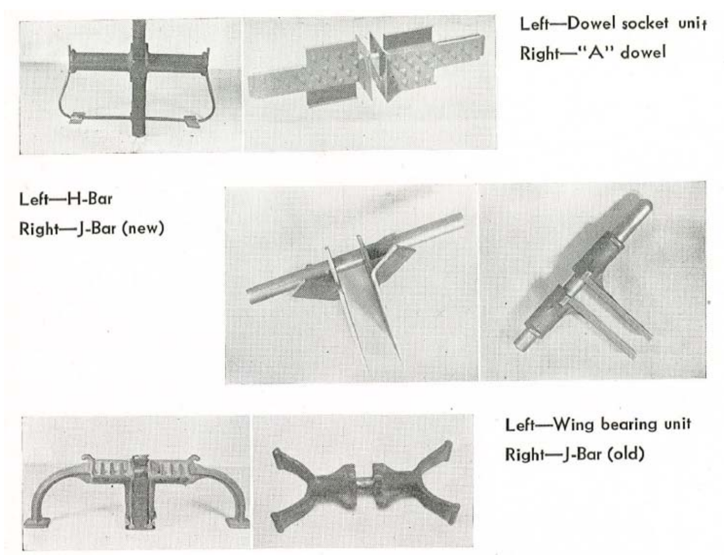

FIGURE 3.1. EARLY JOINT LOAD TRANSFER DEVICES

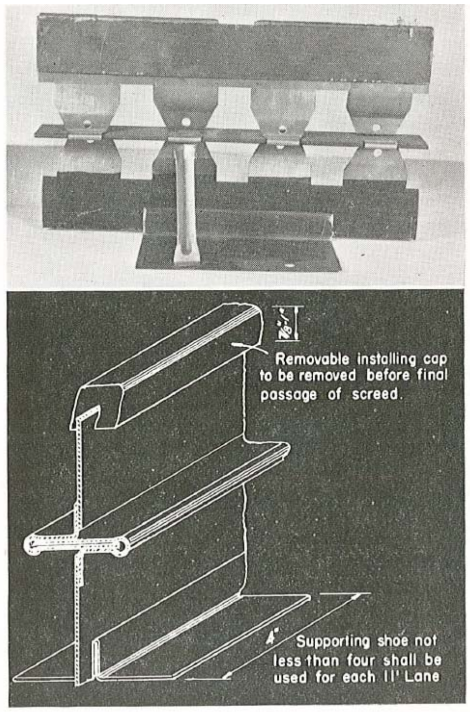

FIGURE 3.2. EARLY JOINT LOAD TRANSFER DEVICES: TOP – PLATE DOWELS, MIDDLE – KEY LODE, BOTTOM- CONTINUOUS PLATE.

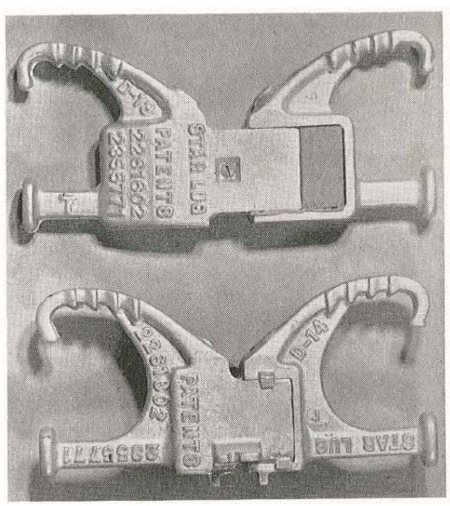

FIGURE 3.3. EARLY JOINT LOAD TRANSFER DEVICES – STAR LUG UNITS.

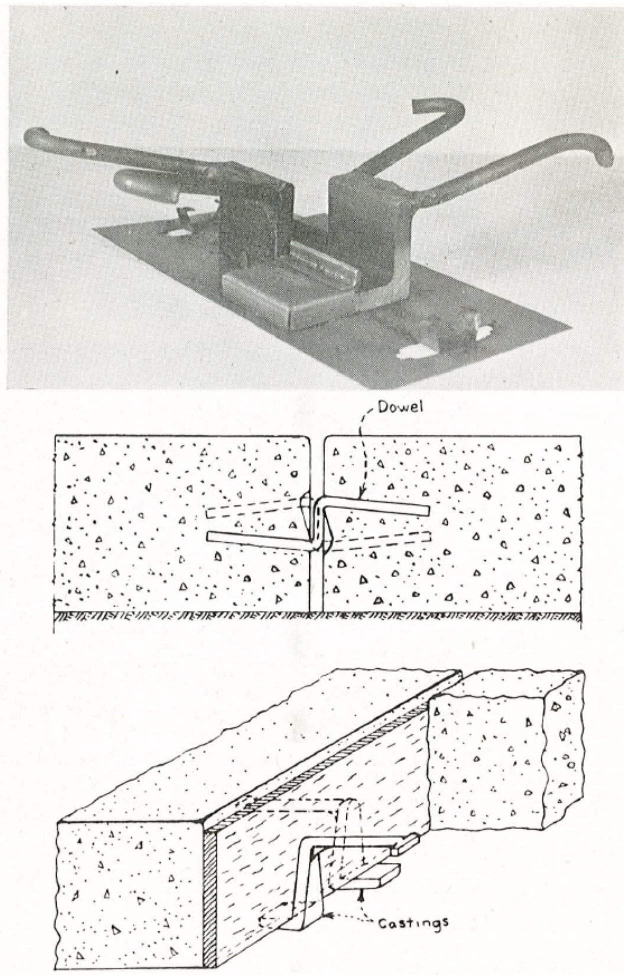

Fig. 5—Hinge action units. Top—Translode angle. Center—Z-Bar. Bottom—Spade unit

FIGURE 3.4. EARLY JOINT LOAD TRANSFER DEVICES: TOP – TRANSLODE ANGLE, CENTER: Z-BAR, BOTTOM – SPADE UNIT.

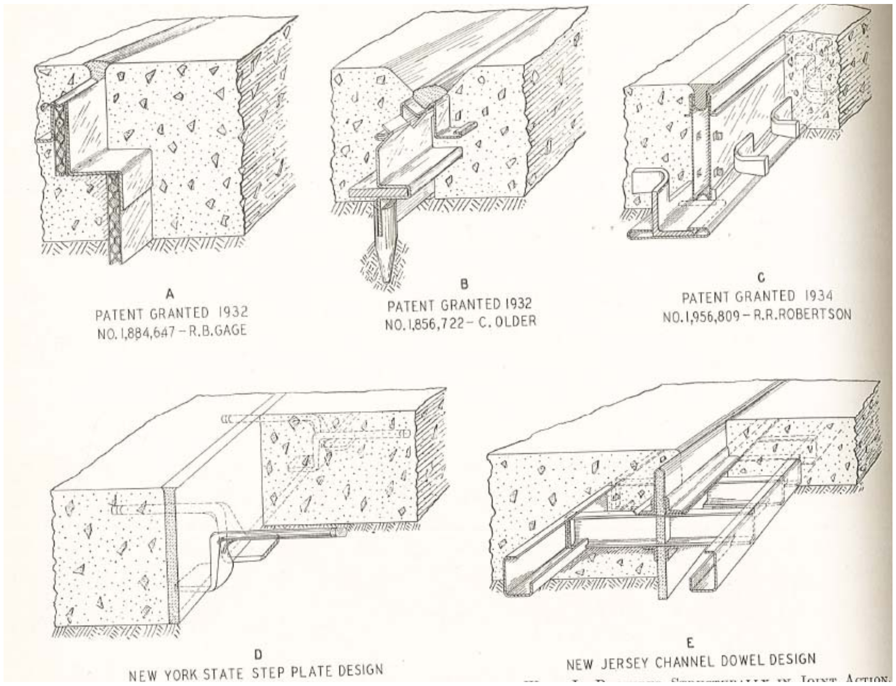

FIGURE 3.5. EARLY JOINT LOAD TRANSFER DEVICES.

- Keyed Joints: Although this joint type was used extensively for many years, currently it is not being used for new construction of major airfields in the United States. Early keyed joints used in the United States had a simple single shear key shape. These keyed joints suffered from poor performance under heavy loads and often had sudden tearing off or spalling of the upper outer wall portions of the side of the keys under heavy loads. The shape of the keyway was critical to performance. A keyed-tied construction joint is similar to a keyed construction joint but has deformed steel bars across the joint to tie the slabs together to prevent the joint from opening. Teller and Sutherland (1936) performed a detailed analysis of key shape considering how slabs rotate at ends due to curling and warping deformation. Barenberg and Smith (1979) performed detailed 3-D FE studies of key shape showing critical aspects. A sine-wave shaped keyed joint slip-form, having several wavelengths, like an aggressive ripple pattern along the face, was still in common use in Germany in 2001.

- Free Edge Expansion Joint: These joints have a thick layer of compressible material placed between the slab ends with no steel reinforcement across the joint. Although easy to construct, these joints are no longer used in heavy traffic areas.

3.2.2 Current Practices

In the last few decades, the jointing schemes have become simpler, and today agencies managing large pavement areas are using a similar general scheme for constructing joints. In more severe climatic regions, most highway agencies provide for load transfer at transverse joints by using dowel bars and use tie bars across the paving lane joint. In airfield pavements, steel ties are commonly provided at the longitudinal paving joint. However most airfield pavements in use today do not have load transfer devices in the joints that are perpendicular to the paving lane. Currently, lane ties placed at paving lane joints as well as dowels if placed at joints perpendicular to the paving lane are generally placed at the mid-depth position of the slab. The FAA AC No. 150/5320-6E presents joint details commonly used in airfield pavements. The FAA AC No. 150/5320-6E includes a new steel reinforced edge expansion joint detail, and does not include any keyed joints in the group of standard recommended joints for designs. Doweled construction joints are the only type of construction joint recommended in FAA AC No. 150/5320-6E. The following is a description of various joint types that are used in airfield pavements:

- Aggregate Interlock Joint: This joint is a thermal or shrinkage contraction-type joint that forms after the PCC is placed, through a partial depth saw-cut or a preformed groove. No steel such as dowels or ties are provided across the joint. FAA AC 150/5260-6E refers to this joint as a Type D dummy joint, and indicates the grove must be formed by sawing. These joints will open and close from winter to summer. Any load transfer ability for this joint type is developed in vertical shear through the crack face roughness interlock. If the crack face that forms is very smooth, just a slight joint opening will result in rapid loss of load transfer ability. If the crack face is very rough and the PCC and aggregates have very high toughness, a greater joint opening will be required before load transfer is lost. An irregular random crack within a slab will behave like an aggregate interlock joint. Load transfer will range from a very low value that is close to zero for large joint openings typically occurring during very cold temperatures, to very high when slabs expand during hot weather.

- Doweled Contraction Joint: This joint is also a thermal or shrinkage contraction-type joint that forms after the PCC is placed, and through a partial depth saw-cut or pre-formed groove. However, smooth steel dowel bars are provided across the joint with the bars being generally placed at the mid-depth position of the slab. FAA AC 150/5260-6E refers to this joint as a FAA Type-C doweled joint, and indicates the groove must be formed by sawing. Typically one half of the smooth steel dowel bar is greased to encourage free opening and closing of the joint from thermal effects. If the joint opening is small, both the crack face aggregate interlock and the steel dowel are available to contribute to load transfer. When the crack is fully open, all load transfer must be developed through the embedded dowel. Doweled joints tend to maintain a relatively constant and high level of load transfer over a wide temperature and joint opening range. The dowels may develop increasing looseness or slack over time causing some loss of load transfer ability.

- Doweled Construction Joint: This joint is the same as a doweled contraction joint, but the joint face typically has a relatively smooth face. The dowels are drilled and grouted into the joint face after the PCC sets, or set into the PCC through the forms before constructing the pavement. FAA AC 150/5260-6E refers to this joint as a FAA Type-E doweled joint. Less aggregate interlock is available for load transfer with this joint type when compared to a doweled contraction joint. Based on the recommended typical dowel-concrete interaction stiffness values in the joint stiffness estimation guidelines for the FAA's new nine-slab FEM analysis model, lower stiffness dowel-concrete interaction factors are recommended for drilling and grouting of dowels compared to dowels installed into fresh PCC and with proper vibration consolidation of the PCC around the dowels. Well formed drilled holes with minimal sidewall damage are needed to achieve good load transfer for drilled and grouted dowels (Snyder 1985).

- Tied Contraction Joint: This type of a joint is similar to a doweled contraction joint, but deformed steel bars are placed across the joint instead of dowel bars. FAA AC 150/5260-6E refers to this joint as a Type B hinged joint. This joint is restrained from opening and is expected to stay closed. These joints are relatively rarely used in airfields and are more common for roadways. There is typically less steel area across the joint face in this type of a joint when compared to a doweled contraction joint. But in this type of joint, by keeping the joint closed, the aggregate interlock remains effective in cold weather. The deformed bar acts to somewhat resist contraction type crack formation below the saw cut or the groove of the joint.

- Doweled Expansion Joint: These joints are rarely used. These joints are sometimes used in very large area placements to relieve potential high compressive stresses that can result from thermal expansion of slabs in the summer. The least expensive version of this joint is a doweled construction joint, with a thick fiber-board joint filler placed between the slab faces. If present, this type of a joint will constitute a very small percentage of the joints on the pavement. Because there is a large joint opening between PCC slabs in this type of a joint, steel dowels with a significant non-embedded length between slabs must develop all load transfer.

- Tied Construction Joint: This joint is similar to a doweled construction joint, but instead of a dowel bars, deformed steel bars are placed across the joint. This joint is restrained to opening and is expected to stay closed. There is typically less steel area across the joint face in this type of a joint compared to a doweled construction joint. Because of the lower steel content, these joints are often oriented parallel to the traffic direction rather than perpendicular to the traffic direction.

- Thickened-Edge Joint: This joint type is used at all outer edges of airfield PCC placements. FAA AC 150/5260-6E refers to this joint as a Type-A thickened edge joint. FAA requires a 25% increase in thickness (2” min. increase) tapered over a full slab length or a minimum of 10 feet.

- Anchored Construction Joint: This joint is similar to a tied construction joint, but load transfer is developed with drilled and grouted anchors such as red-heads or hook-bolts. These joints are more common for rehabilitations and retrofits and are generally not used for new construction or in heavy traffic areas.

3.3. JOINTING CONSIDERATIONS FOR DESIGN

3.3.1 Introduction

In recent years, the general trend in PCC slab design has been to use closely spaced joints with dowels at the joint for load transfer without any reinforcement within the slab. There are two primary theories that are used to help describe the need for joints. Subgrade drag theory estimates the tension build-up in a slab due to friction present at the bottom of the slab acting to resist thermal shrinkage of the slab. In general, if the slab is long enough, the friction buildup from thermal contraction can crack the slab. Thermal and shrinkage gradient theory is used to describe bending moments and associated curling that form in the slabs as they cure and are exposed to changing ambient temperatures and humidity. By using shorter slabs, the tension from subgrade drag is reduced, and the joint openings between slabs remain smaller, resulting in higher load transfer levels between joints.

Some researchers have added subgrade drag to FE models and shown that drag affects curling stress and deflection significantly. The interaction of subgrade drag and curling is complex. By using shorter slabs, the joint lift-off from the foundation caused by morning curling is reduced. By using shorter slabs, the mid-panel bending stresses from thermal curling or warping are reduced. However, a pavement system that uses more joints is subject to more spalling if PCC durability issues occur. If slabs are constructed too short for the types of loads being applied, they are subject to premature permanent rocking or tilting, and faulting of joints. For example, in highways, there is evidence showing that slabs in the 11 to 14 ft long range are more susceptible to developing a permanent tilt or rocking under traffic, when compared to slab lengths of 17 to 20 feet (Byrum 2007).

3.3.2 Differences in Joint Behavior between Airfield and Highway Pavements

Compared to airfield pavements, PCC slabs in highways have more repeated loads such that joint damage deterioration and eventually faulting can occur to a far greater extent than that allowed for airfield pavements. The process of faulting starts as pumping of water beneath a slab begins to erode and move the foundation material from one side of the joint and forcing it beneath the other side of the joint.

As the rolling load moves toward the joint, the load on the subgrade is gradually increased and movement of air and water is relatively slow under the approach slab near the joint. However, when the load suddenly crosses the joint, especially if there is low load transfer, there is a very sudden impact type load applied to the leave slab. This very rapid loading of the leave slab causes the material immediately beneath that area to move rapidly towards the approach slab that has been unloaded. Over time, the approach slab is jacked up, while the leave slab loses foundation support and may drop downward slightly, resulting in faulting occurring at the joint. As this offset and loss of support develops, it significantly affects how load is transferred.

The aggregate interlock at the joint face develops a slack and offset, and the leave side slab aggregate features are essentially dropping down and resting on the approach side features. When the leave slab is loaded, there is no apparent slack. When the approach side is loaded, there is significant slack. So, at a faulted joint, the approach side slab retains stiffer foundation support but less joint load transfer due to the slack, while the leave side slab retains higher load transfer because the slack is closed but has lesser support due to erosion below the slab. These are somewhat balancing effects. Figure 3.6 shows a typical LTE_{δ} response for the approach and leave sides of a highway joint that has experienced rolling traffic loads only in one direction across the joint (Prozzi et al. 1993). Even when just a small level of faulting is present, large differences in LTE_{δ} from one side to the other across a joint that only has aggregate interlock will be observed as shown in figure 3.6.

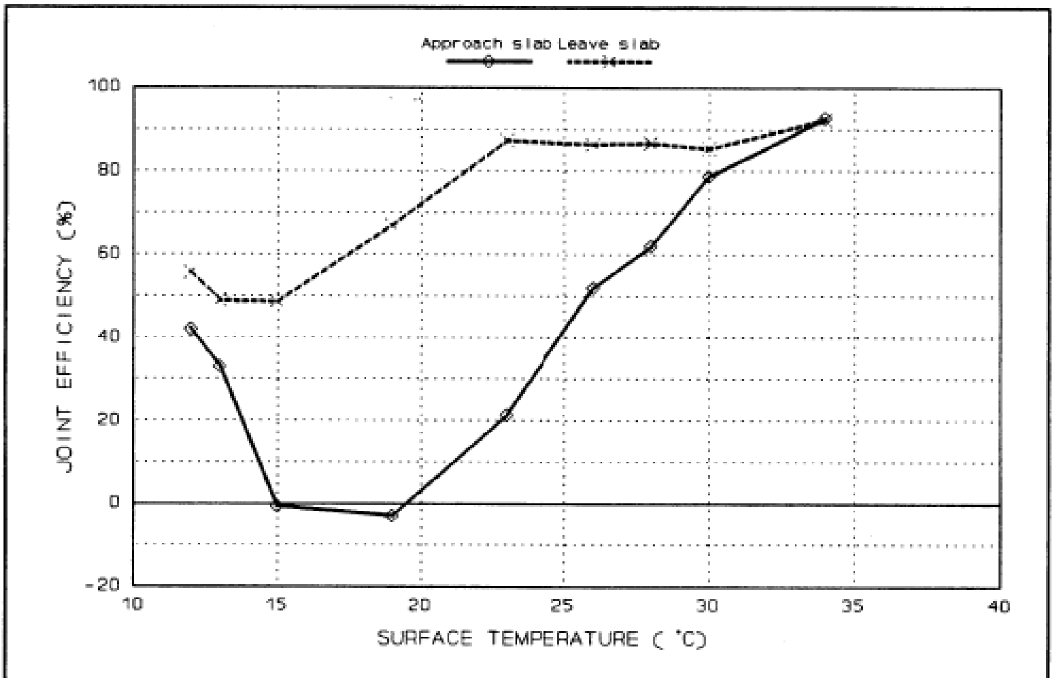

FIGURE 3.6. PLOT SHOWING HOW UNDER-SLAB EROSION AND FAULT OFFSET SLACK AFFECTS LTE_{δ} FOR TYPICAL HIGHWAY JOINTS STARTING TO EXPERIENCE SLIGHT FAULTING (PROZZI ET AL 1993).

3.3.3 Evolution of Joint Spacing in FAA Advisory Circulars

The current FAA advisory for pavement thickness design is FAA AC 150/5320-6E (FAA 2009), which was issued on 30 September, 2009, and superseded the previous AC for pavement design, which was AC 150/5320-6D (FAA 1995).

In AC 150/5320-6E, joint spacing tables are provided for both stabilized and non-stabilized bases and no reference to radius of relative stiffness is indicated relating this parameter with joint spacing. The tables limit the joint spacing on stabilized and non-stabilized bases to less than 20 feet. Therefore, in AC 150/5320-6E, the 20 feet maximum joint spacing is a requirement and not a recommendation as it was in AC 150/5320-6D. If a reinforced PCC pavement system with internal slab steel bar or mat reinforcement is designed, joint spacing of up to 75 feet is allowed in AC 150/5320-6E.

In AC 150/5320-6D, there is a table showing maximum slab lengths of 25 feet for thicker PCC slabs on unbound aggregate bases. For stabilized bases, maximum slab lengths were recommended to be less than 4 to 6 times the radius of relative stiffness and an equation was provided. In change 2 to AC 150/5320-6D released in 2002, a new note appeared in the jointing requirements stating that joint spacing for all sites should be less than 20 feet unless the design engineer had good reason to allow longer joints, and that joint spacing for stabilized bases should be less than 5 times the radius of relative stiffness.

CHAPTER 4: ANALYTICAL STUDIES OF LOAD TRANSFER AT JOINTS

4.1. DOWELED JOINT ANALYSIS (Non FEM)

4.1.1 Early Studies (Prior to 1990)

Perhaps the first analysis of dowel bar stiffness and looseness at a joint was performed by Teller and Sutherland (1936). They plotted the ratios of apparent stiffness of the loaded and unloaded slabs (p/k), and if the ratio was constant over a range of loads then they indicated no looseness was present. Figure 4.1 from Teller and Sutherland (1936) shows how the joint in Section 6 has apparent looseness and lower load transfer when compared to the joint in Section 7.

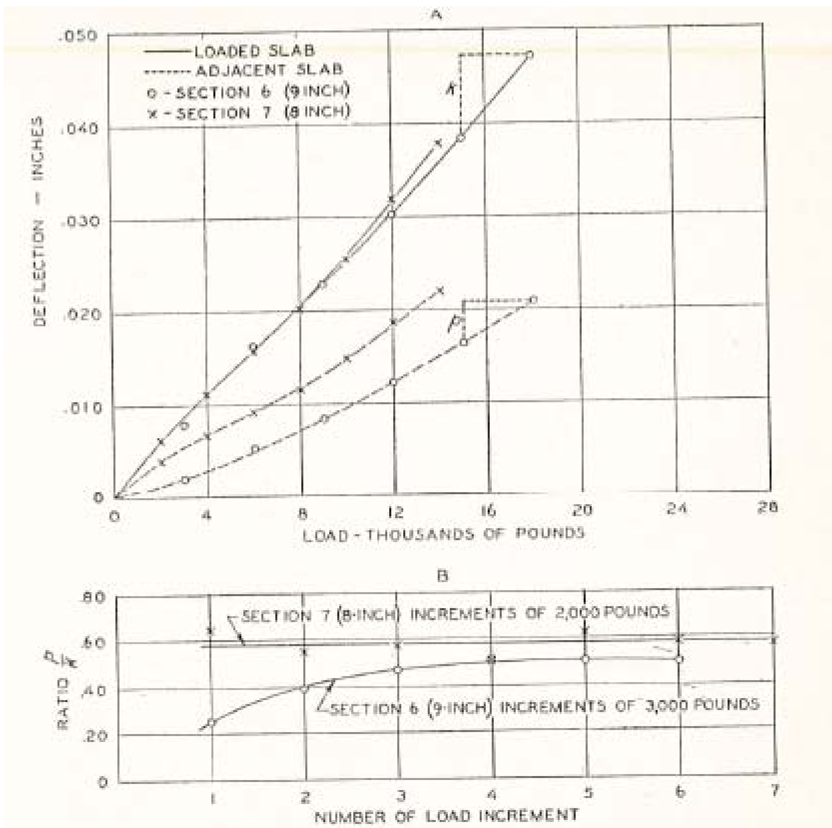

FIGURE 4.1. DEFINITIONS OF DOWEL LOOSENESS FOR JOINTS IN PCC PAVEMENTS (TELLER AND SUTHERLAND 1936).

Shortly after Teller and Sutherland, some of the first theoretical joint considerations were presented by Friberg (1938). Friberg developed a dowel response model based on a structural analysis of laterally loaded elastic steel dowels of infinite length embedded in an elastic half-space. He defined the parameter described in the nine slab FEAFAA as *K*, the modulus of dowel concrete interaction, representing the stiffness of the concrete surrounding the dowel.

Shortly after that, Skarlatos (1949) who was developing an extension of Westergaard's equations to quantify load transfer at joints, defined a parameter called joint stiffness (q_0), a constant value in units of lb/in/in, meaning lb of load transferred in shear, per inch of relative vertical slab displacements (deflection difference) at the joint, per inch along the joint line. This constant value is the most simplified relation that could possibly be used to numerically analyze joint load transfer. This is still today the general form used by most analytical models for PCC pavements and for the state of the art FEAFAA model being developed by FAA.

Most joint research has attempted to find the equivalent constant joint stiffness for various design details, aggregate types, joint openings, and other factors. However, we know that the mobilization of joint stiffness is highly non linear with respect to differential deflection at the joint, and not a constant independent of joint relative displacement magnitude.

Teller and Cashell (1958), performed some of the first full scale repeated load tests of doweled joints in a controlled laboratory environment, that were designed to test some of the theory presented by Friberg (1938). These were perhaps the first detailed controlled studies of load transfer deterioration and joint looseness development for doweled joints using full scale slab models. These studies are often referred to as the Bureau of Public Roads (BPR) dowel looseness studies. The thickest slabs evaluated were 10 inches in thickness and used 1.25 inch diameter dowel bars. Special test apparatus were constructed to apply hundreds of thousands of repeated heavy loads, alternating from one side to the other over the joint, simulating a passing wheel load. Figure 4.2 provides an image of the test apparatus that was used. These tests resulted in a parameter referred to as dowel looseness by the authors.

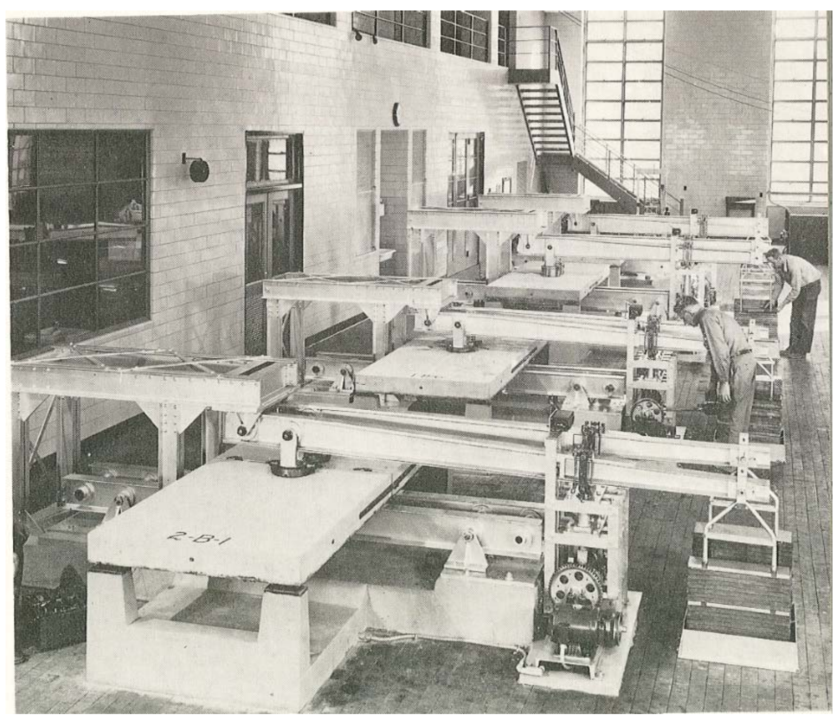

FIGURE 4.2. BUREAU OF PUBLIC ROADS REPEATED LOAD JOINT TESTING APPARATUS (TELLER AND CASHELL 1958)

Figure 4.3 shows a plot from these studies for a joint, and the dowel looseness values are the zero load intercept values indicated on the vertical axis. Figures 4.4 and 4.5 show the thickness and subgrade stiffness trends obtained by Teller and Cashell (1958). Two interesting and strong general trends from the BPR doweled joint studies are that as slab thickness and subgrade stiffness increases, the percent load transferred through otherwise equal joints significantly decreases.

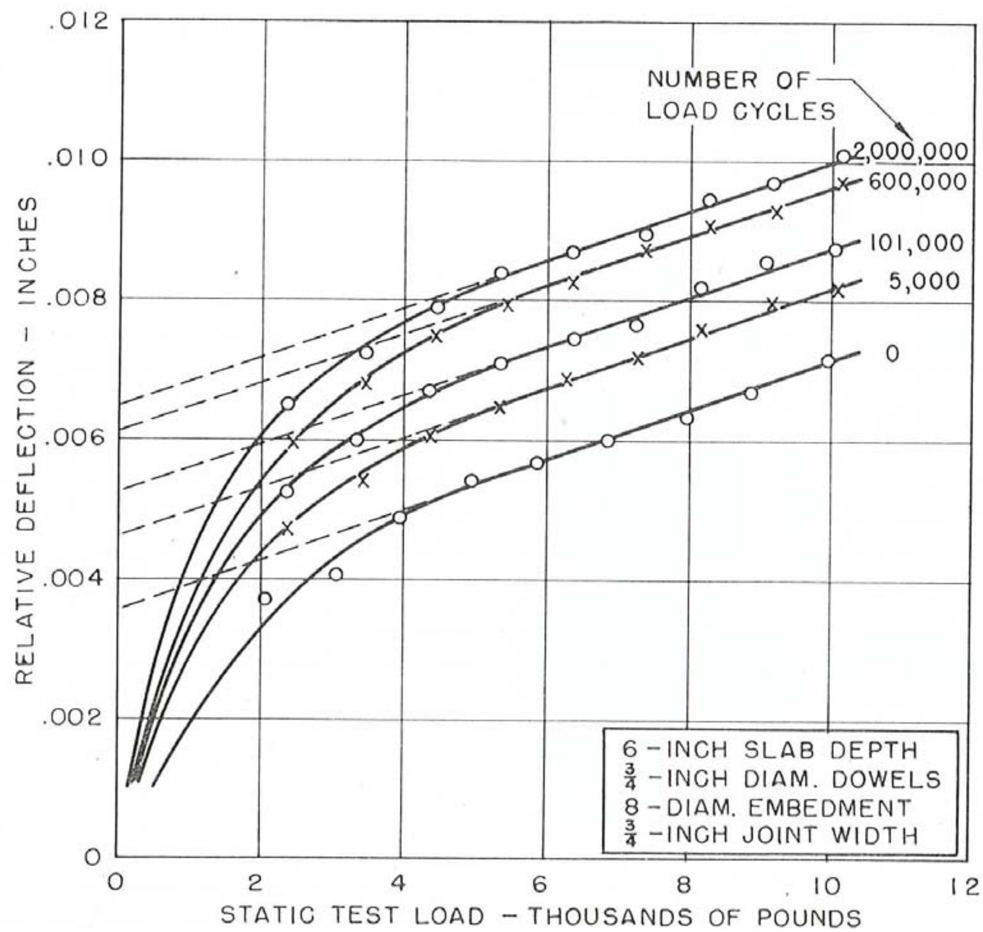

FIGURE 4.3. TELLER & CASHELL (1958) DEFINITION OF DOWEL LOOSENESS.

It is difficult to imagine how those plots would extrapolate out to slab thickness values of 18 to 24 inches. With a stiffer subgrade, there is less overall deflection and therefore less ability to mobilize shear stiffness across a joint, especially if looseness is present. With increasing slab thickness, flexural rigidity increases as a function of slab thickness cubed, while joint shear area is only increasing linearly with increasing slab thickness, indicating joints should be less efficient as thickness increases. In general, these tests showed that once a doweled joint experiences a few thousand relatively heavy loads, the resulting permanent deformation of the dowel concrete interaction zone near the edge of the joint face can cause a significant loss of ability to transfer future loads, especially loads that are significantly smaller than these initial heavy loads that caused the dowel socket damage. For a given repeated load magnitude, the socket damage or looseness shows up relatively quickly and appears to reach a somewhat stable damaged condition for that load. If the load is then increased, damage rate will again be high initially and then somewhat stabilize to a new increased socket damage level.

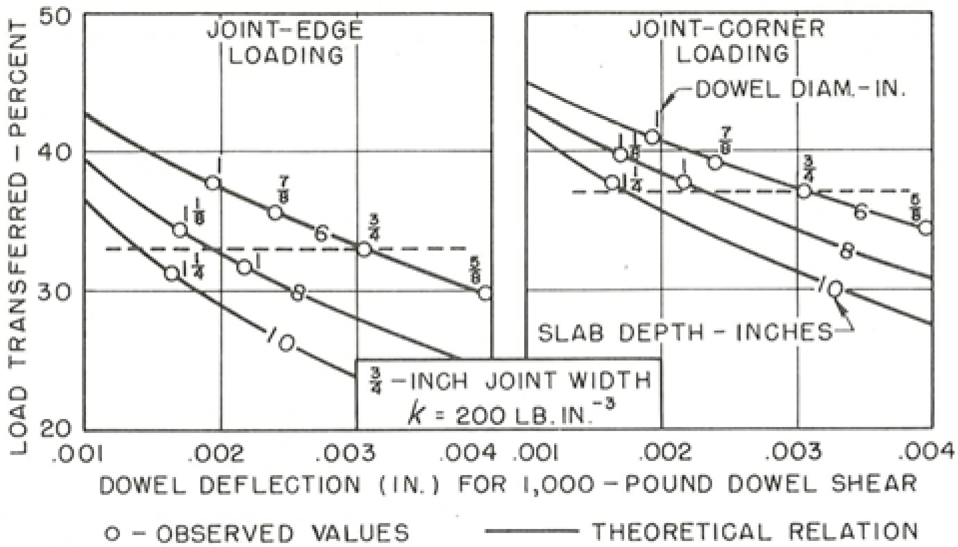

FIGURE 4.4. EFFECT OF DOWEL DEFLECTION AND SLAB DEPTH ON LOAD TRANSFER FOR A SINGLE DOWEL (TELLER AND CASHELL 1958).

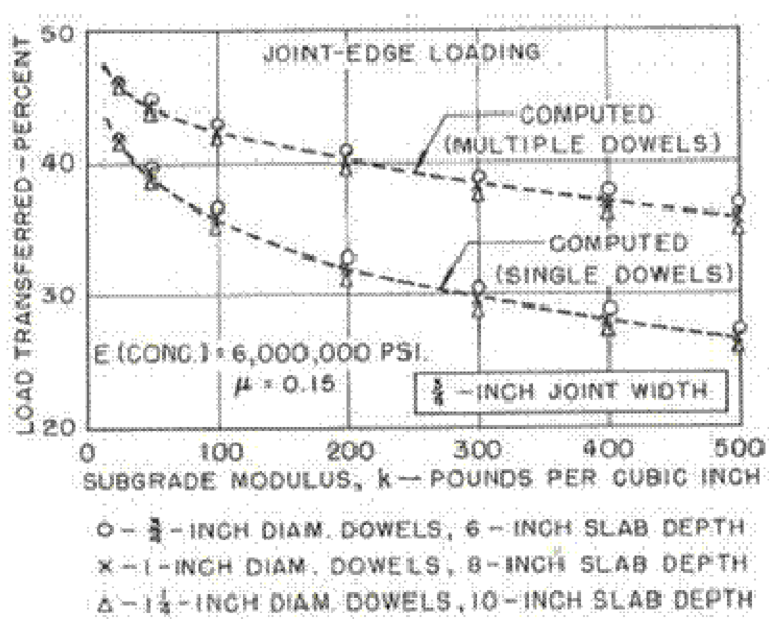

FIGURE 4.5. SUBGRADE EFFECTS ON LOAD TRANSFER, TELLER AND CASHELL (1958).

Snyder (1985) studied dowel looseness further and developed a general function for loss of load transfer as a function of dowel looseness magnitude as shown in figure 4.6.

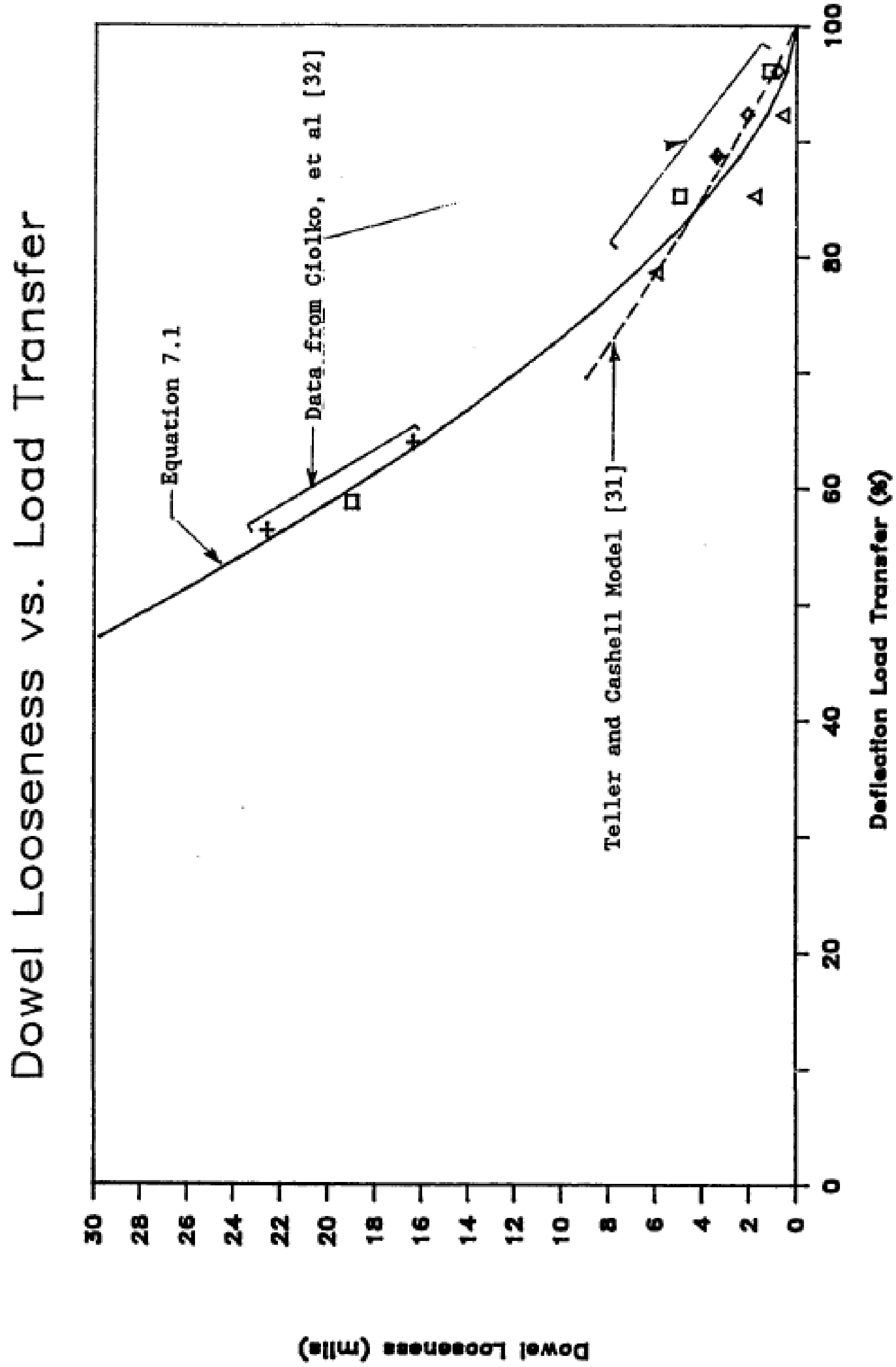

FIGURE 4.6. DOWEL LOOSENESS TRENDS FROM SNYDER (1985).

4.1.2 Recent Studies (Post 1990)

Ioannides and Hammons (1996) presented the Skarlatos closed form solution to the load transfer equation based on the Westergaard equations. Figure 4.7 shows how the Skarlatos trend falls on the dimensionless stiffness trends from Ioannides and Korovesis (1990). Figure 4.8 shows how the Skarlatos trend compares with the FEM trends. Data from Teller and Sutherland (1936) is also shown in this plot. At a given LTE_δ value, the FEM model was predicting significantly lower LTE_σ than that predicted by Westergaard/Skarlatos infinite slab trends. This general trend for finite-slab FEM models compared to infinite-slab Skarlatos/Westergaard equations has been encountered by several researchers.

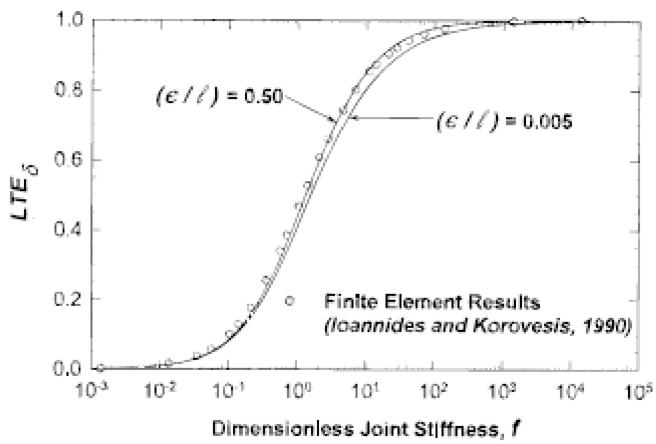

FIGURE 4.7. VARIATION OF LOAD TRANSFER EFFICIENCY WITH RESPECT TO DEFLECTION WITH DIMENSIONLESS JOINT STIFFNESS AND DIMENSIONLESS LOAD SIZE RATIO, IOANNIDES AND HAMMONS (1996).

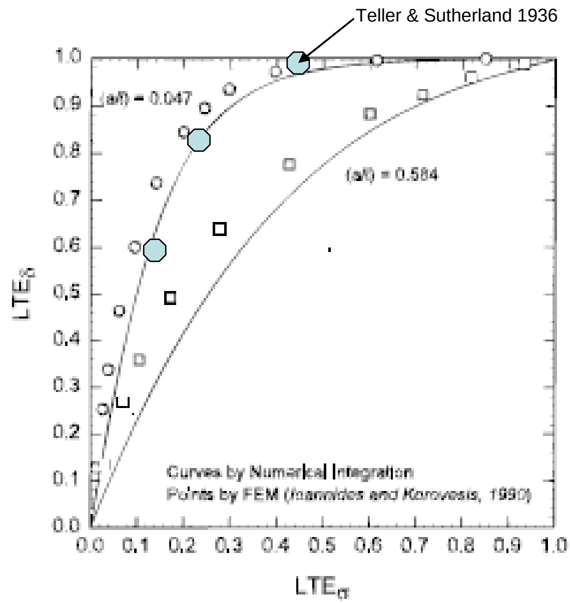

FIGURE 4.8. COMPARISON OF SKARLATOS TREND WITH FEM TRENDS, IOANNIDES AND HAMMONS (1996).

4.2 FINITE ELEMENT STUDIES OF JOINTS

Guo et al. (1993) attempted to simulate the behavior observed by Teller and Cashell (1958) using FE modeling. Figure 4.9 shows the non-linear joint stiffness model used by them, where the effective joint stiffness is a function of the load versus displacement function for the joint. Figure 4.10 shows the results for the FE analysis of joint loading and load transfer for dowel looseness magnitudes ranging from zero to 30 mils. Of key note is that a small dowel looseness value of 6 mils was predicted to result in LTE$_\delta$ dropping from near 90 percent at zero looseness to about 50 percent at 6 mils looseness. Figure 4.11 shows the total shear forces in the dowels as a function of the magnitude of looseness and how the dowels along the slab edge mobilize shear. As looseness increases, less dowels are mobilized. With no looseness, the total load is transferred close to equally to both slabs and the foundation layers beneath have low shear stress at the joint. If large looseness develops, all load is transmitted to the loaded slab and the foundation layer shear stresses become higher at the joint.

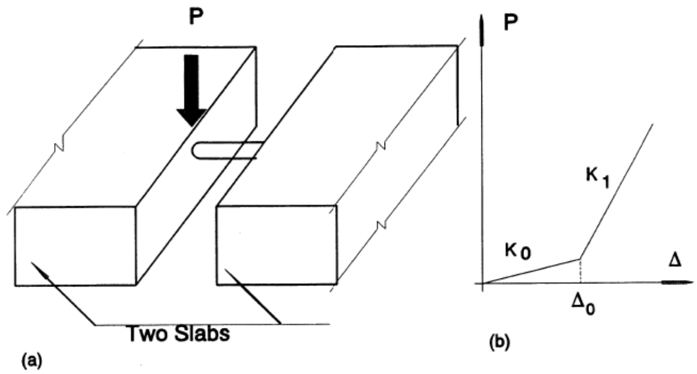

(a) Bilinear structural stiffness model for a single loose dowel.

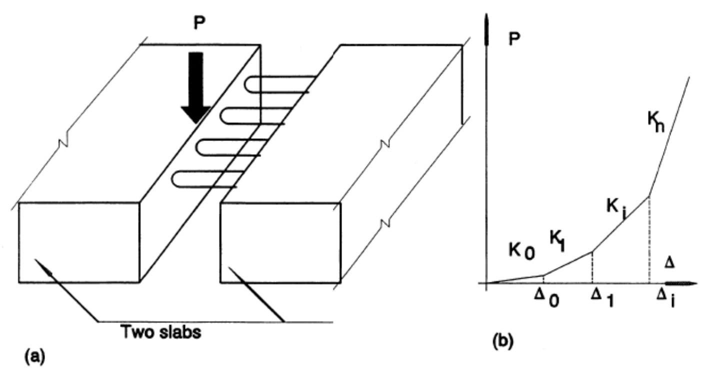

(b) Multilinear structural stiffness model for multiple loose dowels.

FIGURE 4.9. MODELING OF DOWEL LOOSENESS IN THE FE ENVIRONMENT AS DESCRIBED BY GUO ET AL. (1993).

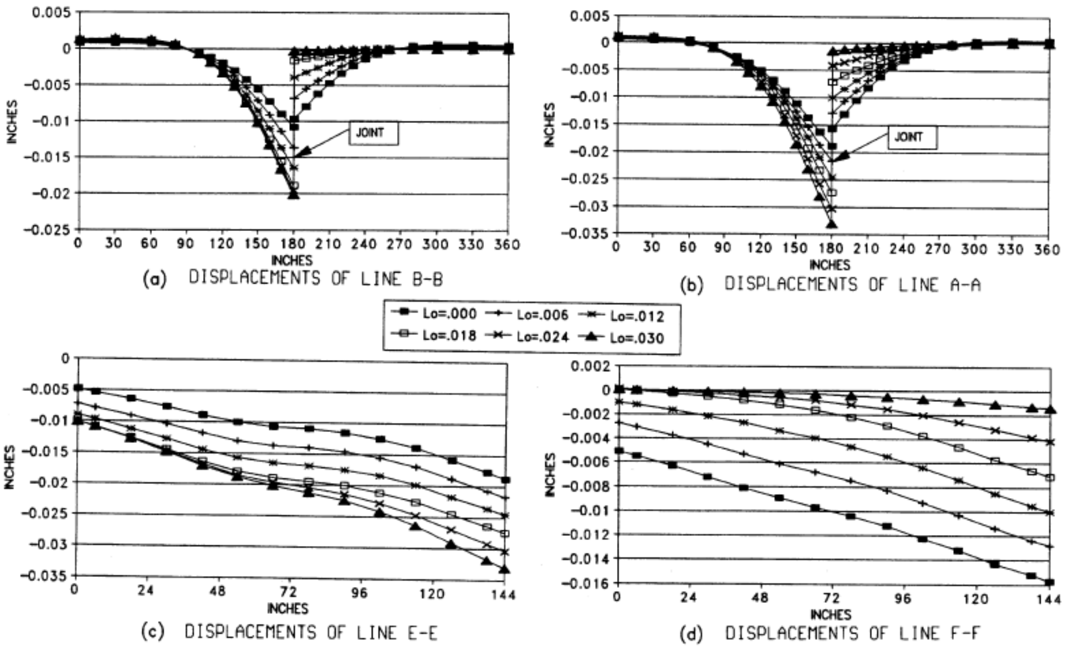

Figure 8. Displacement distributions (load case two).

FIGURE 4.10. RESULTS FROM FE ANALYSIS USING THE VARIABLE JOINT STIFFNESS FUNCTION REPRESENTING DOWEL LOOSENESS, GUO ET AL. (1993).

Nishizawa et al. (1989) presented a FE joint model that was designed to account for both shear stiffness and rotational stiffness from dowel bars. In general, the flexural rigidity of the dowel assemblies is almost negligible with respect to the magnitude of the flexural rigidity of theslab. It has been shown by several researchers that for the most part the moment resistance contribution offered by dowels is small and does not affect load transfer much compared to assuming that none is present. Figure 4.12 shows their results for deflection load transfer efficiency versus joint stiffness. Figure 4.13 shows both LTE_δ and LTE_σ trends observed for doweled and aggregate interlock joints. A key observation is the predicted lower LTE_σ for thicker slabs

Nishizawa et al. (2001) presented results from further studies on dowel bar modeling in the FE environment. The following model form was used in that study:

$$\begin{Bmatrix} \Delta v' \\ \Delta \theta_{x'} \end{Bmatrix} = a_0 \begin{bmatrix} a_1 & -a_2 \\ -a_2 & a_3 \end{bmatrix} \cdot \begin{Bmatrix} \Delta f_{y'} \\ \Delta m_{x'} \end{Bmatrix}$$

in y'-z' plane, where

$$a_0 = \frac{2\beta^2}{k(S^2 - s^2)},\ a_1 = \frac{1}{\beta}(SC - sc),\ a_2 = (S^2 + s^2),\ a_3 = 2\beta(SC + sc),\ \beta = \sqrt[4]{\frac{K_c\phi}{4E_d I_d}}$$

K_c = interaction spring coefficient of surrounding concrete,
ϕ = diameter of dowel bar,
$E_d I_d$ = bending rigidity of dowel bar,
$s = \sin(\beta L)$, $c = \cos(\beta L)$, $S = \sinh(\beta L)$, $C = \cosh(\beta L)$,
L = embedded length of dowel bar,
$f_{y'}$ = shear force in y' direction, and
$m_{x'}$ = moment for x' axis.

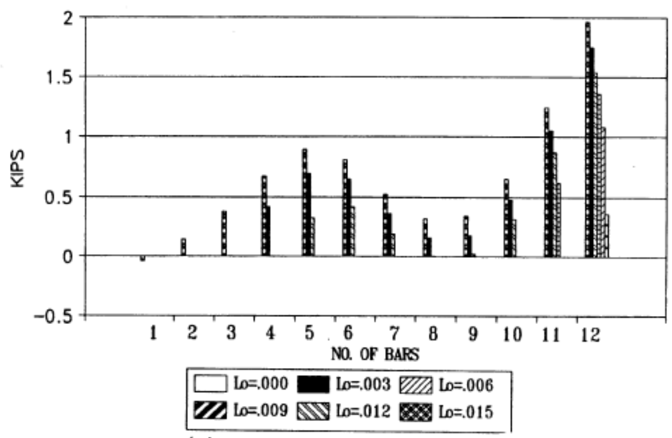

(a) SHEAR FORCES OF DOWEL BARS

5.4 mm
4.4 kN

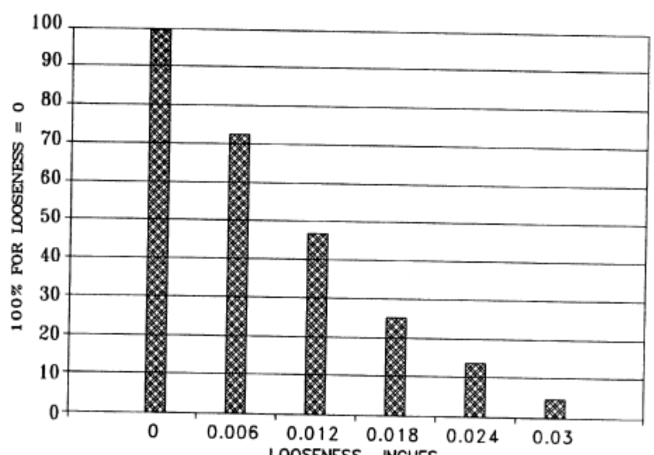

(b) TOTAL SHEAR FORCES TRANSMITTED BY BARS

FIGURE 4.11. SHEAR TRANSFER THROUGH DOWEL BARS AS A FUNCTION OF DOWEL LOOSENESS (GUO ET AL. 1993)

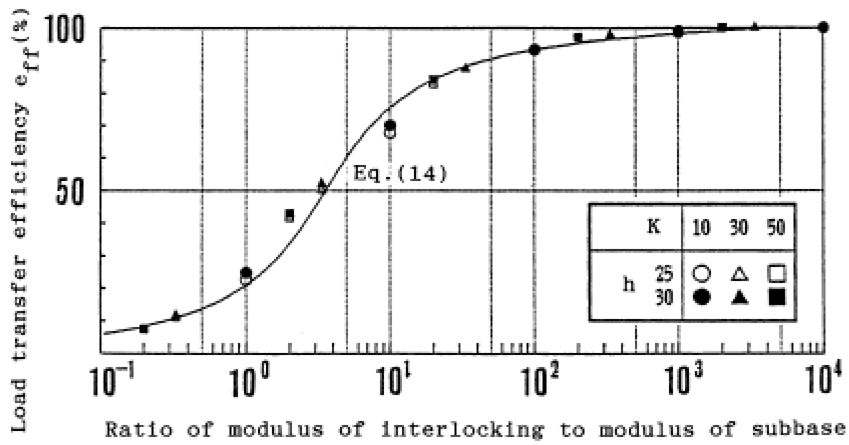

Note: h=slab thickness(cm),
K=modulus of subbase reaction(kg/cm^3),
$1kg/cm^2$=0.098MPa, $1kg/cm^3$=9.8MPa/m

FIGURE 4.12. DEFLECTION LOAD TRANSFER VS. JOINT STIFFNESS (NISHIZAWA ET AL. 1989).

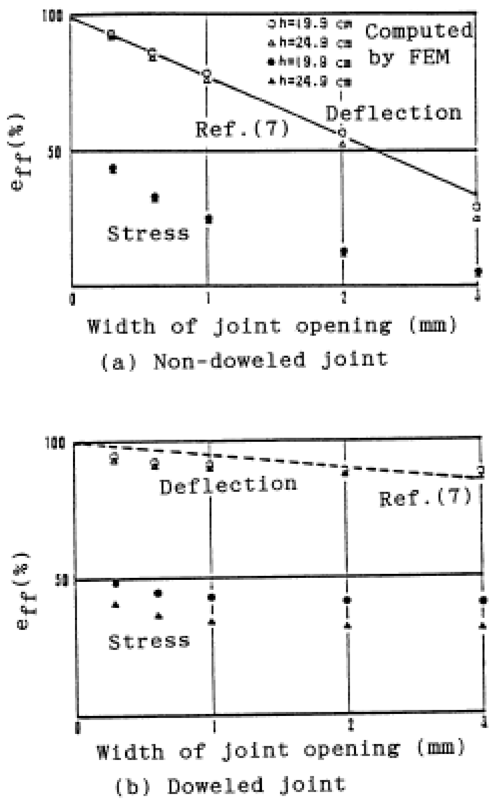

Note: $e_{ff}=s_2/s_1$x100,
s_1=maximum value in loaded slab
s_2=maximum value in unloaded slab
h=thickness of concrete slab

FIGURE 4.13. RELATIONSHIP BETWEEN JOINT EFFICIENCY AND WIDTH OF JOINT OPENING (NISHIZAWA ET AL. 1989).

Kazuyuki et al. (1993) showed results from an FE model that was calibrated to FWD joint testing data. They modeled the joints as a simple constant stiffness spring. Figure 4.14 shows how the joint stiffness affected slab bending stress and also the stress applied to the top of the subbase. Stress applied to the subbase nearly tripled as joint stiffness varied from very high to very low.

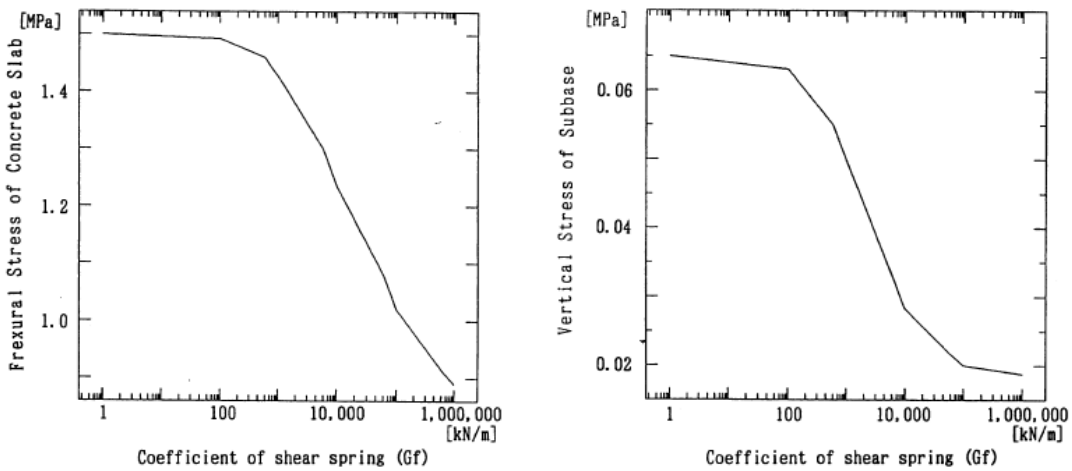

FIGURE 4.14. AFFECT OF JOINT STIFFNESS ON BENDING STRESS (LEFT) AND STRESS APPLIED TO THE TOP OF THE SUBBASE (RIGHT) (KAZUYUKI ET AL. 1993).

Figure 4.15 shows FE model results from research conducted in South Africa by Prozzi et al. (1993) that show how LTE_{δ} and subgrade stiffness affect apparent maximum tensile stress in the test slabs.

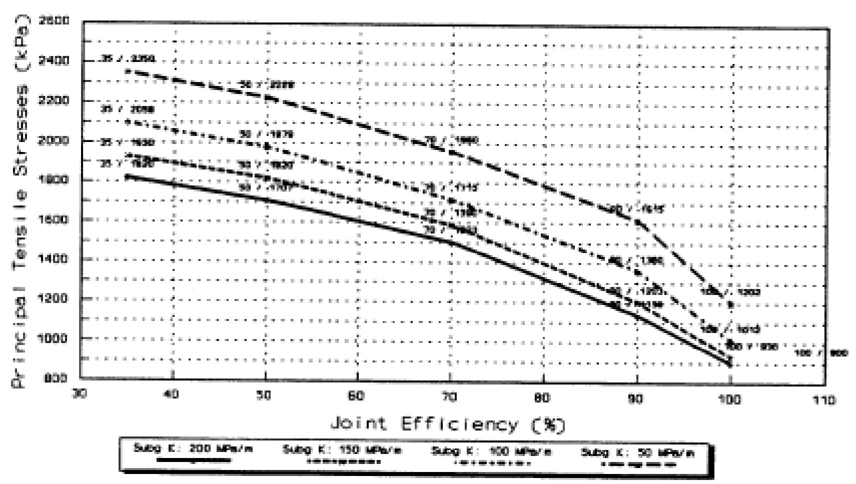

FIGURE 4.15. FE MODEL RESULTS SHOWING HOW LTE_{δ} AND SUBGRADE STIFFNESS AFFECT APPARENT MAXIMUM TENSILE STRESS IN THE TEST SLABS (PROZZI ET AL 1993).

4.3. AGGREGATE INTERLOCK JOINT ANALYSIS

The primary factor controlling the behavior of aggregate interlock joints is the joint opening. Some aggregate type effects can also influence joint performance, where harder and larger aggregates and tougher PCC mixtures require greater joint openings to cause full loss of load transfer. Jensen and Hansen (2001) performed laboratory studies of joint width and aggregate type effects on load transfer. Figure 4.16 shows observed joint opening and aggregate type effects, and figure 4.17 shows apparent joint looseness, similar to dowel looseness, as a function of joint opening for aggregate interlock joints. The slack index shown is equal to the deflection difference as defined by Teller and Cashell (1958). Larger top-size aggregates appear to significantly affect aggregate interlock joint looseness for a given joint opening magnitude.

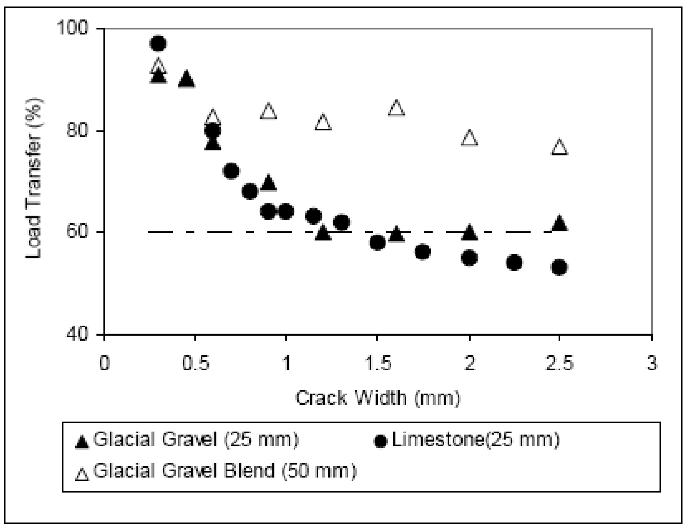

FIGURE 4.16. JOINT OPENING AND AGGREGATE TYPE EFFECTS OBSERVED BY JENSEN AND HANSEN (2001).

4.4 OVERSEAS STUDIES (Non FEM)

4.4.1 Chinese Research

Researchers in China have studied the load transfer problem for airfield pavements and developed a traditional style nomograph for pavement thickness design incorporating the LTE_{δ} value as shown in figure 4.18 (Jun et al. 1997). According to the nomograph in figure 4.18, the design thickness difference for 70% versus 85% LTE_{δ} (where *E* in figure 4.18 represents LTE_{δ}) is about 2.5 cm (about 1 inch) for the example design shown (Jun et sl. 1997). If a low LTE_{δ} of about 20% is assumed, versus the 70% shown, a thickness of about 39 cm would be required, which is an extra 8 cm (3.15 inches).

Researchers in China also evaluated the loss of load transfer over time (Jun et al. 1997). Figures 4.19 and 4.20 show their general results for loss of LTE_{δ} (shown as E in the figures) for different joint types and joint widths. These trends were observed from smaller scale test sections.

The method reported by Jun et al. (1997) shows the design thickness to be relatively sensitive to assumed load transfer. Fatigue models commonly used to determine the number of allowable load cycles, or coverages, are very sensitive to changes in stress, and would imply it is important to accurately account for load transfer when estimating the design stress level.

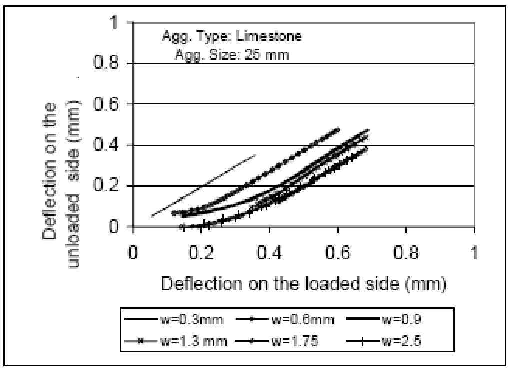

w (mm)	slack (mm)	slope (-)
0.30	0.002	0.99
0.60	0.133	1.00
0.90	0.237	1.00
1.30	0.278	1.00
1.75	0.292	0.95
2.50	0.291	0.96

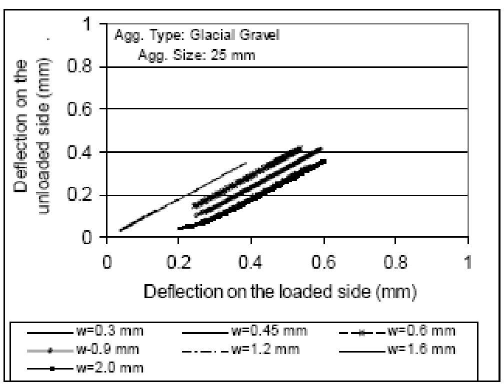

w (mm)	slack (mm)	slope (-)
0.30	0.002	0.92
0.45	0.005	0.92
0.60	0.088	0.93
0.90	0.151	0.93
1.20	0.187	0.90
1.60	0.187	0.90
2.00	0.201	0.90
2.50	0.200	0.90

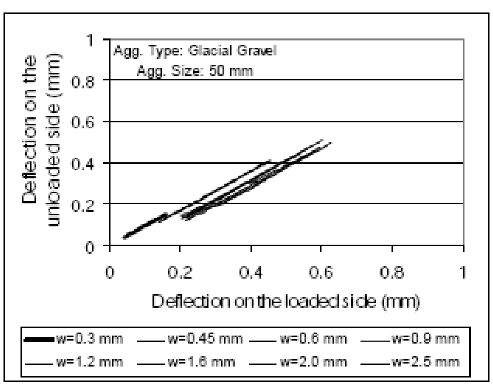

w(mm)	slack (mm)	slope (-)
0.30	0.002	0.94
0.45	0.023	0.95
0.60	0.069	0.95
0.90	0.069	0.95
1.20	0.089	0.93
1.60	0.069	0.95
2.00	0.080	0.90
2.50	0.081	0.89

FIGURE 4.17. AGGREGATE INTERLOCK JOINT LOOSENESS MEASURED BY JENSEN AND HANSEN (2001).

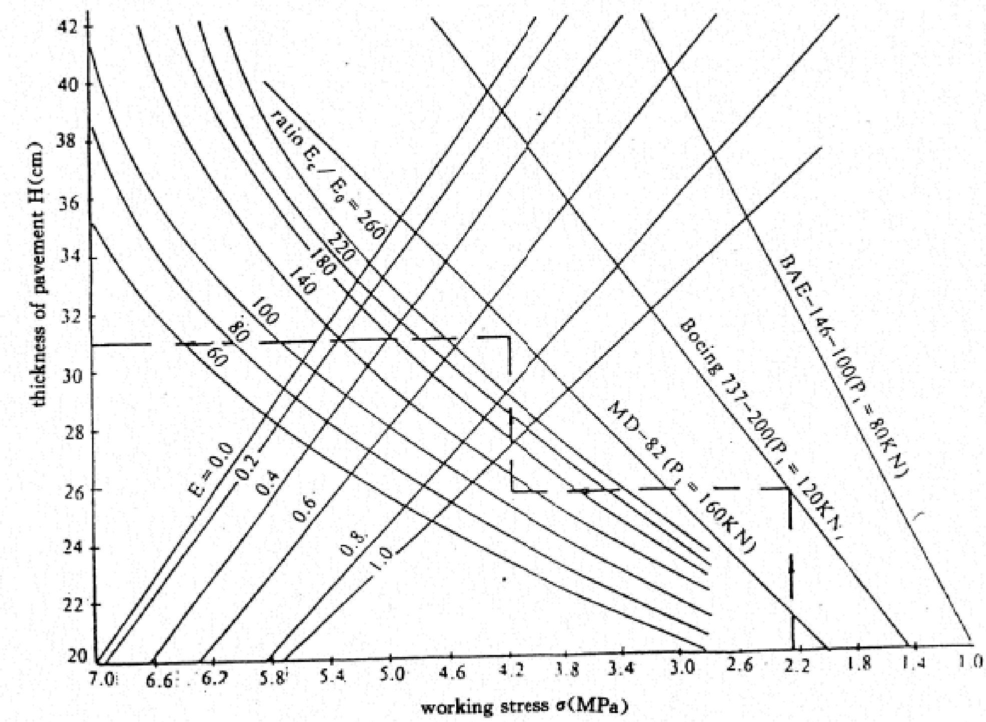

FIGURE 4.18. THICKNESS DESIGN NOMOGRAPH FROM RESEARCH IN CHINA, INCLUDING LTE$_\delta$ (SHOWN AS E IN THE FIGURE) AS A DESIGN PARAMETER, JUN ET AL. (1997).

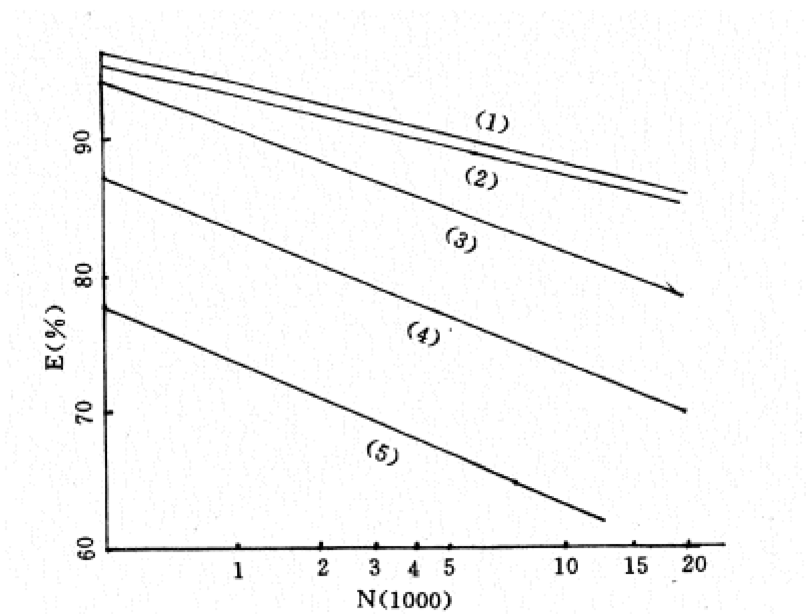

notes:
N——repetitive numbers of wheel load
E——coefficient of load—transfer of joint
(1)Engaged; (2)Thin key; (3)Dowelled;
(4)Thick key; (5)Dummy joint.

FIGURE 4.19. LOSS OF LTE_{δ} (SHOWN AS E IN THE FIGURE) OBSERVED FOR DIFFERENT JOINT TYPES (JUN ET AL. 1997).

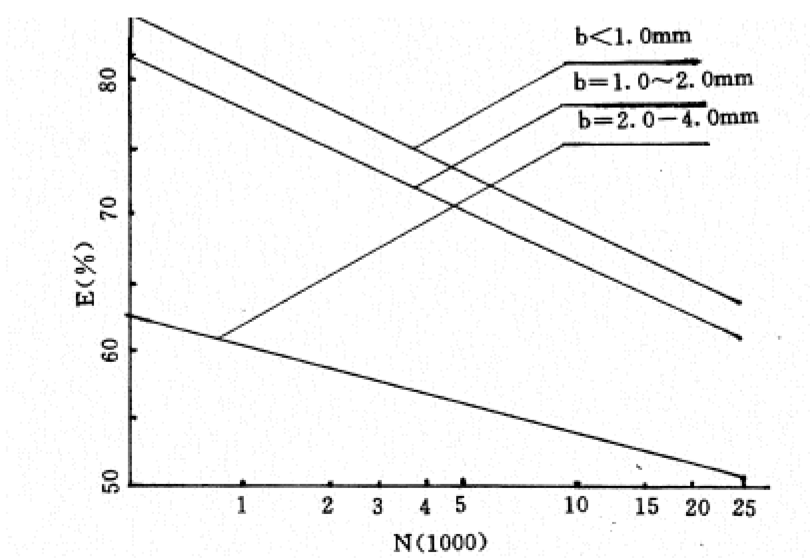

Note b---width of dummy joint (mm)

FIGURE 4.20. LOSS OF LTE_{δ} (SHOWN AS E IN THE FIGURE) TRENDS OBSERVED FOR DIFFERENT JOINT WIDTHS FOR DUMMY JOINTS (JUN ET AL. 1997).

4.4.2 South African Research

Strauss et al. (2005) provided an update on joint modeling in South Africa. A study was performed where test slabs were built and loaded to failure using a heavy vehicle simulator. FWD testing of in service highways was used to supplement the test site data. This team developed a modified version of the RILEM concrete shrinkage model to estimate joint opening development over time, and used the field data to calibrate the models to match observations. The results of their study are included in the South African mechanistic empirical pavement design procedure called *cncPAVE*. This joint opening and load transfer model is perhaps the most sophisticated that has been developed. The model is however calibrated based on thinner highway slabs. The equations shown below are used in *cncPAVE*.

$$\Delta y = 0.118(1 - e^{-((v + 11.4/agg)\Delta x)^{1.881}})$$

where Δy = relative vertical movement at joint/crack
v = factor influenced by speed of loading
Δx = crack/joint width
agg = nominal size of the 20% biggest particles in the concrete mix

The following equation shows movement at a joint or crack in which steel bars are installed that was developed by Yoder and Witczak (1975).

$$\Delta y = P\,(2 + \beta x) / (4\beta^3 EI)$$

where $\beta = [Kb / 4EI]^{0.25}$
K = Winkler stiffness of the concrete around the steel bar
b = steel bar diameter
E = modulus of elasticity of the steel bar
I = moment of inertia of the steel bar
P = load on the steel bar
x = crack width

The following equations are used to calculate the shrinkage strain in concrete (RILEM 1995):

$$\text{Strain with time} = S(t)\ k_h\ \varepsilon$$

where: $S(t) = \tanh\ \{(t\text{-}t_0)/4.9D^2\}^{\ 0.5}$

$\varepsilon = \alpha_1\ \alpha_2\ [0.019\ w^{2.1}/f^{\ 0.28} + 270]$

$k_h = 1\text{-}\ h_u^{\ 3}$

$k_h = 1\text{-}\ h_u^{\ 3}$
t = age of the concrete
t_0 = age when drying starts
D = effective cross section thickness = 2 v/s (v/s is the volume to surface ratio)
α_1 = cement type
α_2 = factor for curing
w = water content of the concrete
f = cylinder compressive strength of the concrete
h_u = factor for relative humidity (where 100% humidity = factor of

$$\text{Strain} = C_1\ \alpha_1\ \alpha_2\ \alpha_3/h\ [0.019\ w^{2.1}/f^{\ 0.28}+270]+(T_0 - T_t).\eta$$

where α_3 = aggregate type
C_1 = constant
h = slab thickness

T_0 and T_t = temperature at time of paving and present temperature respectively

η = thermal coefficient of the concrete

Shrinkage strain over the long term (ε_t) is computed using the following equation developed by Troxell (1958):

$$\varepsilon_t = C_2\,[900\text{-}t]\,[t\text{-}0.08]^{0.18}\,[1\text{-}h_u]$$

where: h_u = relative humidity (value of 1 = 100% humidity)
t = time (years)
C_2 = constant

Crack width Δx is calculated using the following equation:

$$\Delta x = [C_3/h\{\alpha_1\,\alpha_2\,\alpha_3\,(0.019w^{2.1}/f^{0.28}+270) + (900\text{-}t)\,(t\text{-}0.08)^{0.18}\}(1\text{-}h_u) + (T_0 - T_t)\,\eta].L$$

The following equations were generated from regression techniques using 1475 data sets obtained from HVS testing:

$$\Delta y = 8.37\,(\Delta x_m^{\ 1.5} / Agg) + 0.030.n.\ ACV - 0.254 \qquad (10)$$

$$\Delta y = 2.22\,(\Delta x_c^{\ 1.5} / Agg) + 0.030.n.\ ACV - 0.040 \qquad (11)$$

where: Δy = relative vertical movement (mm)

Δx_m = crack width using actually measured values in equation 10 (mm)

Δx_c = calculated crack width using equation 9 to calculate crack width (mm)

Agg = nominal size of the 20% biggest particles in the concrete mix (mm)

n = number of load applications actually applied (million E 80's)

$$\Delta y = 8.37\,(\Delta x_m^{\ 1.5} / Agg) + 0.030.n.\ ACV - 0.254$$

$$\Delta y = 2.22\,(\Delta x_c^{\ 1.5} / Agg) + 0.030.n.\ ACV - 0.040$$

where: Δy = relative vertical movement (mm)

Δx_m = crack width using actually measured values in equation 10 (mm)

Δx_c = calculated crack width using equation 9 to calculate crack width (mm)

Agg = nominal size of the 20% biggest particles in the concrete mix (mm)

n = number of load applications actually applied (million E 80's)

Strauss et al. (2005) performed a sensitivity study of the joint model. Figure 4.21 shows how the crack width is predicted to grow over time in two different climates (different relative humidity). Figure 4.22 shows the design relative movement (deflection difference) at the joint for three cases, showing the effect of subgrade drag, traffic rate, and aggregate durability (indicated as ACV) on the relative movement at joints for designs. Figure 4.23 shows how the dowel diameter and PCC stiffness affect the design relative joint movement in that model. In *cncPAVE*, the LTE is varied over the life of the pavement as a function of many parameters including, climate, traffic, materials, and age.

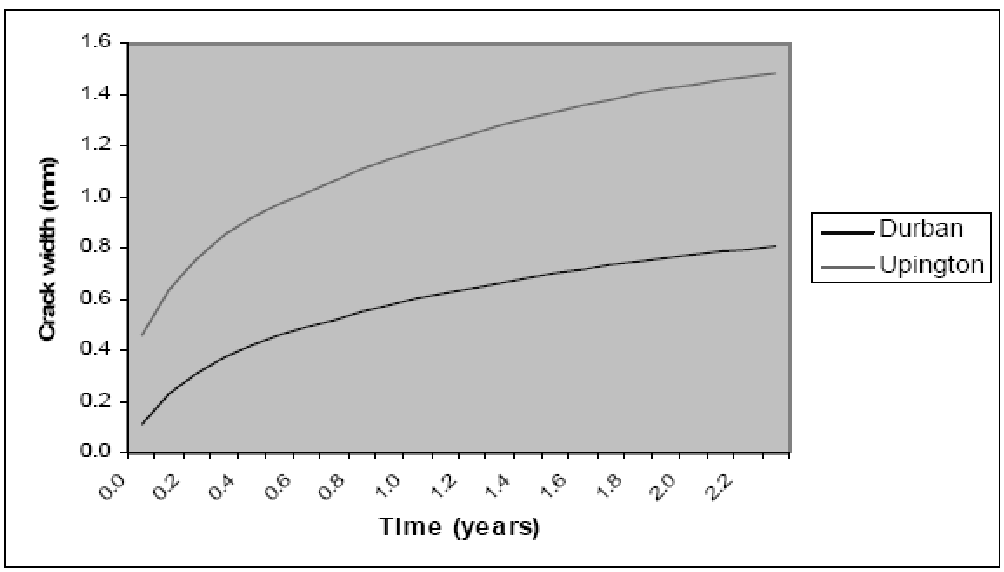

FIGURE 4.21. CRACK WIDTH AS A FUNCTION OF TIME FOR DIFFERENT CLIMATES (STRAUSS ET AL. 2005).

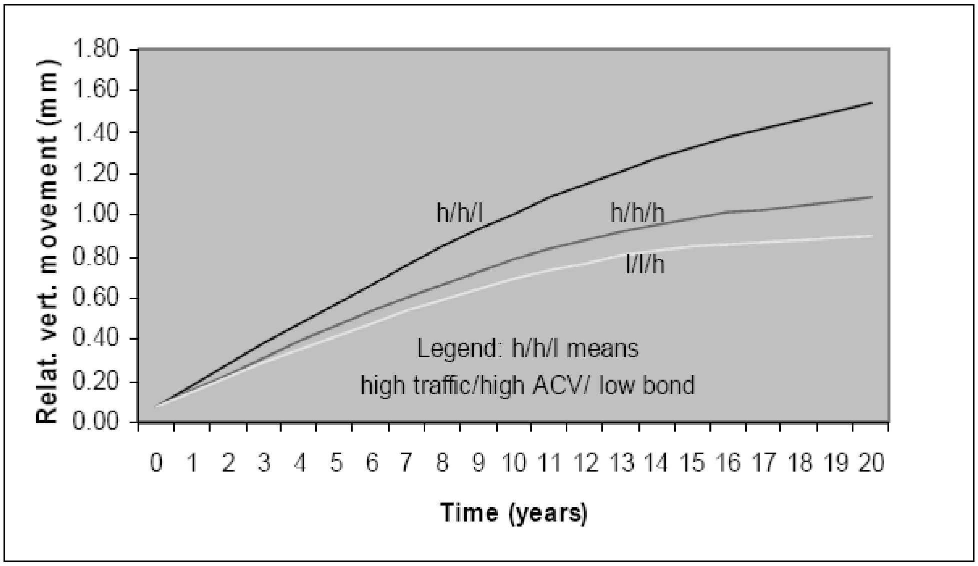

FIGURE 4.22. CALCULATED RELATIVE VERTICAL MOVEMENT AS A FUNCTION OF TIME, TRAFFIC LOADING, ACV OF AGGREGATE, AND BOND BETWEEN SUBBASE AND SLAB IN A DRY HOT CLIMATE (STRAUSS ET AL, 2005).

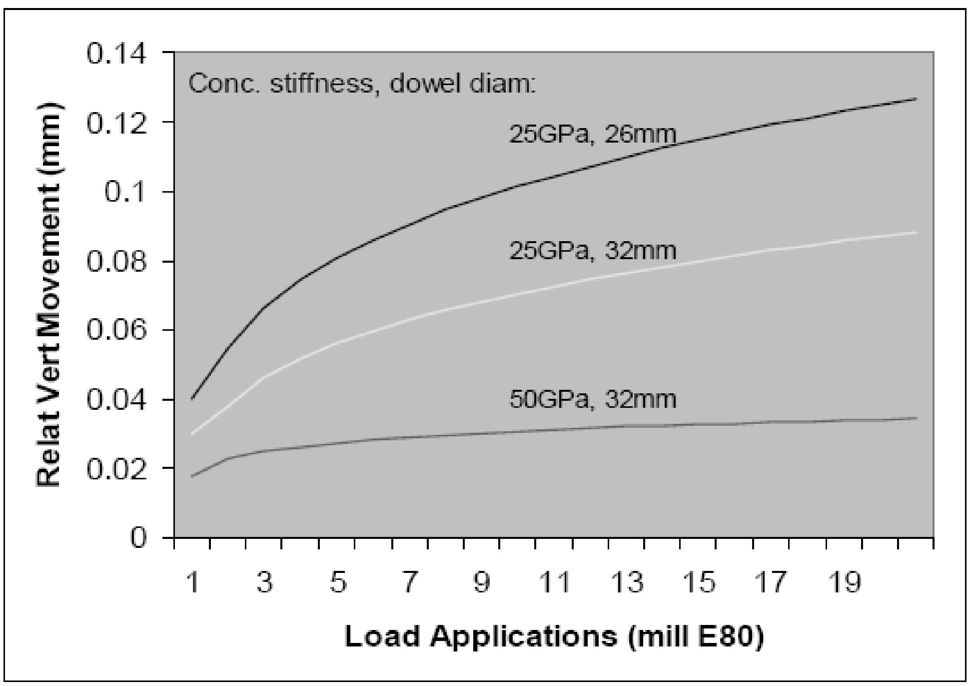

FIGURE 4.23. RELATIVE MOVEMENT AT THE JOINT OF A DOWELED PAVEMENT (STRAUSS ET AL. 2005).

4.5. SUMMARY

In general, the past analytical studies of joints have shown that the moment contribution provided by dowel bars placed at the mid-depth in the slabs is very small and has an almost negligible effect on the relation between LTE_{σ} and LTE_{δ} for jointed PCC pavements. The enhancement provided by dowels is nearly a pure vertical shear load transfer mechanism. Past studies that have compared jointed slab FE models to the semi-infinite slab Westergaard type models have observed significant differences in the relationship between LTE_{σ} and LTE_{δ}. Crack opening size is the primary factor causing changes in load transfer efficiency for aggregate interlock type joints. Dowels are effective in keeping load transfer high when joint openings become large. Tie bars are effective in keeping joints closed and retaining high load transfer capability.

CHAPTER 5: FIELD EVALUATION OF JOINT BEHAVIOR

5.1. OVERVIEW

This chapter describes field studies that have been conducted to evaluate joint behavior. Results from field studies that were performed to evaluate the effect of climatic factors on joint behavior (e.g., temperature effects on joint opening, variation of load transfer with temperature and season) are described in Chapter 6.

5.2. WATERWAYS EXPERIMENT STATION INSTRUMENTED TESTING

The WES developed a 16-kip vibratory test device that is shown conceptually in figure 5.1 in the late 1970's (Bush III and Hall, 1981). Figure 5.2 shows a deflection plot for that device from a 15 Hz test. Data from these vibratory devices is more difficult to analyze, as the system damping effect and associated dynamic magnification coefficients versus frequency of loading effects cannot be easily accounted for. These vibratory devices are capable of performing frequency sweep testing and defining the full dynamic response characteristics of a pavement system.

This research team used the 16-kip vibrator to evaluate load transfer efficiency at a test site that was instrumented for bending strain. Figure 5.3 shows the location of the load plate and deflection transducers for the joint tests. Figure 5.4 shows the results from testing. Based on their strain gage measurements, the overall average LT was above 25%, but LT values less than 25% were observed for LTE_{δ} values greater than 85%.

These vibratory type devices are no longer in use and have been replaced by the FWD.

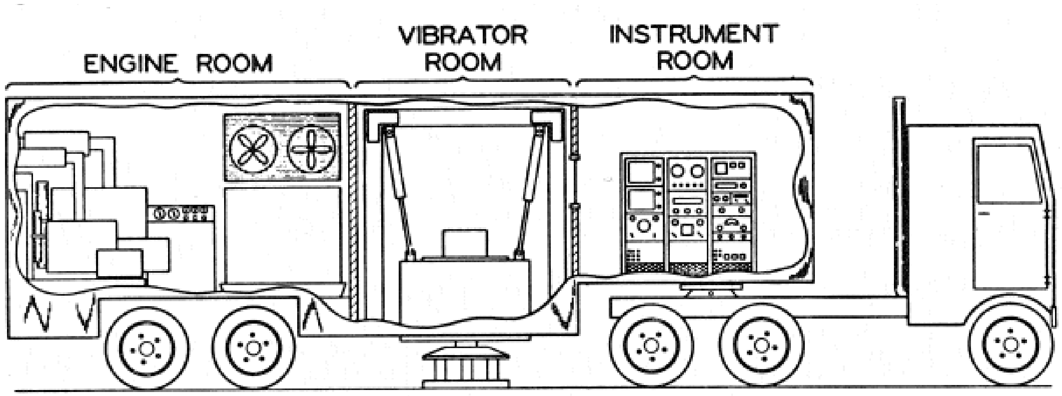

FIGURE 5.1. WES NDT DEVICE FOR PAVEMENT TESTING USING A VIBRATORY LOAD (BUSH III AND HALL 1981).

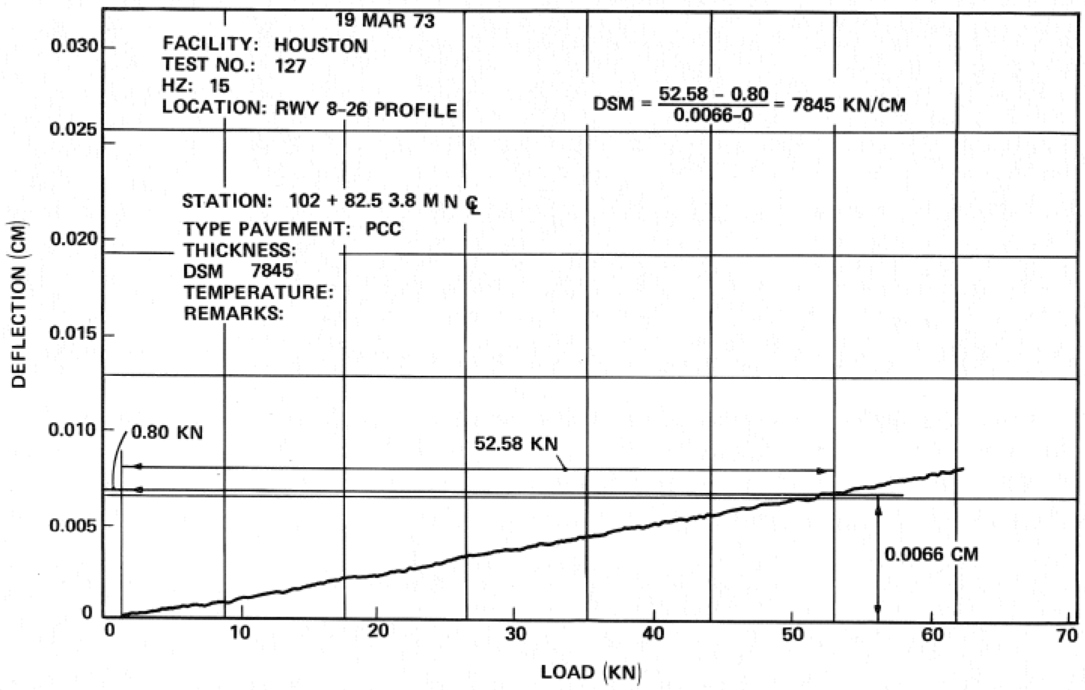

Note: 1 cm = 0.3937 in.; 1 kN = 0.225 kip.

FIGURE 5.2. TYPICAL DEFLECTION DATA FROM THE WES 16 KIP VIBRATORY DEVICE (BUSH III AND HALL 1981).

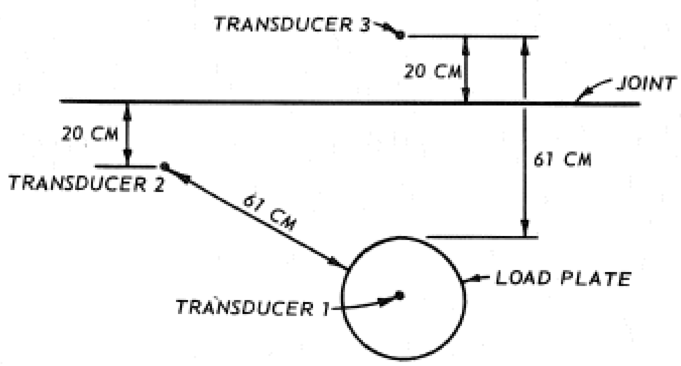

FIGURE 5.3. LOCATION OF LOAD PLATE AND TRANSDUCERS FOR JOINT DEFLECTION TESTS.

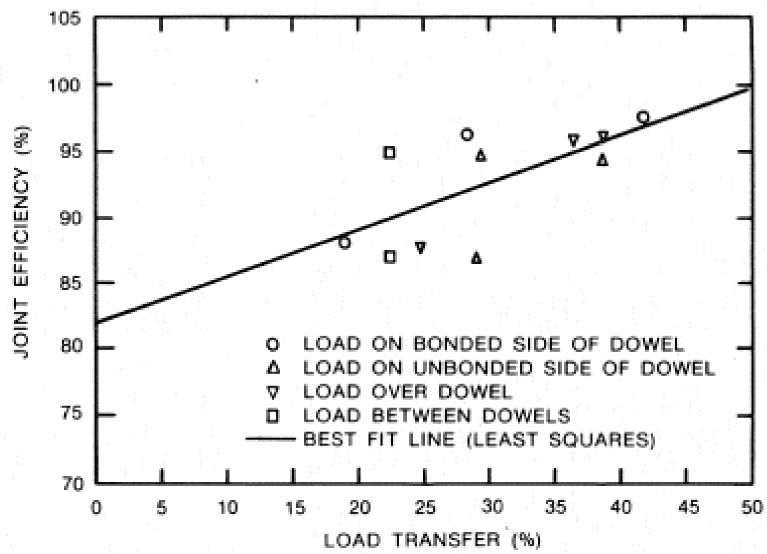

FIGURE 5.4. COMPARISON OF JOINT LTE_δ FROM THE WES 16-KIP VIBRATOR TO STRAIN GAGE BASED LT MEASUREMENTS FOR A DOWELED JOINT (BUSH III AND HALL 1981).

5.3. NAPTF INSTRUMENTED TESTING

Guo (2008) summarized findings from joint studies conducted at NAPTF. In their work, they defined LTE(S) as a strain-based estimate of the load transfer value, defined as the unloaded slab strain divided by the sum of the loaded and unloaded strains. (This parameter is same as LT described in Chapter 1.) Guo (2008) identified that as the radius of relative stiffness increases, for a given value of LT the value of LTE_δ drops as shown in figure 5.5.

Figure 5.6 shows a test slab configuration and the loading that was used by Guo (2008). His team analyzed strain histories from embedded strain gages at NAPTF. They encountered a typical challenge associated with strain gages, which is permanent locked-in strains (offsets) before or after loads, causing offsets in response signals as shown in figure 5.7 and 5.8. The LT calculation points for comparing adjacent strain sensors are shown as vertical lines in the plots. Table 5.1 shows the peak strains and calculation of LTE (S) at two joints, while table 5.2 shows the average and standard deviation values. (In these tables ε_U is the strain on the unloaded slab and ε_L is the strain on the loaded slab.) Based on their testing, LT(S) average values of 32 to 39 percent were achieved for joints with LTE_δ between about 82 and 88 percent. However it should be noted that low LT(S) values of 22 to 23 percent were observed when all four tires were on one side of a joint at two locations (i.e., positions AI and BIV).

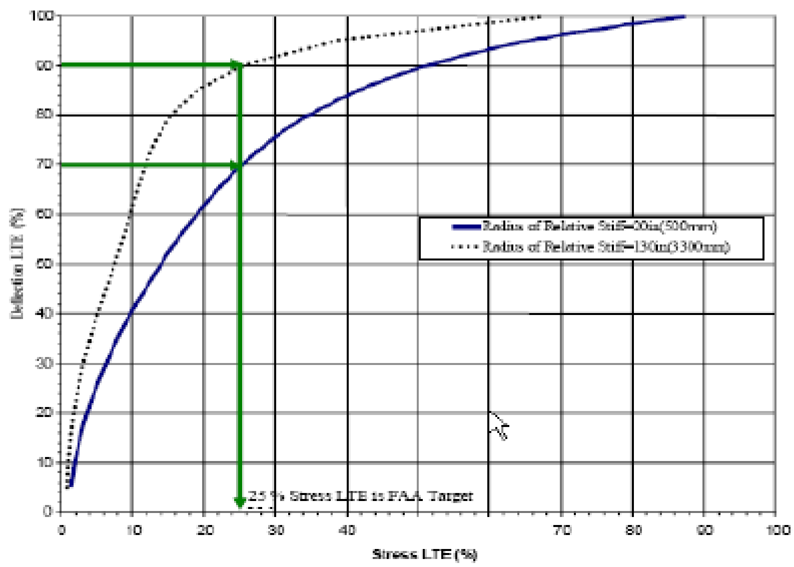

FIGURE 5.5. LTE$_\delta$ VERSUS LT TRENDS OBSERVED BY GUO (2008) FOR A 12-INCH DIAMETER LOAD PLATE.

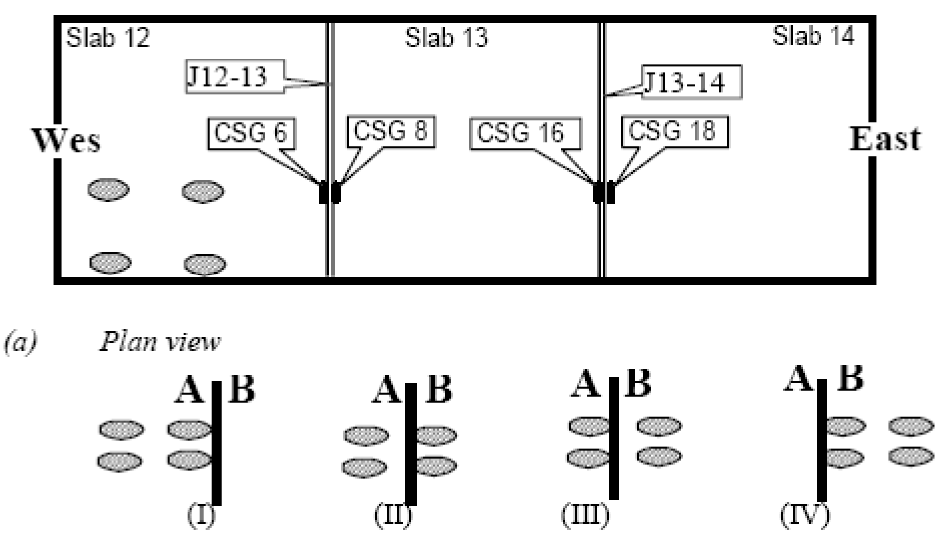

FIGURE 5.6. TEST SLAB CONFIGURATION AND LOADING AT NAPTF BY GUO (2008).

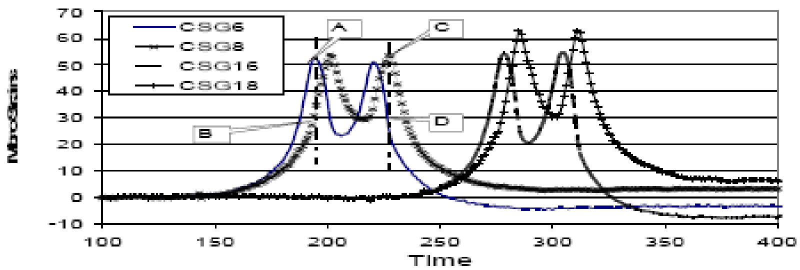

(a) From the West to the East

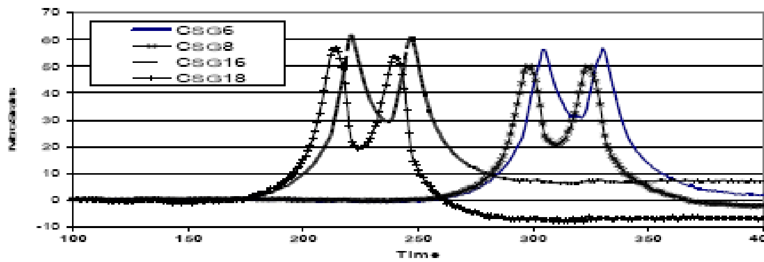

(b) From the East to the West

FIGURE 5.7. STRAIN HISTORIES OF FOUR STRAIN GAGES 6, 8, 16, AND 18 (LEFT OFFSET SET AS ZERO) FROM THE NAPTF STUDIES BY GUO (2008).

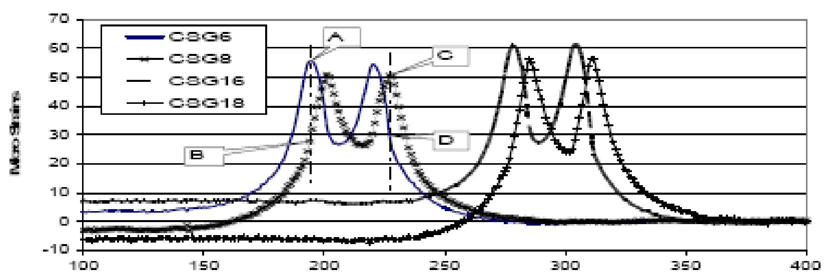

FIGURE 5.8. STRAIN HISTORIES OF FOUR STRAIN GAGES 6, 8, 16, AND 18 (FROM WEST TO EAST, RIGHT OFFSET SET AS ZERO) FROM NAPTF STUDIES BY GUO (2008).

TABLE 5.1. PEAK STRAINS AND CALCULATION OF LTE(S) OF THE TWO JOINTS FROM NAPTF STUDIES, GUO (2008).

	(I)		(II)		(III)		(IV)	
Joint(12-13) Left offset=0	=>	<=	=>	<=	=>	<=	=>	<=
(1) ε_L	52.5	***57.5***	53.0	***50.0***	51.0	***56.5***	53.7	***50.0***
(2) ε_U	33.0	***26.0***	29.0	***37.5***	35.0	***26.0***	25.0	***34.0***
(3) SUM	85.5	***83.5***	82.0	***87.5***	86.0	***82.5***	78.7	***84.0***
(4) LTE(S)	38.6	***31.1***	35.4	***42.9***	40.7	***31.5***	31.8	***40.5***
LTE(D) by FWD	**81.8**						**88.1**	
Joint(13-14) Left offset = 0	=>	<=	=>	<=	=>	<=	=>	<=
(5) ε_L	54	***61***	63	**54**	55	***62***	63	***57***
(6) ε_U	33	***18***	26.5	**32.5**	36.5	***23***	19	***32***
(7) SUM	87.0	***79.0***	89.5	**86.5**	91.5	***85.0***	82.0	***89.0***
(8) LTE(S)	37.9	***22.8***	29.6	**37.6**	39.9	***27.1***	23.2	***36.0***
LTE(D) by FWD	72.5						82.6	
Joint(12-13) Right offset=0	=>		=>		=>		=>	
(9) ε_L	***56***		***51***		***54.8***		***50.8***	
(10) ε_U	***30***		***31.8***		***32.5***		***28***	
(11) SUM	***86.0***		***82.8***		***87.3***		***78.8***	
(12) LTE(S)	***34.9***		***38.4***		***37.2***		***35.5***	
Joint(13-14) Right offset=0	=>		=>		=>		=>	
(13) ε_L	***61***		***56.5***		***61.5***		***57***	
(14) ε_U	***26.2***		***32.5***		***30***		***27***	
(15) SUM	***87.2***		***89.0***		***91.5***		***84.0***	
(16) LTE(S)	***30.0***		***36.5***		***32.8***		***32.1***	

TABLE 5.2. AVERAGE AND STANDARD DEVIATION VALUES OF THE PARAMETERS FROM NAPTF STUDIES, GUO (2008).

Table 2 Averages and standard deviations

		Ave. =>	STD =>	Ave. <=	STD. <=	Ave. Total	STD. Total
Joint(12-13) App. offset = 0	(1) ε_L	52.6	1.1	53.5	4.1	**53.0**	2.8
	(2) ε_U	30.5	4.4	30.9	5.8	**30.7**	4.8
	(3) SUM	83.1	3.4	84.4	2.2	**83.7**	2.7
	(4) LTE(S)	36.6	3.9	36.5	6.1	**36.6**	4.7
Joint (13-14) App. offset = 0	(5) ε_L	58.8	4.9	58.5	3.7	**58.6**	4.0
	(6) ε_U	28.8	7.7	26.4	7.1	**27.6**	7.0
	(7) SUM	87.5	4.1	84.9	4.3	**86.2**	4.1
	(8) LTE(S)	32.7	7.7	30.8	7.1	**31.7**	6.9
Joint (12-13) Lea. Offset = 0	(9) ε_L	**53.2**	2.6	Standard Deviation of All SUMs		Joint(12-13)	
	(10) ε_U	**30.6**	2.0			***0.54***	
	(11) SUM	**83.7**	3.8			Joint(13-14)	
	(12) LTE(S)	**36.5**	1.6			***1.38***	
Joint (13-14) Lea. Offset = 0	(13) ε_L	**59.0**	2.6	Standard deviation of all LTE(S)		Joint(12-13)	
	(14) ε_U	**28.9**	2.9			***0.05***	
	(15) SUM	**87.9**	3.2			Joint(13-14)	
	(16) LTE(S)	**32.9**	2.7			***0.93***	

5.4. DENVER INSTRUMENTED TESTING

Rufino et al. (2001) attempted to match joint deflection responses observed at Denver International Airport (DIA) to FE models by simulating multiple wheel gear assemblies. An influence function approach was used to develop FE simulated deflection histories for points on the FE model slab matching vertical deflection gage sensors embedded at DIA. Figure5.9 shows the sensor layout in the test area that was evaluated, and the two cases that were analyzed, corresponding to two gear types. Figure 5.10 shows the deflection histories for the gear types as the actual aircraft gear passed over the joint. Figure5.10 also shows how this team defined LTE_{δ} for the deflection history traces. LTE_{δ} values between about 30 and 50 percent were calculated from the deflection history plots.

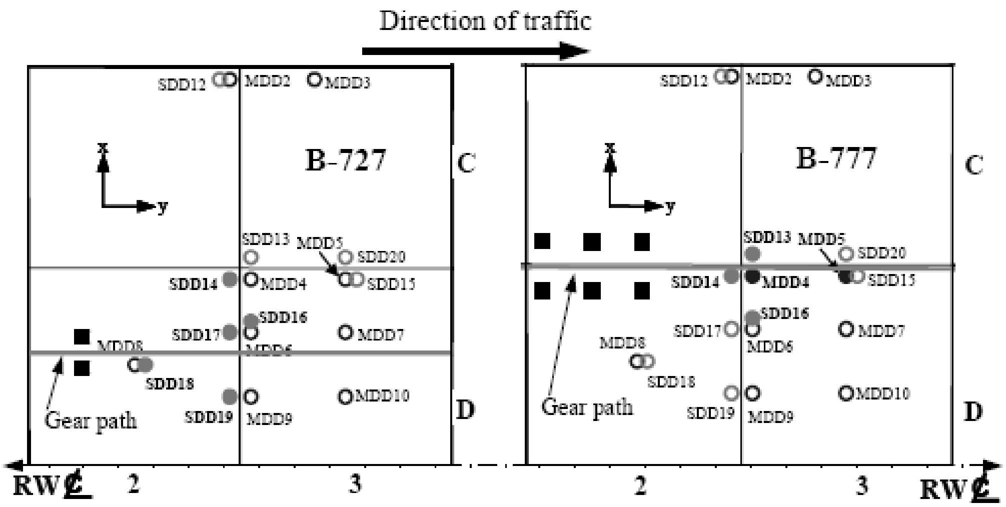

FIGURE 5.9. SENSOR LAYOUT IN THE DIA TEST AREA EVALUATED BY RUFINO ET AL (2001).

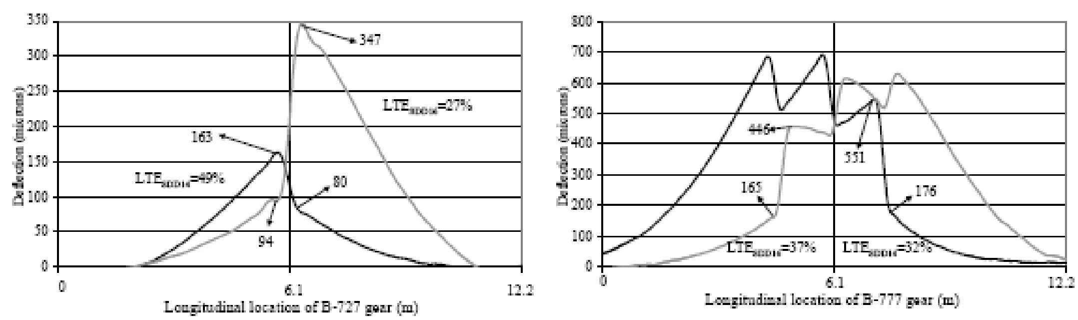

FIGURE 5.10. DEFLECTION HISTORY PLOTS FROM AN ACTUAL AIRCRAFT PASS AT DIA (RUFINO ET AL. 2001).

Rufino et al. (2001) used a form of visual backcalculation to evaluate apparent subgrade stiffness and also apparent load transfer efficiency. Figures 5.11 and 5.12 show the DIA deflection sensor history compared to FE runs for three different subgrade stiffness levels for a corner sensor

(SDD14) and transverse joint sensor (SDD16). Figure 5.13 shows how the real deflection traces match traces from FE models set at different load transfer efficiency values for the corner sensor (SDD 14). Based on these plots, it appears that the DIA joints may have some small slack/looseness, and some slab warp or foundation deformation along the edges.

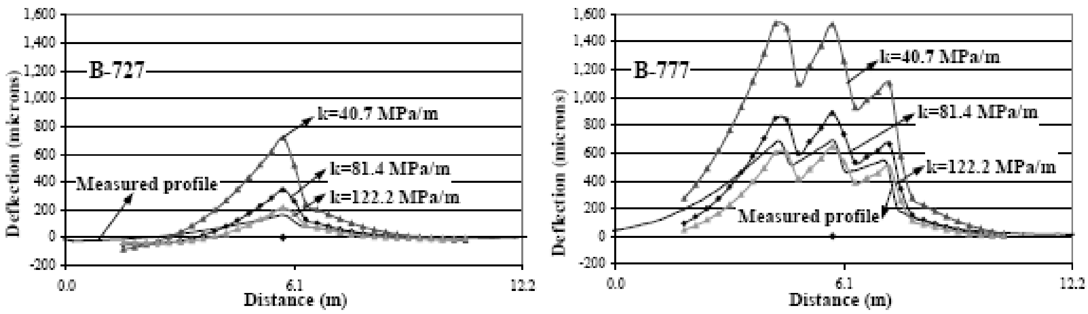

FIGURE 5.11. MATCHING DEFLECTION HISTORIES FROM DIA TO FE MODELS FOR A CORNER SENSOR (SDD14) (RUFINO ET AL. 2001).

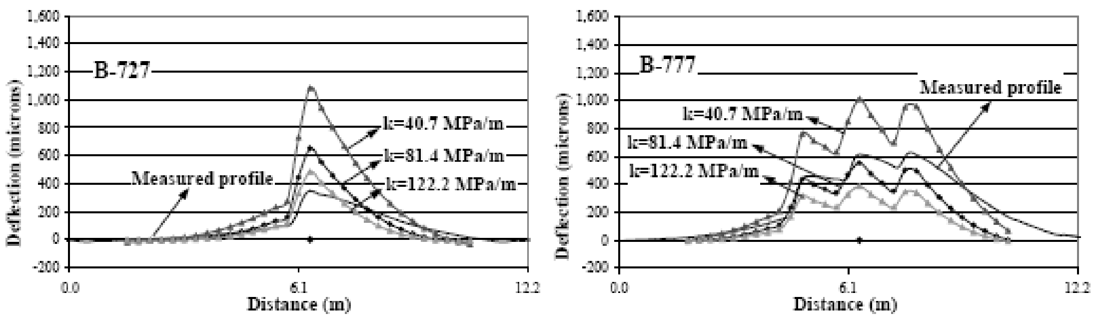

FIGURE 5.12. MATCHING DEFLECTION HISTORIES FROM DIA TO FEM MODELS FOR TRANSVERSE JOINT SENSOR (SDD16) (RUFINO ET AL 2001).

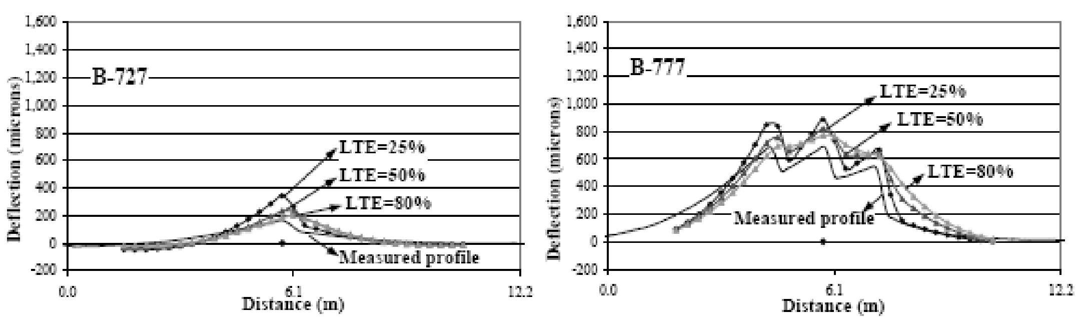

FIGURE 3.13. MATCHING DEFLECTION HISTORIES FROM DIA TO FEM MODELS USING VARIOUS JOINT EFFICIENCIES AT CORNER (SDD14) (RUFINO ET AL 2001).

Results from joint opening sensors installed at DIA are presented in Chapter 6 that addresses climatic effects on load transfer at joints,

5.5. FALLING WEIGHT DEFLECTOMETER TESTING

An interesting and perhaps the first example of a study that used a multi-slab FE model to backcalculate apparent joint stiffness and load transfer from FWD data is the study by Florida DOT and the University Florida (Armaghani et al. 1986). In this study, the joint stiffness models in FEACONS III FE model were calibrated based on FWD test data performed at multiple times of day (curling effects), multiple times of the year (joint opening and warp effects), and at multiple load levels (effects of gaps and voids). This research team took detailed measurements of the shape of the loaded and unloaded slabs during FWD testing and then varied joint spring stiffness values and subgrade stiffness values simultaneously within the FE model until the model slab deflection shapes matched the measured shapes from FWD data. Armaghani et al. (1986) reported a joint stiffness value of about 10,000 lb/in/in at 60°F. Armaghani et al (1986) did not perform an analysis of apparent stress load transfer.

Bush III et al. (1989) showed us one of the first WES methodologies for use of the FWD for airfield PCC pavements. WES was in the process of moving away from the more complicated 16 kip vibratory NDT device and towards the use of the FWD for NDT. WES developed the Volumetric k index to estimate the modulus of subgrade reaction from FWD data. The following equation was used to compute volumetric k:

$$\text{Volumetric k, pci} = \frac{\text{Force (lb)}}{\sum_{N=1}^{7} \text{Area}_N * (\text{Dist. to Centroid}) * 2 * \pi}$$

Figure 5.14 shows a plot of FE model results that Bush III et al. (1989) developed in an attempt to correlate LTE_δ from FWD devices to the percent of free edge stress, LT, concept. An LTE_δ of about 77% or greater would be needed to achieve an LT of 25% for this model.

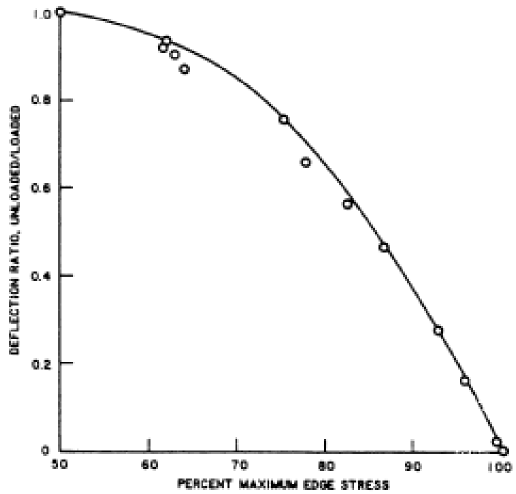

FIGURE 5.14. FEM MODEL RESULTS FROM BUSH III ET AL, (1989) SHOWING FWD LTE_{δ} VS. FEM LT.

Owusu-Antwi et al. (1989) performed an early evaluation of FWD methods for joint evaluations. This team developed plots showing the apparent effects of thermal gradients and joint opening size on LTE_{δ} for aggregate interlock type joints as shown in figure 5.15.

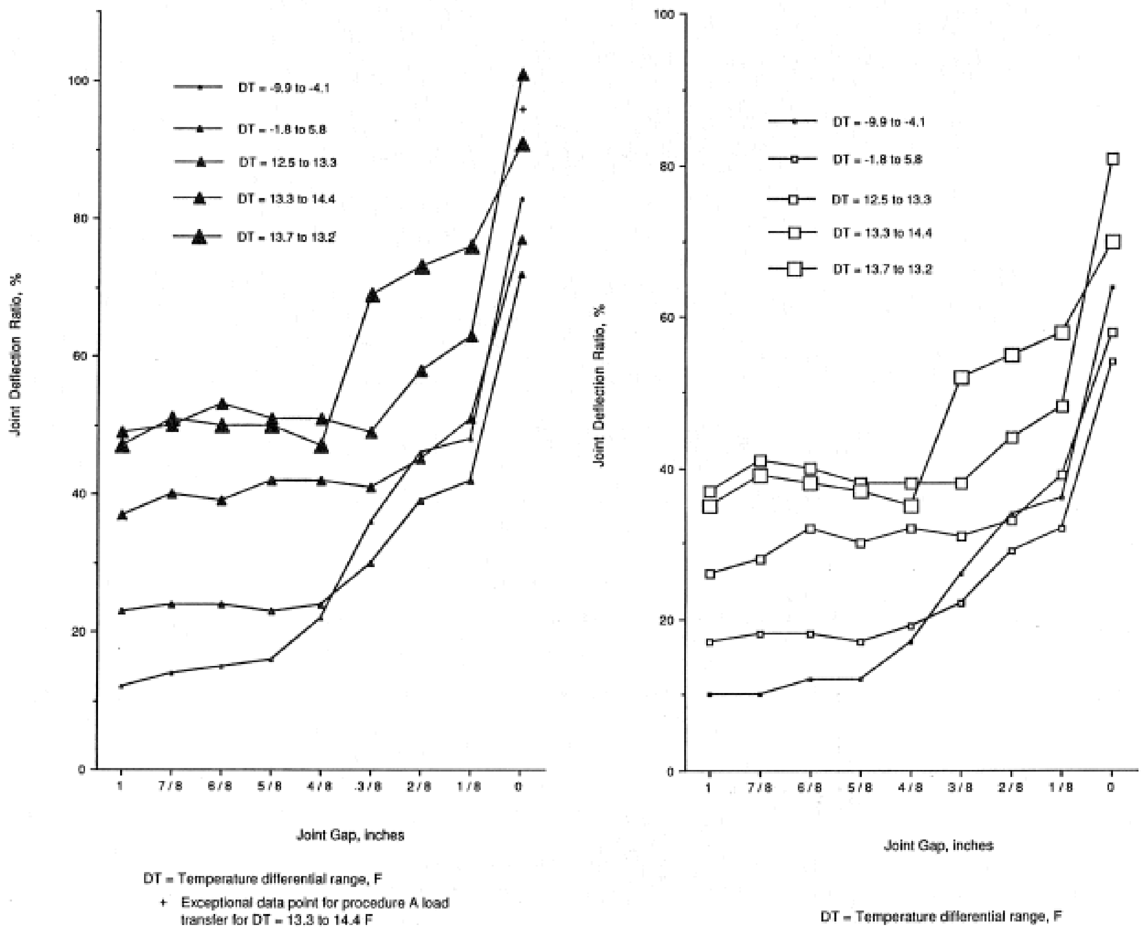

(a) Load transfer using procedures A and B.

(b) Load transfer using procedure C.

FIGURE 5.15. PLOTS FROM OWUSU-ANTWI ET AL (1989) SHOWING HOW THERMAL GRADIENT AND JOINT OPENING SIZE AFFECT LTE_{δ} DETERMINED FROM FWD DATA.

A theoretical treatment of the load transfer issue was also developed by a doctoral student of Professor Westergaard (Skarlatos) under contract with the Army Corps of Engineers, but it received little attention until recently (Ioannides and Hammons 1996, Skarlatos 1949). Ioannides and Hammons (1996) provided a summary of the closed form Skarlatos extension of the Westergaard equations for the load transfer problem and presented a methodology for use with the FWD to evaluate load transfer at joints. Figure 5.16 shows the general equations for the closed form Skarlatos method. Figure 5.17 show the definitions for the parameter *f,* referred to as the dimensionless joint stiffness, which is used in the closed form solution.

Free Edge Deflection:

$$\Delta_f^* = \frac{\Delta_f\, k\, \ell^2}{P} = \left[0.4314 - 0.3510 \left(\frac{\varepsilon}{\ell} \right) + 0.06525 \left(\frac{\varepsilon}{\ell} \right)^2 \right]$$

Free Edge Bending Stress:

$$\overline{\sigma}_f^* = \overline{\sigma}^* + \sigma_c^* = \frac{(\overline{\sigma} + \sigma_c)\, h^2}{P}$$

$$\overline{\sigma}^* = \frac{\overline{\sigma}\, h^2}{P} = 1.3945 \left[0.22215 - \log_e \left(\frac{\varepsilon}{\ell} \right) \right]$$

$$\sigma_c^* = \frac{\sigma_c\, h^2}{P} = 1.3945 \left[-0.2419 + 0.3822 \left(\frac{\varepsilon}{\ell} \right) - 2.1125 \left(\frac{\varepsilon}{\ell} \right)^2 + 4.02 \left(\frac{\varepsilon}{\ell} \right)^3 \right]$$

Unloaded Side Deflection:

$$\Delta_U^* = \frac{\Delta_U\, k\, \ell^2}{P} = 0.215 \left[\frac{f - 0.6 \log (1 + f)}{f + 0.4} \right] *$$

$$\left[1 - 0.7 \left(\frac{\varepsilon}{\ell} \right) \left\{ 1 + 0.06 \log (1 + f) - 0.01\, f^{0.2} \right\} \right] + \Delta_U^{*\prime}$$

$$\Delta_U^{*\prime} = \frac{1}{2} \left[0.015 + 0.005 \log f \right] \left(\frac{\varepsilon}{\ell} \right)^2$$

Unloaded Side Bending Stress:

$$\sigma_U^* = \frac{\sigma_U\, h^2}{P} = 0.54 \left[0.42 + \log (1 + f) + 0.1\, \frac{\sqrt{f} - 4.2}{f + 1} \right] *$$

$$\left[1 - 0.54 \left(\frac{\varepsilon}{\ell} \right)^{4.1}\sqrt{f + 5.0} \right] + \sigma_U^{*\prime}$$

$$\sigma_U^{*\prime} = 3.75 \log^{-1} \left[0.74 \log f - 1.94 \right] \left(\frac{\varepsilon}{\ell} \right)^2 \quad \text{for } f > 10; = 0, \text{ otherwise}$$

Note: The unloaded side bending stress should not exceed half the corresponding free edge bending stress.

FIGURE 5.16. CLOSED-FORM SOLUTIONS FOR THE EDGE LOAD TRANSFER PROBLEM FOR SQUARE LOADS, IOANNIDES AND HAMMONS (1996).

$$f = \frac{q_o}{kl} = \frac{AGG}{kl} \qquad \text{for undoweled joints}$$

or

$$f = \frac{D}{skl} \qquad \text{for doweled joints}$$

FIGURE 5.17. DEFINITIONS FOR THE PARAMETER *f*.

Tables 5.3 through 5.6 show results from using this Skarlatos based FWD analysis method at three airports.

5.6. SUMMARY

The Skarlatos method as implemented by Ioannides and Hammons (1996) is judged to be the simplest way to connect FWD data to the stress load transfer problem. However, it cannot directly account for thermal stresses. Several researchers have attempted to match FE models to FWD responses and this approach is probably more precise but it takes a great deal of time, knowledge and effort to execute. Most of these past studies have focused on matching measured deflections. In general, very little published work was found that was attempting to analyze in detail the FWD sensor responses during joint testing.

Our literature review did not find any procedure that has been developed for estimating joint stiffness directly from field load testing of joints using the FWD. The only procedure for estimating joint stiffness and converting LTE_δ to LTE_σ that was available for FWD that didn't require extensive FE back-calculation efforts was the Skarlatos based procedure described by Ioannides and Hammons (1996), which does not account for the actual joint deflections measured at the site. Two additional methods for estimating joint stiffness from FWD data are available (Crovetti 1994, Zollinger et al. 1999). These three existing joint stiffness estimation procedures use mid-panel drops to establish system structural properties, and then use only the joint LTE_δ ratios, not magnitudes, to estimate joint stiffness characteristics. During our literature review we also did not find any literature that had reviewed in detail the effect of thermal curling on stress load transfer.

TABLE 5.3. SKARLATOS ANALYSIS RESULTS FROM IOANNIDES ET AL. (1996) FOR DIA (DAY TESTING).

Feature / STATISTIC	Midslab Load (lbs)	AREA (in.)	ℓ (in.)	a/ℓ	Edge Load (lbs)	$LTE_δ$	HPM LT %	SRA LT %	ANN LT %
Runway 17-35									
AVG	52026	31.34	40.37	0.15	52104	0.73	17.77	20.22	21.59
MIN	51150	29.88	32.07	0.11	50880	0.57	11.29	14.78	15.60
MAX	53231	32.80	51.82	0.18	53660	0.86	24.15	26.16	28.33
COV %	1.13	2.79	15.44	14.13	1.15	9.61	18.56	13.69	14.39
COUNT	8				48				
Runway 16-34									
AVG	63851	31.27	39.26	0.15	56834	0.71	17.03	19.87	21.09
MIN	62142	30.20	33.41	0.13	52484	0.27	3.47	6.97	6.85
MAX	65065	32.00	44.18	0.18	62110	0.92	28.67	31.90	32.87
COV %	1.32	1.52	7.24	7.52	3.51	18.71	32.82	26.29	26.55
COUNT	12				132				
Concourse B/C									
AVG	53578	31.93	46.11	0.13	52824	0.87	24.65	25.98	28.30
MIN	52643	30.33	34.02	0.08	51356	0.82	22.12	23.09	25.14
MAX	54358	34.00	71.47	0.17	54517	0.91	27.34	29.32	31.34
COV %	1.00	3.72	24.06	21.66	1.47	2.13	4.35	5.01	4.51
COUNT	12				70				
Apron 8-26									
AVG	53409	31.14	38.54	0.15	54391	0.84	23.09	25.38	27.11
MIN	52754	30.30	33.84	0.13	52563	0.71	16.40	19.28	32.22
MAX	54231	32.18	45.65	0.17	56011	0.91	27.92	31.21	32.22
COV %	0.72	1.68	8.44	8.14	1.72	5.02	10.10	10.09	10.01
COUNT	12				48				
All 4 Features									
AVG	56051	31.43	41.13	0.15	54737	0.77	19.92	22.25	23.83
MIN	51150	29.88	32.07	0.08	50880	0.27	3.47	6.97	6.85
MAX	65065	34.00	71.47	0.18	62110	0.92	28.67	31.90	32.87
COV %	8.65	2.77	18.09	14.44	4.49	15.30	26.60	21.46	22.02
COUNT	44				298				

Notes: 1 lb=4.444 N; 1 in.=25.4 mm.
HPM: Hammons, et al. *(9)*
SRA: Statistical Regression Analysis (Equations 9 and 5)

TABLE 5.4. SKARLATOS ANALYSIS RESULTS FROM IOANNIDES ET AL. (1996) FOR ATLANTA HATFIELD INTERNATIONAL AIRPORT (NIGHT TESTING).

Feature STATISTIC	Midslab Load (lbs)	AREA (in.)	ℓ (in.)	a/ℓ	Edge Load (lbs)	LTE_s	HPM LT %	SRA LT %	ANN LT %
Runway 8R-26L									
AVG	54373	30.19	34.76	0.18	48808	0.85	24.39	27.99	29.22
MIN	53421	27.08	23.66	0.13	47655	0.23	3.21	6.27	6.48
MAX	54946	32.18	45.71	0.25	50403	0.96	34.17	38.53	38.18
COV %	0.89	5.39	19.54	21.71	1.06	11.82	22.02	18.87	17.98
COUNT	12				140				
Runway 9L-27R									
AVG	50196	30.51	35.90	0.17	48535	0.70	18.45	21.87	22.86
MIN	49291	28.14	26.26	0.13	46035	0.10	2.04	2.61	2.28
MAX	51178	32.18	45.71	0.22	50991	0.97	35.56	40.14	39.80
COV %	1.17	4.27	16.96	18.21	1.46	32.28	49.19	40.88	40.65
COUNT	12				249				
Taxiway E									
AVG	53947	31.37	40.00	0.15	53270	0.59	12.63	15.79	16.70
MIN	52881	30.35	34.08	0.13	48116	0.18	2.75	4.66	4.46
MAX	54708	32.32	46.90	0.17	55788	0.87	24.97	26.95	29.06
COV %	0.98	1.87	9.55	9.47	2.46	28.78	44.52	32.73	34.23
COUNT	12				86				
Taxiway M									
AVG	50055	32.24	47.28	0.13	49113	0.72	18.22	19.87	21.56
MIN	49037	31.13	38.18	0.10	47163	0.19	2.83	4.72	4.21
MAX	51118	33.31	58.54	0.15	51388	0.96	34.65	36.51	36.56
COV %	1.22	2.39	15.06	14.88	1.54	24.56	37.25	30.12	31.56
COUNT	12				189				
All Four Features									
AVG	52143	31.08	39.49	0.16	49370	0.72	18.88	21.80	23.03
MIN	49037	27.08	23.66	0.10	46035	0.10	2.04	2.61	2.28
MAX	54946	33.31	58.54	0.25	55788	0.97	35.56	40.14	39.80
COV %	1.07	3.48	15.28	16.07	1.53	25.31	39.46	32.12	32.45
COUNT	48				664				

Notes: 1 lb=4.444 N; 1 in.=25.4 mm.
HPM: Hammons, et al. *(9)*
SRA: Statistical Regression Analysis (Equations 9 and 5)

TABLE 5.5. SKARLATOS ANALYSIS RESULTS FROM IOANNIDES ET AL. (1996) FOR ATLANTA HATFIELD INTERNATIONAL AIRPORT (DAY TESTING).

Feature / STATISTIC	Midslab Load (lbs)	AREA (in.)	ℓ (in.)	a/ℓ	Edge Load (lbs)	LTE_{δ}	HPM LT %	SRA LT %	ANN LT %
Runway 8R-26L									
AVG	54373	30.19	34.76	0.18	48941	0.87	25.52	29.08	30.33
MIN	53421	27.08	23.66	0.13	47814	0.61	12.73	16.81	17.63
MAX	54946	32.18	45.71	0.25	50149	0.94	32.34	36.22	36.24
COV %	0.89	5.39	19.54	21.71	1.11	7.18	16.77	14.48	13.45
COUNT	12				58				
Taxiway M									
AVG	50055	32.24	47.28	0.13	48537	0.72	18.28	20.09	21.62
MIN	49037	31.13	38.18	0.10	46591	0.34	4.76	8.23	7.83
MAX	51118	33.31	58.54	0.15	50880	0.97	35.71	38.16	38.21
COV %	1.22	2.39	15.06	14.88	1.83	23.17	41.26	33.37	33.48
COUNT	12				40				
Both Features									
AVG	52214	31.22	41.02	0.16	48776	0.81	22.57	25.42	26.77
MIN	49037	27.08	23.66	0.10	46591	0.34	4.76	8.23	7.83
MAX	54946	33.31	58.54	0.25	50880	0.97	35.71	38.16	38.21
COV %	1.06	3.89	17.30	18.30	1.41	13.70	26.76	22.19	21.63
COUNT	24				98				

Notes: 1 lb=4.444 N; 1 in.=25.4 mm.
HPM: Hammons, et al. *(9)*
SRA: Statistical Regression Analysis (Equations 9 and 5)
Midslab Data from the corresponding night tests

TABLE 5.6. SKARLATOS ANALYSIS RESULTS FROM IOANNIDES ET AL. (1996) FOR DALLAS-FORT WORTH AIRPORT (DAY TESTING).

Feature STATISTIC	Midslab Load (lbs)	AREA (in.)	ℓ (in.)	a/ℓ	Edge Load (lbs)	LTE_δ	HPM LT %	SRA LT %	ANN LT %
Taxiway K									
AVG	50956	30.33	34.85	0.17	50298	0.77	20.23	23.83	24.81
MIN	50355	27.75	25.23	0.14	48846	0.34	4.70	8.89	9.17
MAX	51737	31.54	40.78	0.23	52786	0.94	31.86	35.50	34.44
COV %	1.32	4.47	15.59	18.39	1.22	16.62	29.77	23.99	24.16
COUNT	6				210				
Taxiway J									
AVG					50884	0.70	17.77	21.43	22.29
MIN					48910	0.07	1.61	1.77	1.43
MAX	**Used values from T/w K.*				55995	0.98	37.95	44.06	44.26
COV %					1.99	28.57	44.65	36.21	36.66
COUNT					210				
Runway 31R									
AVG					51468	0.70	17.38	20.94	22.10
MIN					50324	0.19	2.78	4.95	5.05
MAX	**Used values from T/w K.*				52421	0.88	25.82	29.10	30.83
COV %					1.03	30.77	42.65	35.03	35.65
COUNT					44				
Cross-Taxiway 31 S									
AVG					52176	0.76	20.14	23.73	25.02
MIN					51197	0.24	3.30	6.45	6.65
MAX	**Used values from T/w K.*				53644	0.93	30.75	34.21	34.76
COV %					1.23	20.98	33.55	27.14	27.14
COUNT					96				
All 4 Features									
AVG	50956	30.33	34.85	0.17	50932	0.74	19.07	22.69	23.69
MIN	50355	27.75	25.23	0.14	48846	0.07	1.61	1.77	1.43
MAX	51737	31.54	40.78	0.23	55995	0.98	37.95	44.06	44.26
COV %	1.32	4.47	15.59	18.39	1.50	22.96	37.01	29.98	30.26
COUNT	6				560				

Notes: 1 lb=4.444 N; 1 in.=25.4 mm.
HPM: Hammons, et al. *(9)*
SRA: Statistical Regression Analysis (Equations 9 and 5)

CHAPTER 6: CLIMATE EFFECTS ON JOINT LOAD TRANSFER

6.1 SOUTH AFRICAN STUDIES

Perhaps the most detailed attempt for accounting environmental effects on joint behavior within a design model was performed by the South African researchers Prozzi et al. (1993), who performed a detailed evaluation of how daily thermal gradients affect load transfer in highway slabs.

Figure 6.1 shows typical joint deflection versus surface pavement temperature for a South African pavement showing how combined daily thermal curling and joint opening changes affect joint deflections.

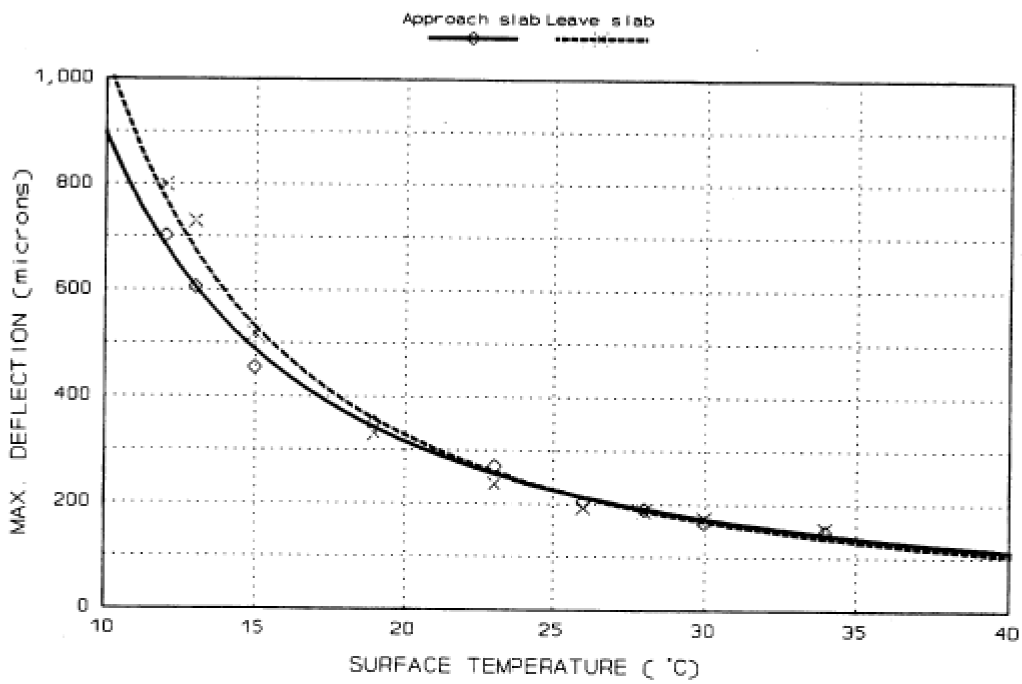

FIGURE 6.1. FWD JOINT DEFLECTION VERSUS PAVEMENT SURFACE TEMPERATURE AT A TEST SITE (PROZZI ET AL. 1993).

Figures 6.2 and 6.3 show how deflection history traces changed for cold and warm conditions, respectively, at the test site. The cold weather deflections were measured at temperatures ranging from 15 to 19°C, while the hot weather deflections were measured at temperatures ranging from 20 to 34°C. The speed of the test vehicle that loaded the slabs was approximately 26 km/h for both series of testing. During the warm weather testing, the joints are in a locked condition, compressed tightly against each other. During the cold weather testing, the effects of joint slack caused by slab faulting are clearly visible. Note how the leave-side slab does not move until the load crosses the joint. Figure 6.4 shows how LTE_{δ} varied with temperature for the approach and leave sides of the joints. As seen in this figure, the LTE was different for the approach and leave side of the joint.

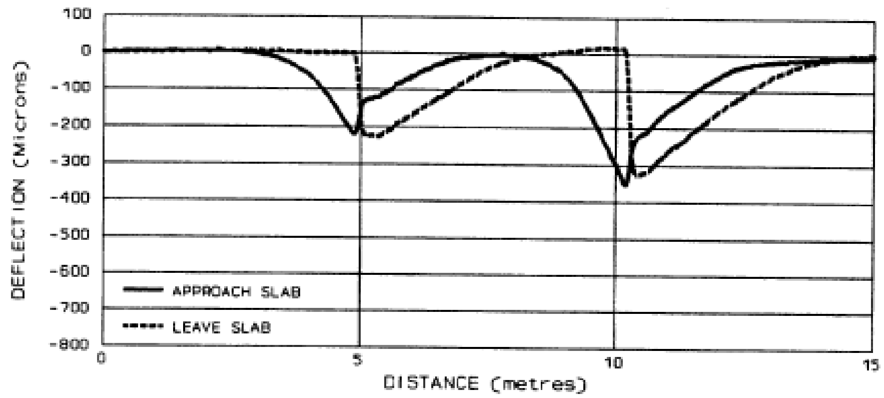

FIGURE 6.2. COOL WEATHER JOINT DEFLECTION HISTORIES FOR A SOUTH AFRICAN TEST SITE (PROZZI ET AL 1993).

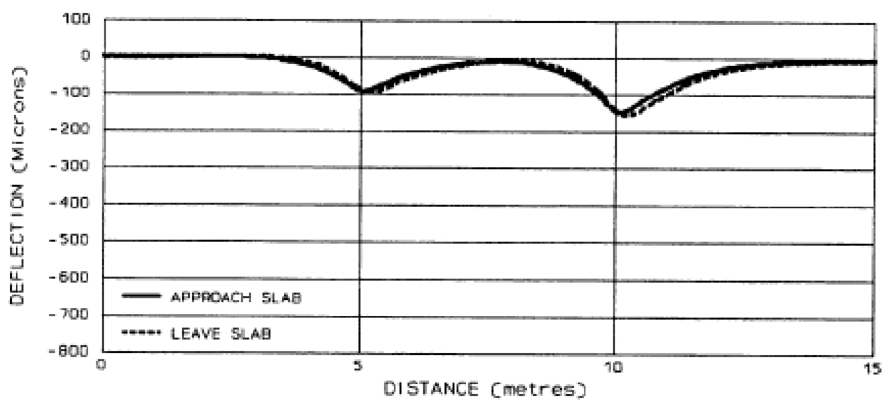

FIGURE 6.3. WARM WEATHER JOINT DEFLECTION HISTORIES FOR A SOUTH AFRICAN TEST SITE (PROZZI ET AL 1993).

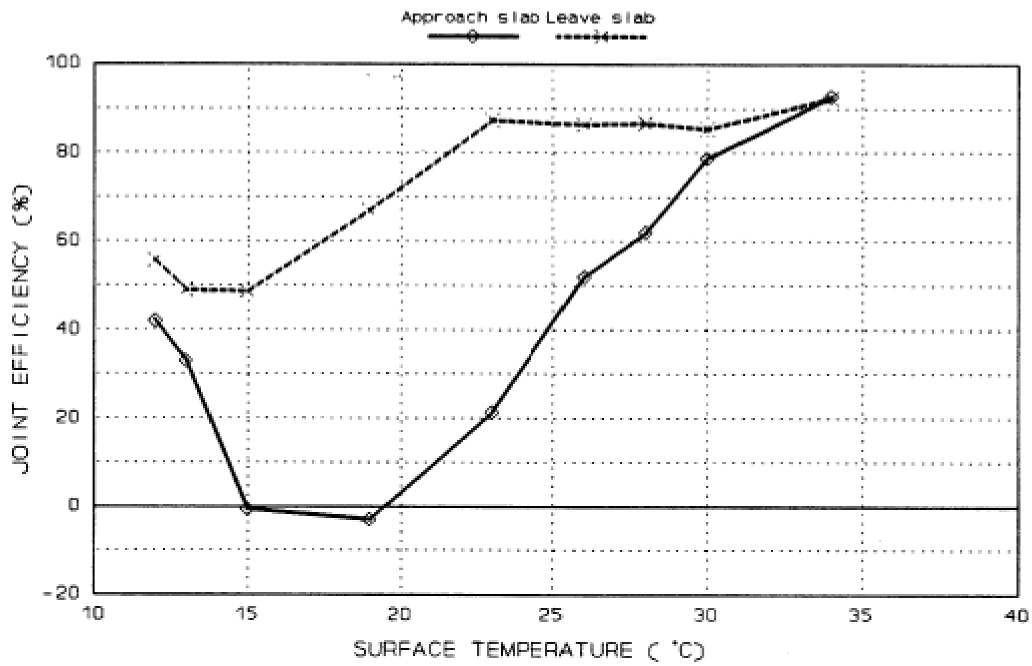

FIGURE 6.4. DIFFERENCE IN LTE$_\delta$ BETWEEN APPROACH AND LEAVE SIDES OF A JOINT FOR A SOUTH AFRICAN TEST SITE (PROZZI ET AL. 1993).

6.2 RESULTS FROM MICHIGAN ROAD TEST

The Michigan Road Test jointed PCC pavement study which commenced in 1940 was monitored for 17 years, and in part was designed to study the effects of joint spacing and temperature on contraction and expansion joint openings (Finney and Oehler 1959). This study was a highly mechanistic pavement performance study for that time, but was somewhat inconclusive. In the Michigan Road Test PCC pavements with contraction joint spacing of 10 to 100 feet were studied. Figures 6.5 to 6.7 show contraction joint opening versus pavement temperature measurements for test sites having 10, 20, and 50 ft joint spacing, respectively. Best fit type regression lines indicated that during the summer all of the joints closed to a value of about 0.02 inches. However, at zero degrees, the average joint openings were about 0.06, 0.10, and 0.27 inches respectively for the 10, 20, and 50 ft joint spacing respectively

Figure 6.8 shows a comparison of joint openings for a site with many expansion joints relative to a site with a few expansion joints. If too much expansion ability is provided, joints will open and lose load transfer. Figures 6.9 and 6.110 show how slabs pushed themselves apart over time due to repeated summer to winter thermal cycles. The ends of the 2700-ft long segment had pushed themselves outward by about 0.9 inches within one year after construction, and had moved out a total of about 1.65 inches after 15 years. Figure 6.11 shows their overall summary plot for the joint opening study.

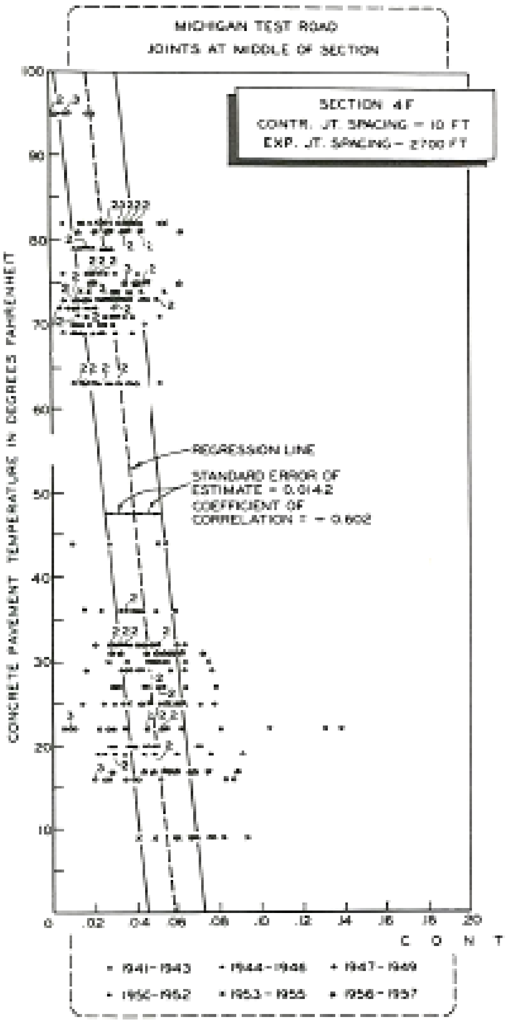

FIGURE 6.5. JOINT OPENING TRENDS FOR CONCRETE SLABS WITH 10-FT JOINT SPACING (FINNEY AND OEHLER 1959).

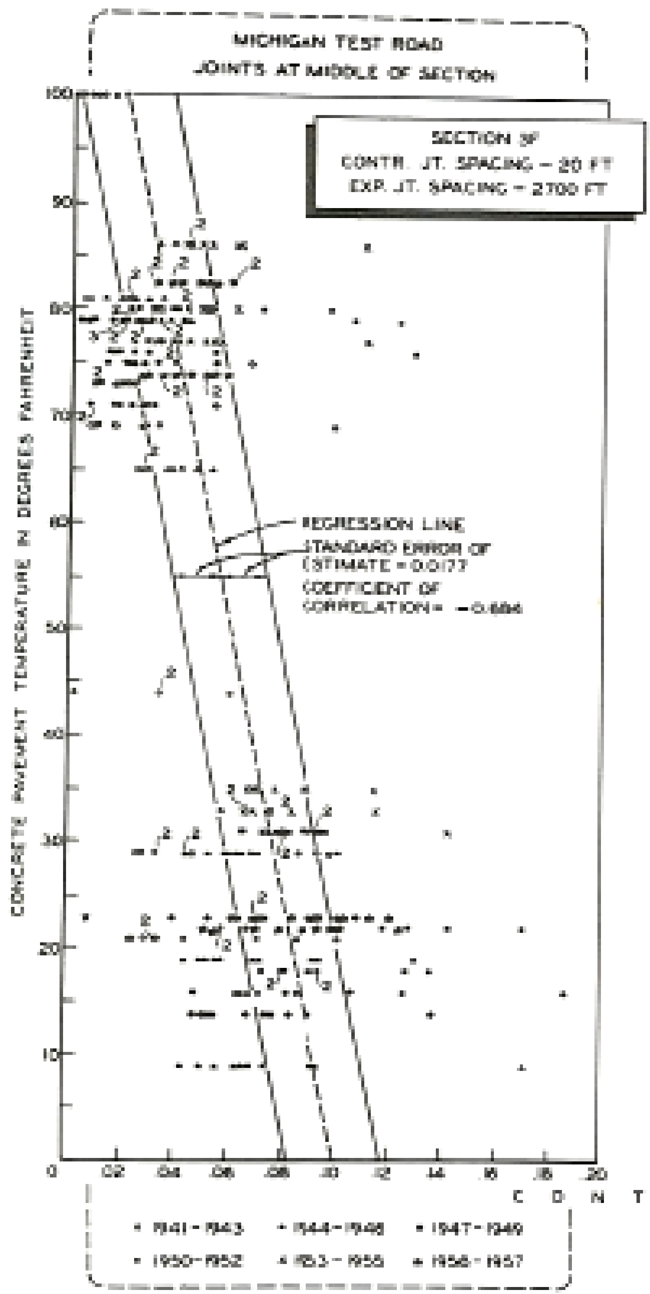

FIGURE 6.6. JOINT OPENINGS TRENDS FOR CONCRETE SLABS WITH 20-FT JOINT SPACING (FINNEY AND OEHLER 1959).

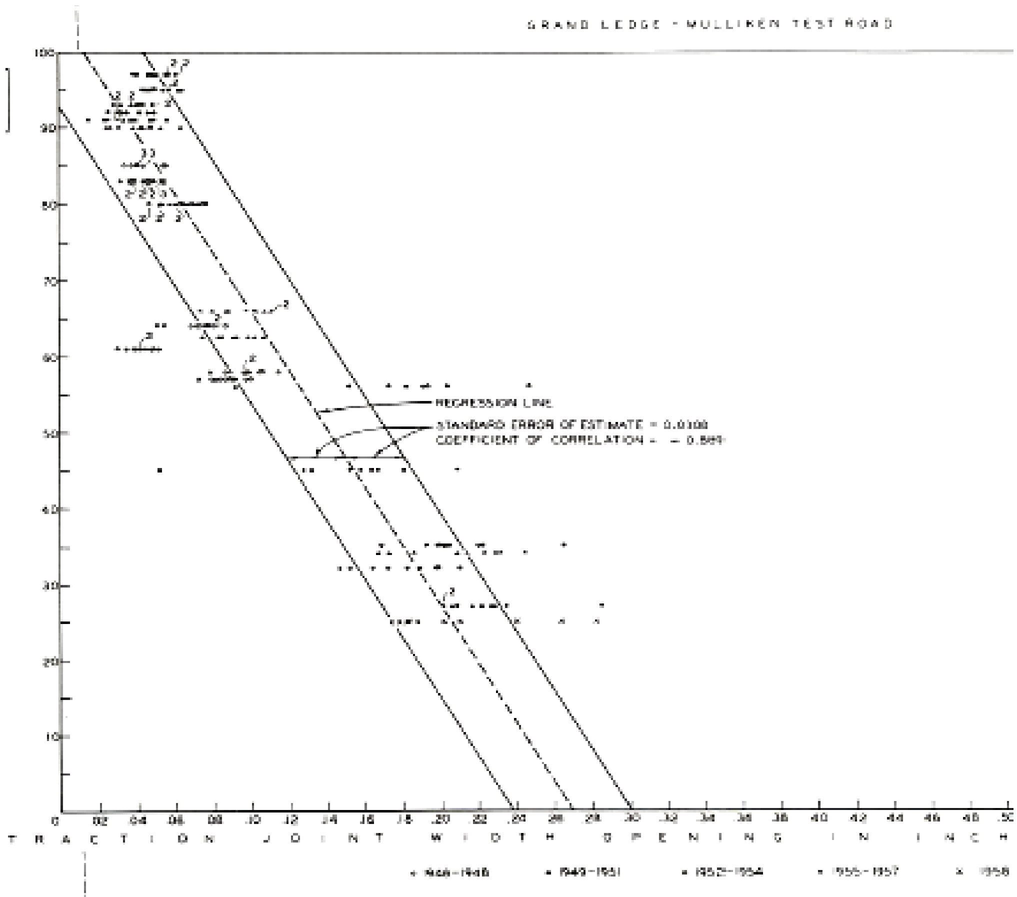

FIGURE 6.7. JOINT OPENING TRENDS FOR CONCRETE SLABS WITH 50-FT JOINT SPACING (FINNEY AND OEHLER 1959).

6.3 RESULTS FROM DENVER INTERNATIONAL AIRPORT

Joint opening sensors installed at DIA were evaluated by Rufino (2003). Figures 6.12 to 6.14 show how joint openings changed over time for a period of seven weeks during winter for an aggregate interlock joint, a doweled joint and a tied joint, respectively. The tied joint is clearly fixed, with little change in joint opening, whereas the doweled and aggregate interlock joints have significant opening and closing movement, which are similar to each other and closely match air temperature trends.

Figures 6.15 and 6.16 show joint opening movements plotted in another way that shows both the daily variations and the total variations from a seasonal perspective for doweled and aggregate interlock joints, respectively. For the doweled joints, the joint openings ranging about 0.14 inches (3.5 mm) did not affect the load transfer much. For the aggregate interlock joints, the joint openings ranging about 0.12 inches (3 mm) dramatically affected load transfer, with the joints being fully locked in summer for temperatures over 70ºF, and the load transfer being nearly zero during winter at temperatures close to 10 ºF. Figure 6.16 demonstrates joint lock-up due to compression of the joint faces due to thermal expansion in the summer.

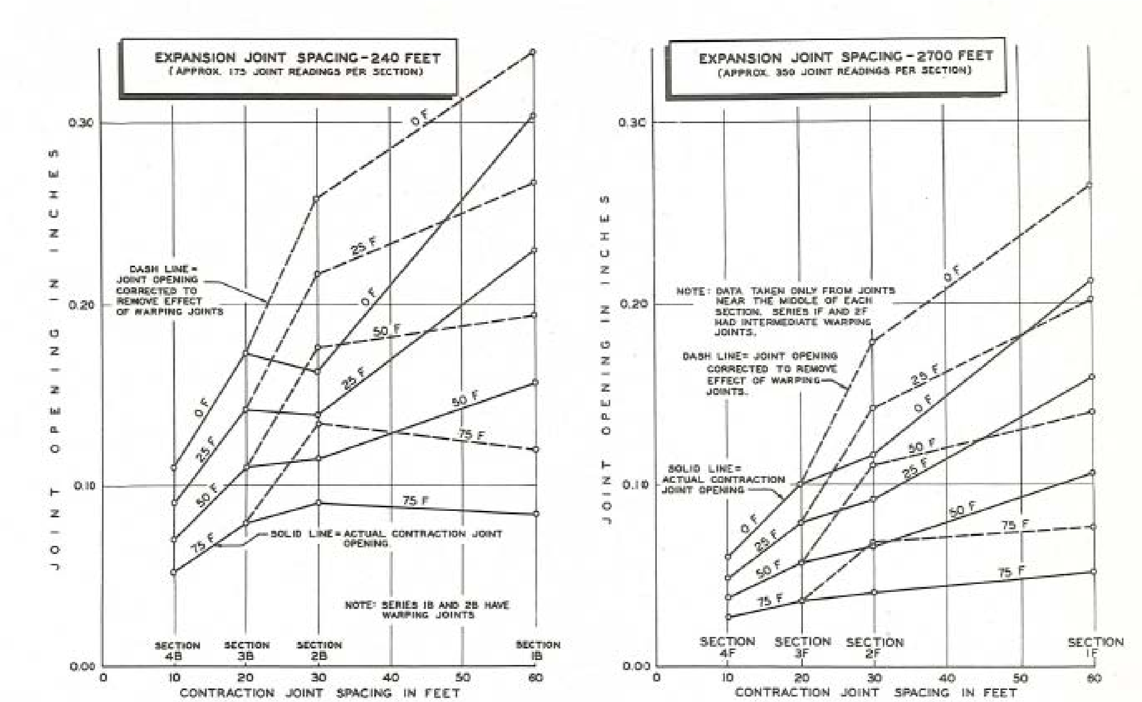

Figure 15. Effect of Contraction Joint Spacing on Contraction Joint Opening

FIGURE 6.8. THE EFFECT OF SPACING OF EXPANSION JOINTS ON CONTRACTION JOINT OPENINGS (FINNEY AND OEHLER 1959).

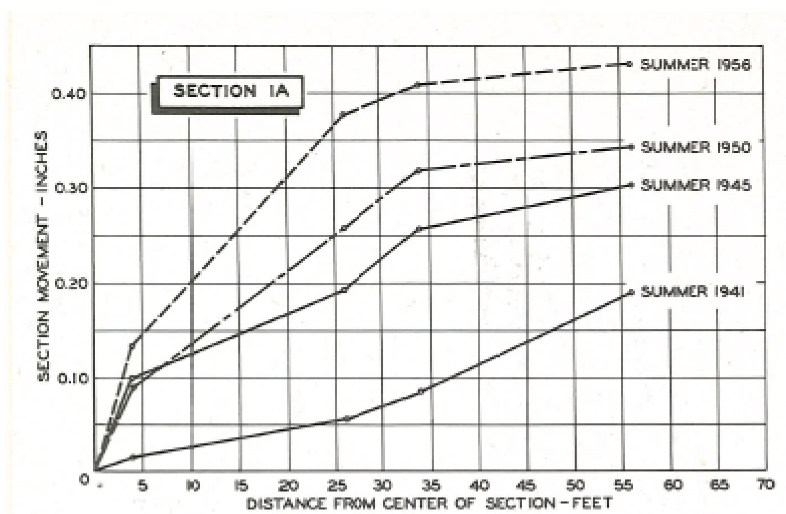

FIGURE 6.9. OUTWARD DRIFT OF THE ENDS OF SLABS IN A 110-FT LONG SEGMENT OF PCC (FINNEY AND OEHLER 1959).

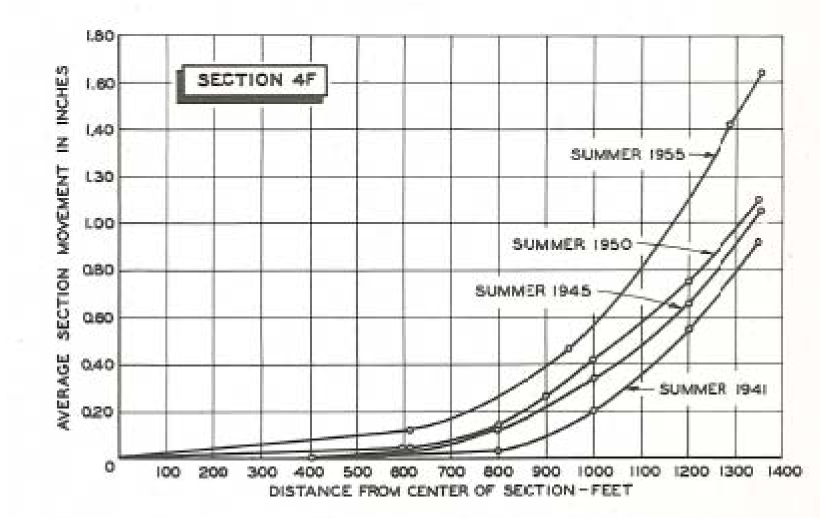

FIGURE 6.10. OUTWARD DRIFT OF A 2700-FT SEGMENT OF PCC PAVEMENT OVER TIME (FINNEY AND OEHLER 1959).

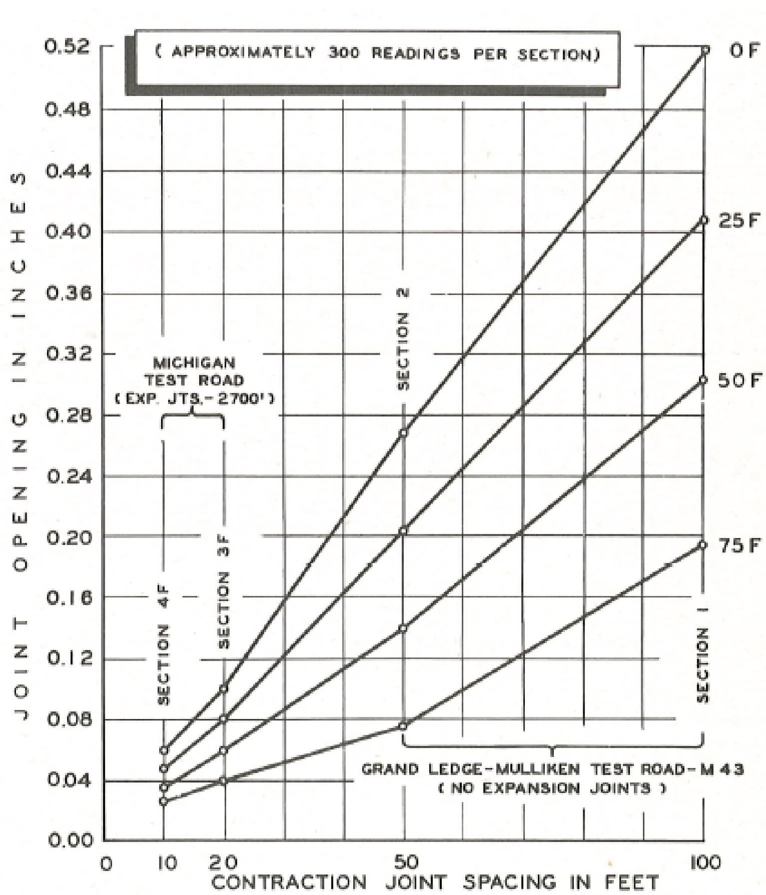

FIGURE 6.11. SUMMARY PLOT FROM THE MICHIGAN ROAD TEST SHOWING EFFECT OF JOINT SPACING AND TEMPERATURE ON JOINT OPENING (FINNEY AND OEHLER 1959).

Figures 6.17 and 6.18 show how these changes in joint openings affected LTE_δ for aggregate interlock joints, where the relationship between LTE_δ and pavement temperature is shown. Figure 6.19 shows the relationship between LTE_δ and pavement temperature for a tied joint.

Figures 6.20 and 6.21 show the relationship between measured deflections and temperature differential at a joint and a corner respectively due to a B-727 loading for an aggregate interlock joint. Figures 6.22 and 6.23 show the relationship between measured deflections and temperature differential at joints due to a B-737 and DC-10, respectively. In figures 6.20 through 6.23, the general trend is the thermal gradient effect, while the scatter around the general trend is the joint opening effect.

Figures 6.24 and 6.25 show the relationship between tensile strain and temperature differential at the slab interior and at the joint (aggregate interlock) respectively for a B-727 loading. In figure 6.26, increased compression is seen in the afternoon, perhaps showing that subgrade drag is stronger than curling stress.

Figures 6.26 and 6.27 show gap magnitude measurements at transverse joints (aggregate interlock) and corners, respectively, for various aircraft for various temperature differentials at DIA. These figures seem to imply slab lift-off at about a 10°F temperature differential.

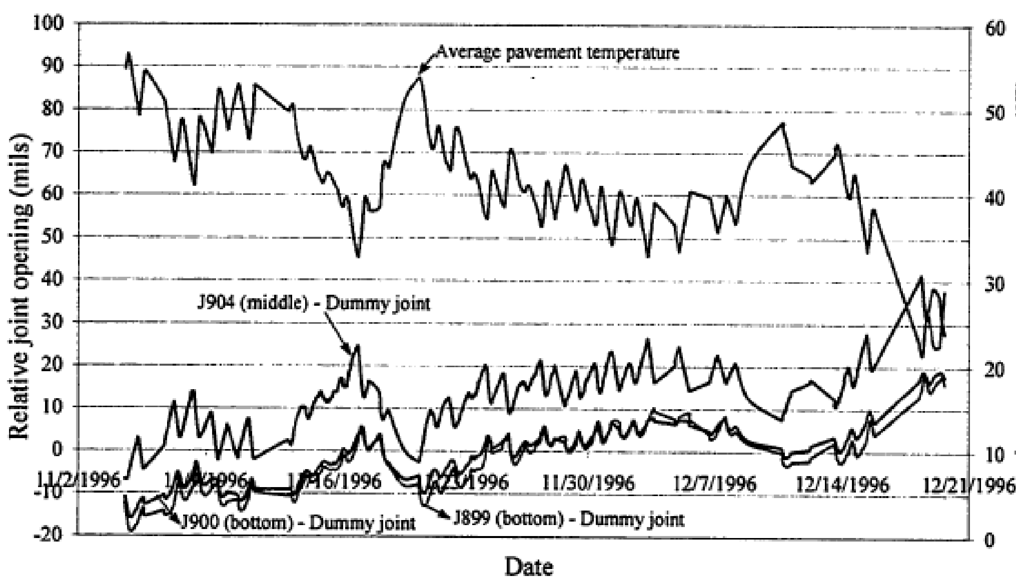

FIGURE 6.12. JOINT OPENINGS IN WINTER OVER A 7 WEEK PERIOD FOR AGGREGATE INTERLOCK JOINTS AT DIA (RUFINO 2003).

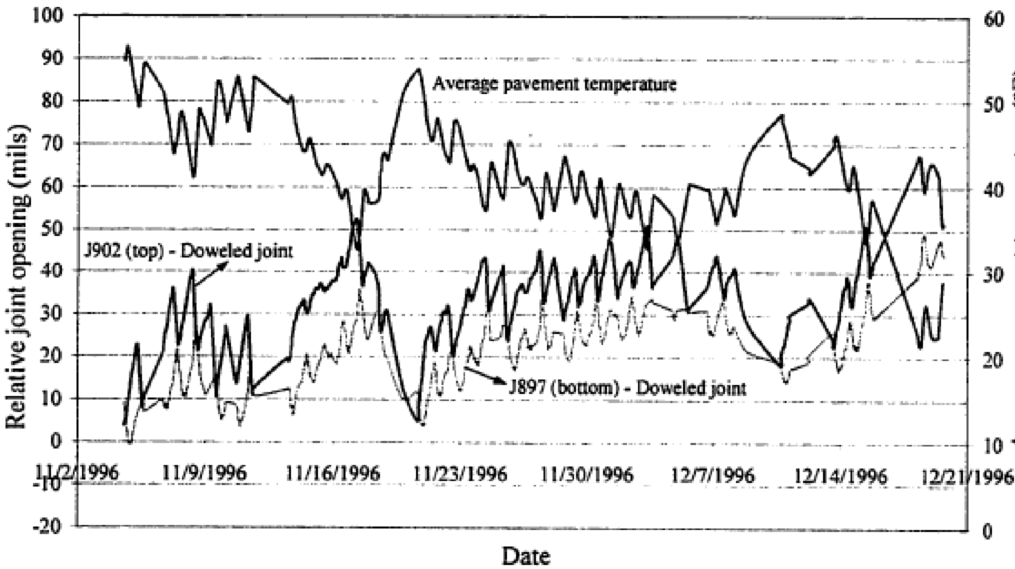

FIGURE 6.13. JOINT OPENINGS IN WINTER OVER A 7 WEEK PERIOD FOR DOWELED JOINTS AT DIA (RUFINO 2003).

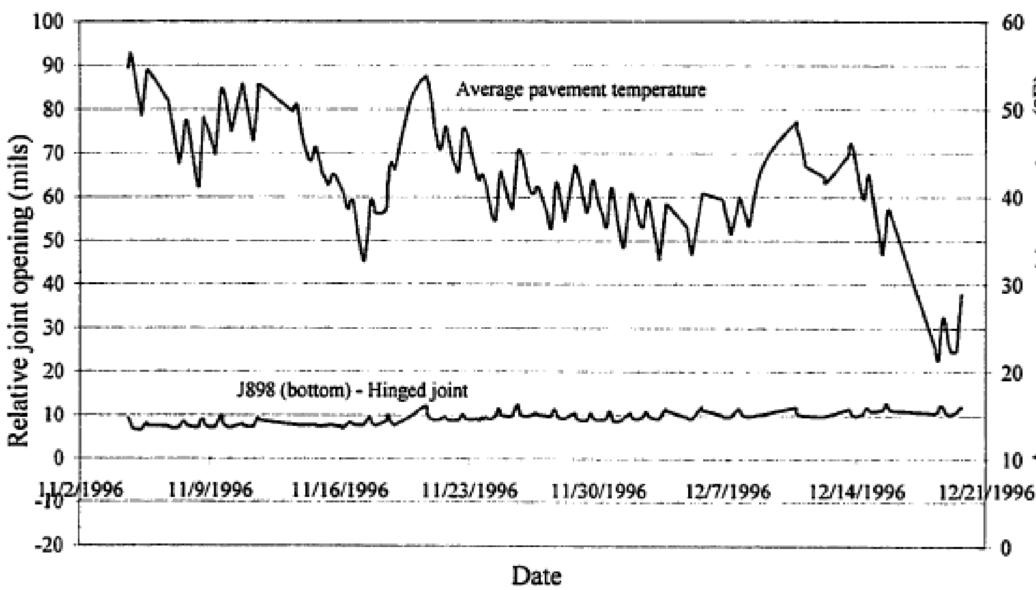

FIGURE 6.14. JOINT OPENINGS IN WINTER OVER A 7 WEEK PERIOD FOR TIED JOINTS AT DIA (RUFINO 2003).

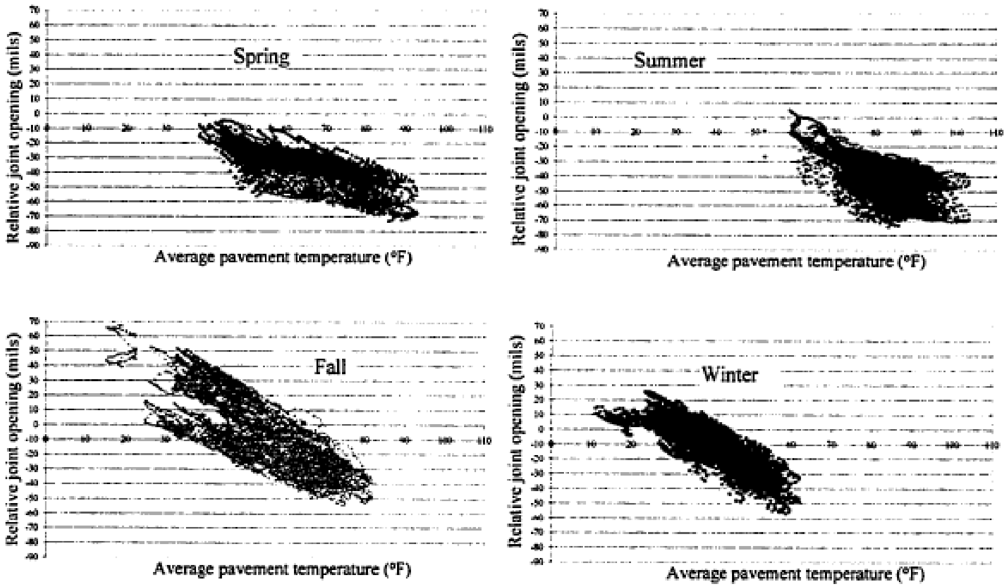

FIGURE 6.15. JOINT OPENINGS SEPARATED BY SEASON FOR DOWELED JOINTS AT DIA (RUFINO 2003).

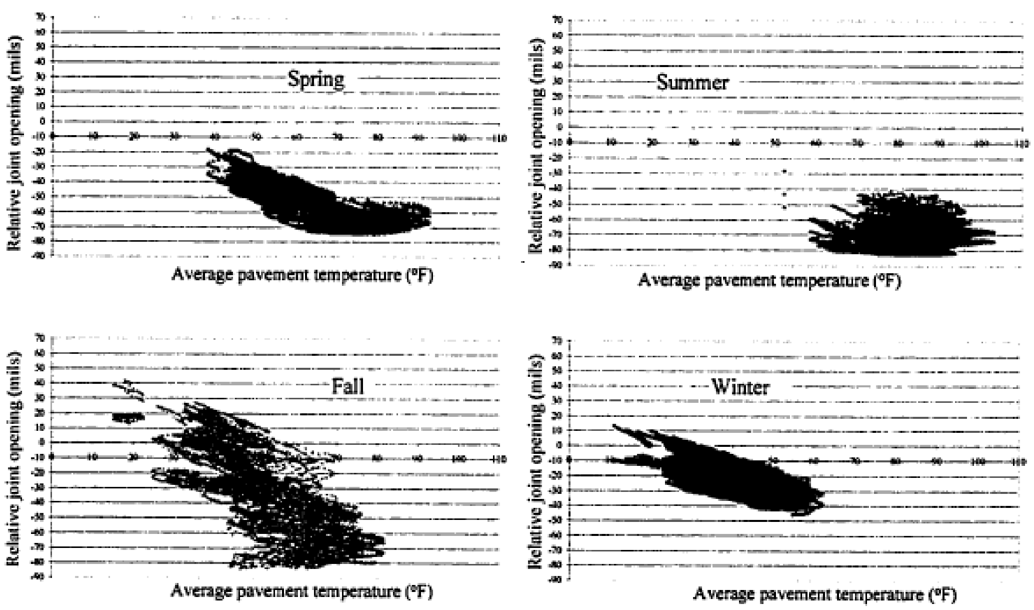

FIGURE 6.16. JOINT OPENINGS SEPARATED BY SEASON FOR AGGREGATE INTERLOCK JOINTS AT DIA (RUFINO 2003).

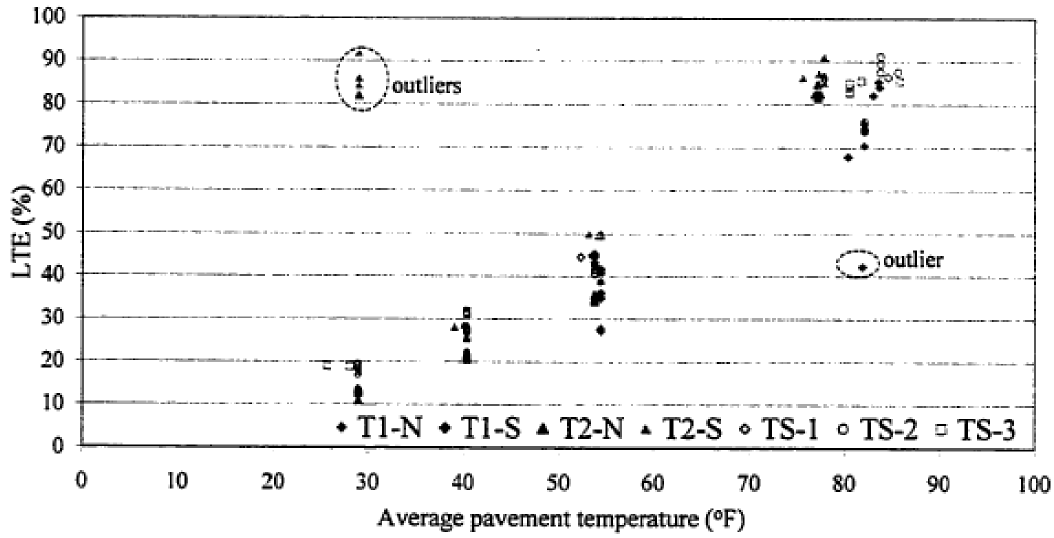

FIGURE 6.17. VARIATION OF LTE_{δ} WITH AVERAGE PAVEMENT TEMPERATURE FOR AGGREGATE INTERLOCK JOINTS AT DIA (RUFINO 2003).

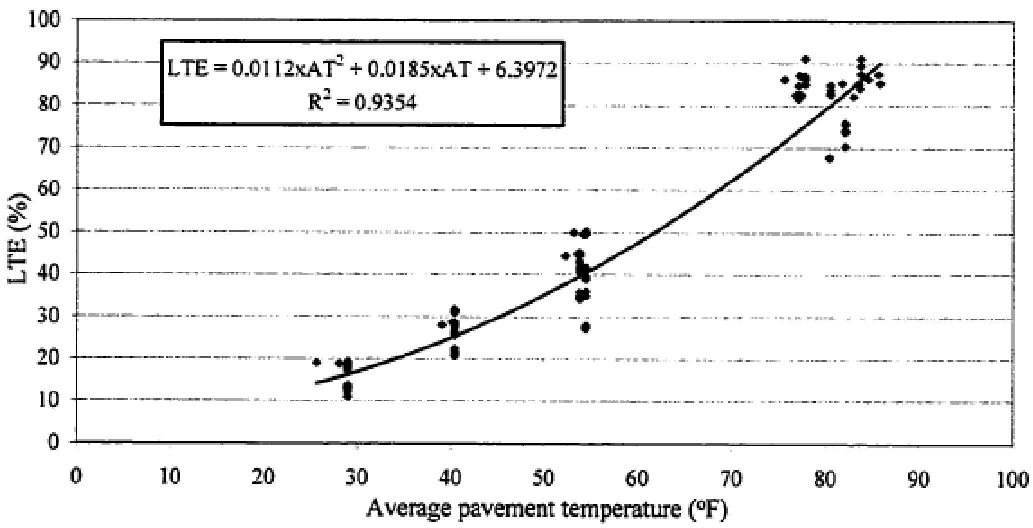

FIGURE 6.18. RELATIONSHIP BETWEEN LTE_{δ} AND AVERAGE PAVEMENT TEMPERATURE FOR AGGREGATE INTERLOCK JOINTS AT DIA (RUFINO 2003).

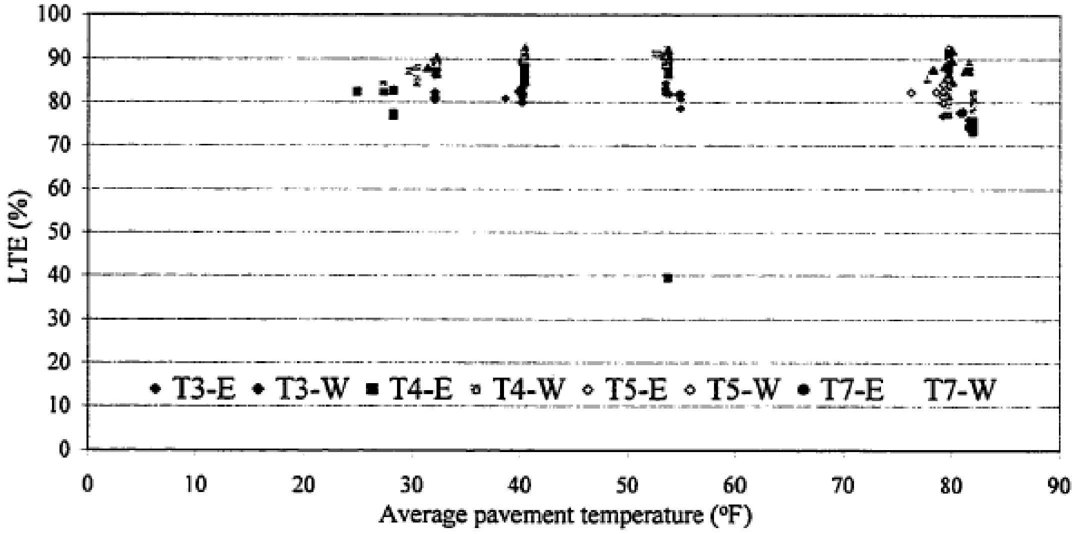

FIGURE 6.19. RELATIONSHIP BETWEEN LTE_{δ} AND AVERAGE PAVEMENT TEMPERATURE FOR TIED JOINTS AT DIA (RUFINO 2003).

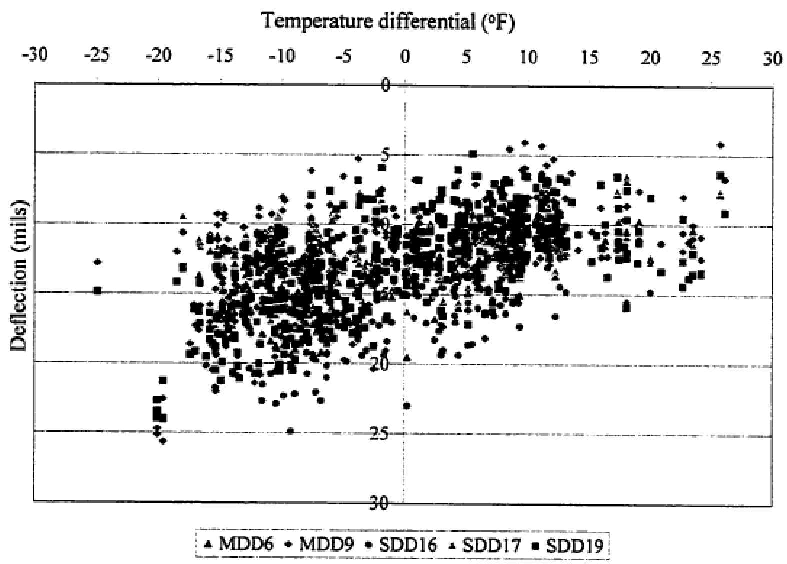

FIGURE 6.20. MEASURED DEFLECTIONS VS. TEMPERATURE DIFFERENTIAL FOR B-727 AT AGGREGATE INTERLOCK TRANSVERSE JOINTS (RUFINO 2003).

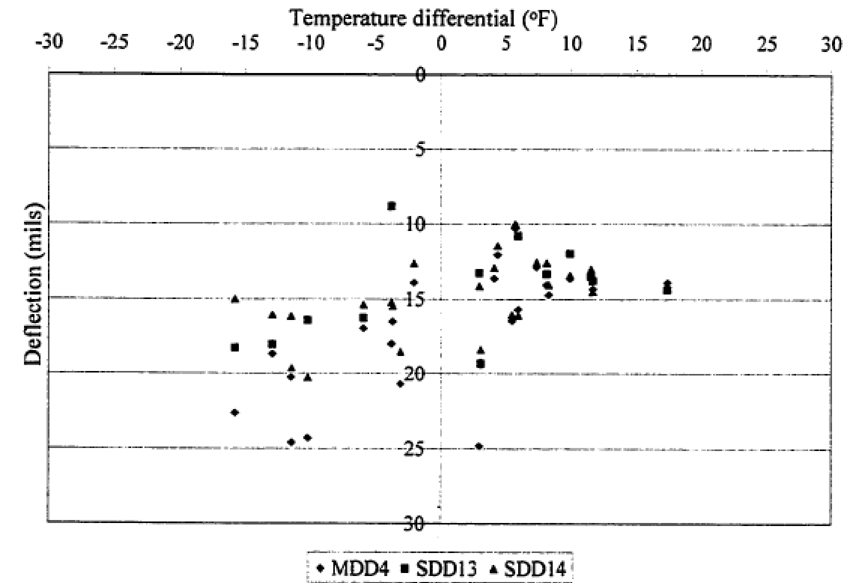

FIGURE 6.21. MEASURED DEFLECTIONS VS. TEMPERATURE DIFFERENTIAL FOR B-727 AT A CORNER (RUFINO 2003).

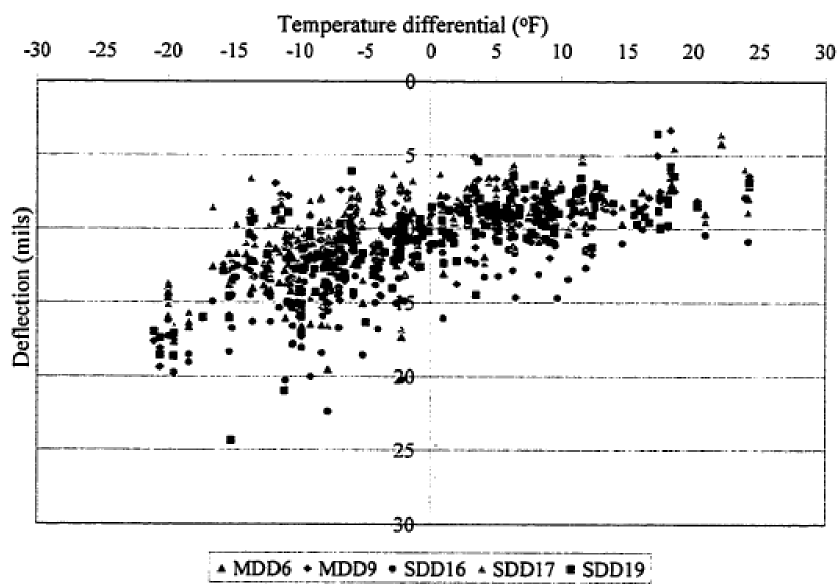

FIGURE 6.22. MEASURED DEFLECTIONS VS. TEMPERATURE DIFFERENTIAL FOR A B-737 AT A TRANSVERSE JOINT (RUFINO 2003).

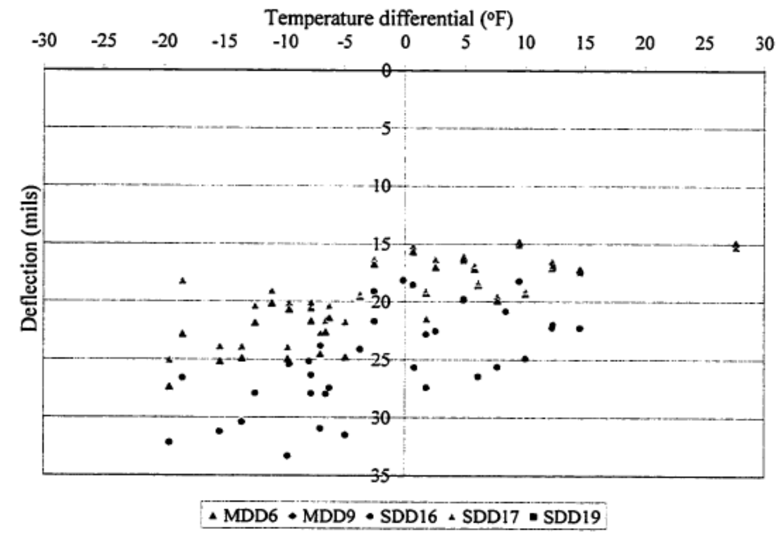

FIGURE 6.23. MEASURED DEFLECTIONS VS. TEMPERATURE DIFFERENTIAL FOR A DC-10 AT A TRANSVERSE JOINT (RUFINO 2003).

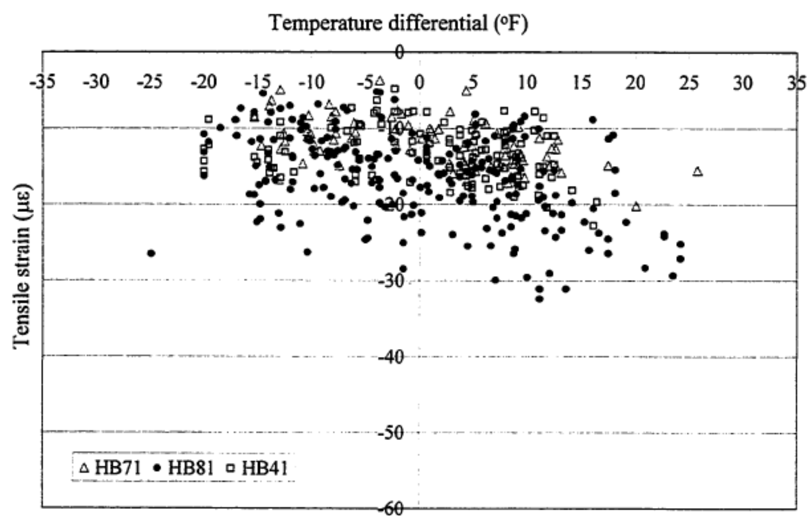

FIGURE 6.24. STRAIN VS. TEMPERATURE DIFFERENTIAL AT THE INTERIOR FOR A B-727 LOADING (RUFINO 2003).

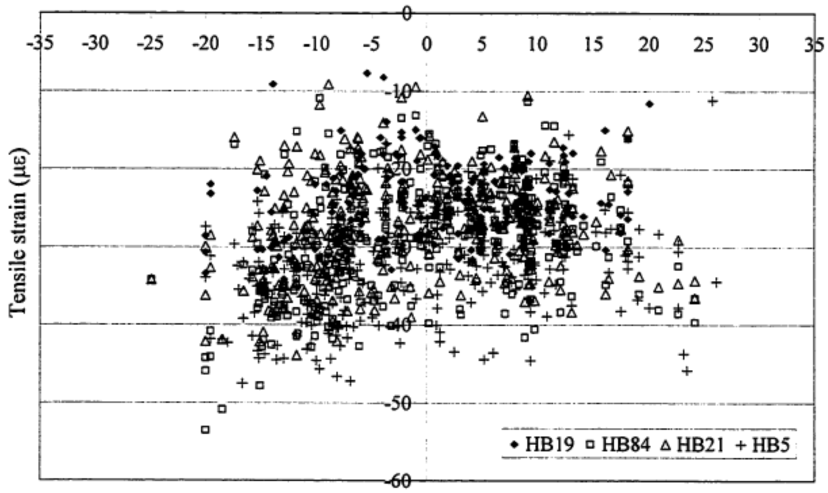

FIGURE 6.25. STRAIN VS. TEMPERATURE DIFFERENTIAL AT AN AGGREGATE INTERLOCK TRANSVERSE JOINT DUE TO A B-727 LOADING (RUFINO 2003).

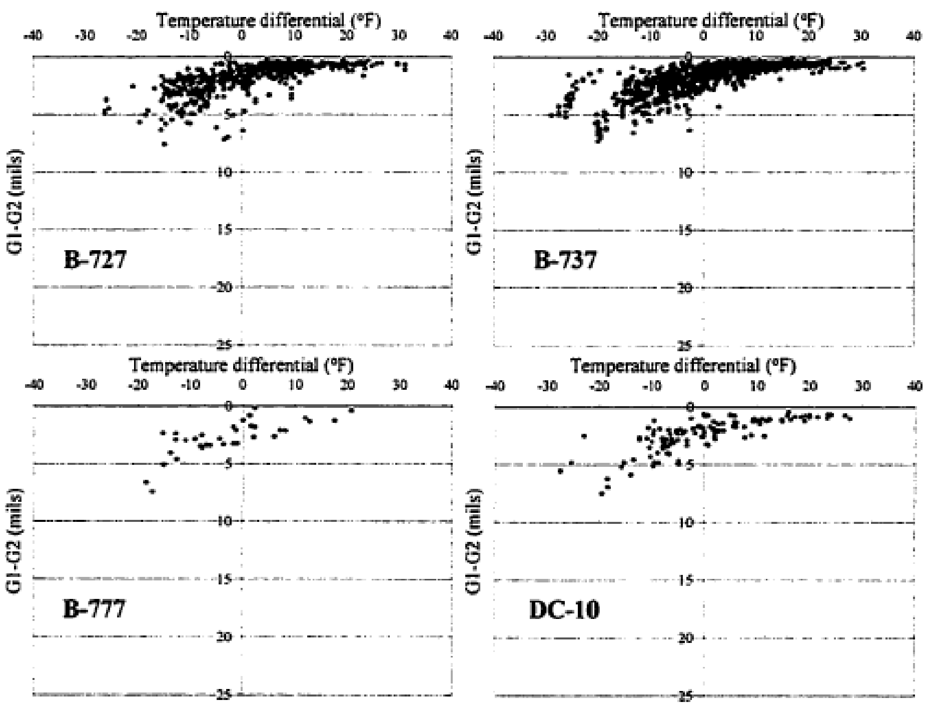

FIGURE 6.26. GAP COMPARISONS AT TRANSVERSE AGGREGATE INTERLOCK JOINTS FOR VARIOUS AIRCRAFTS AT DIA (RUFINO 2003).

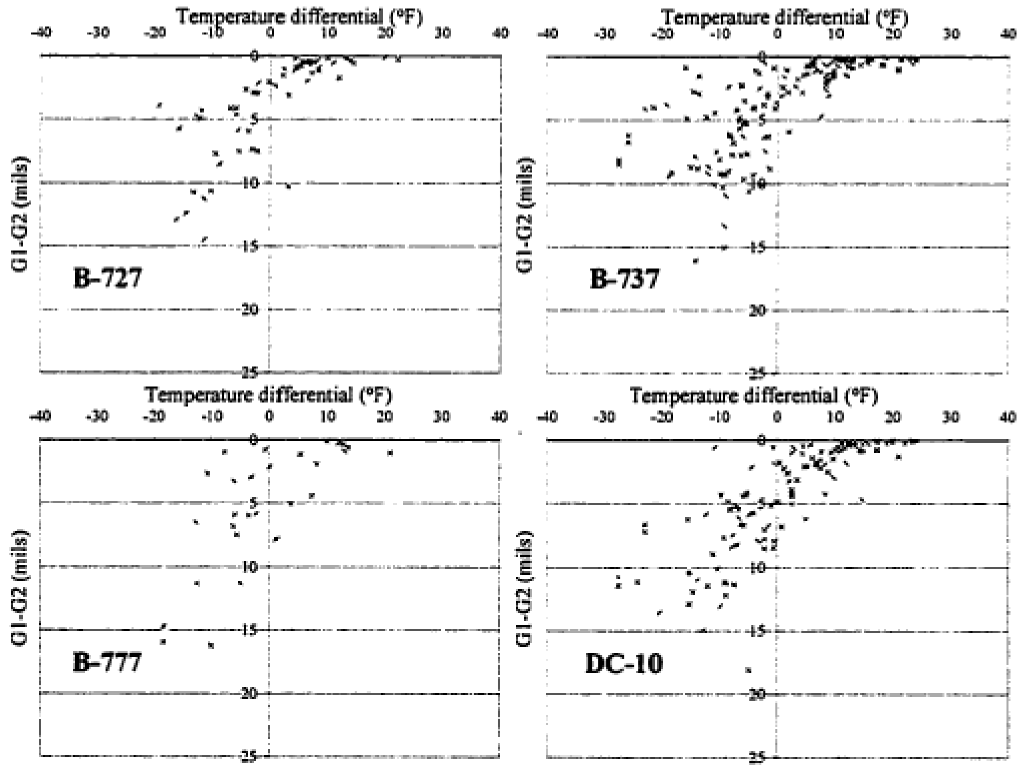

FIGURE 6.27. GAP COMPARISONS AT CORNER FOR VARIOUS AIRCRAFTS AT DIA (RUFINO 2003).

6.4 RESEARCH BY TELLER AND SUTHERLAND

Teller and Sutherland (1936) performed some of the first detailed studies of PCC slab and joint behavior. A focus of their study was the interaction of climate and daily thermal changes on joint and slab behavior. These experiments were designed to compare actual finite slab behavior to theoretical behavior models developed by Westergaard in the 1920's. Figures 6.28 shows the daily changes in joint openings, with negative values indicating the closure of the joint. Figure 6.29 shows the annual changes in joint openings observed by them, with positive values indicating joint opening and negative values indicating joint closing. Figure 6.30 shows the daily maximum day-time thermal curling deflections observed by them showing how joints had similar curling to free edges indicating very little moment resistance offered by joints relative to slab curling moments.

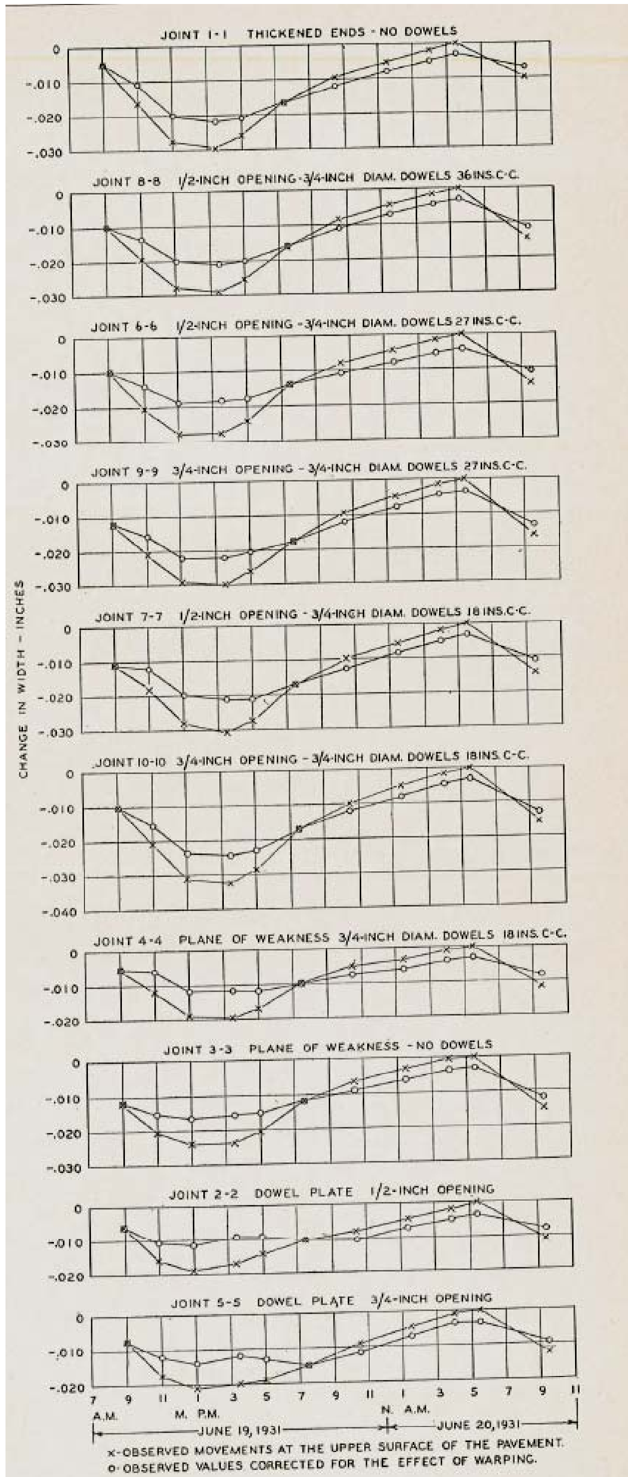

FIGURE 6.28. DAILY CHANGES IN JOINT OPENINGS OBSERVED BY TELLER AND SUTHERLAND (1936).

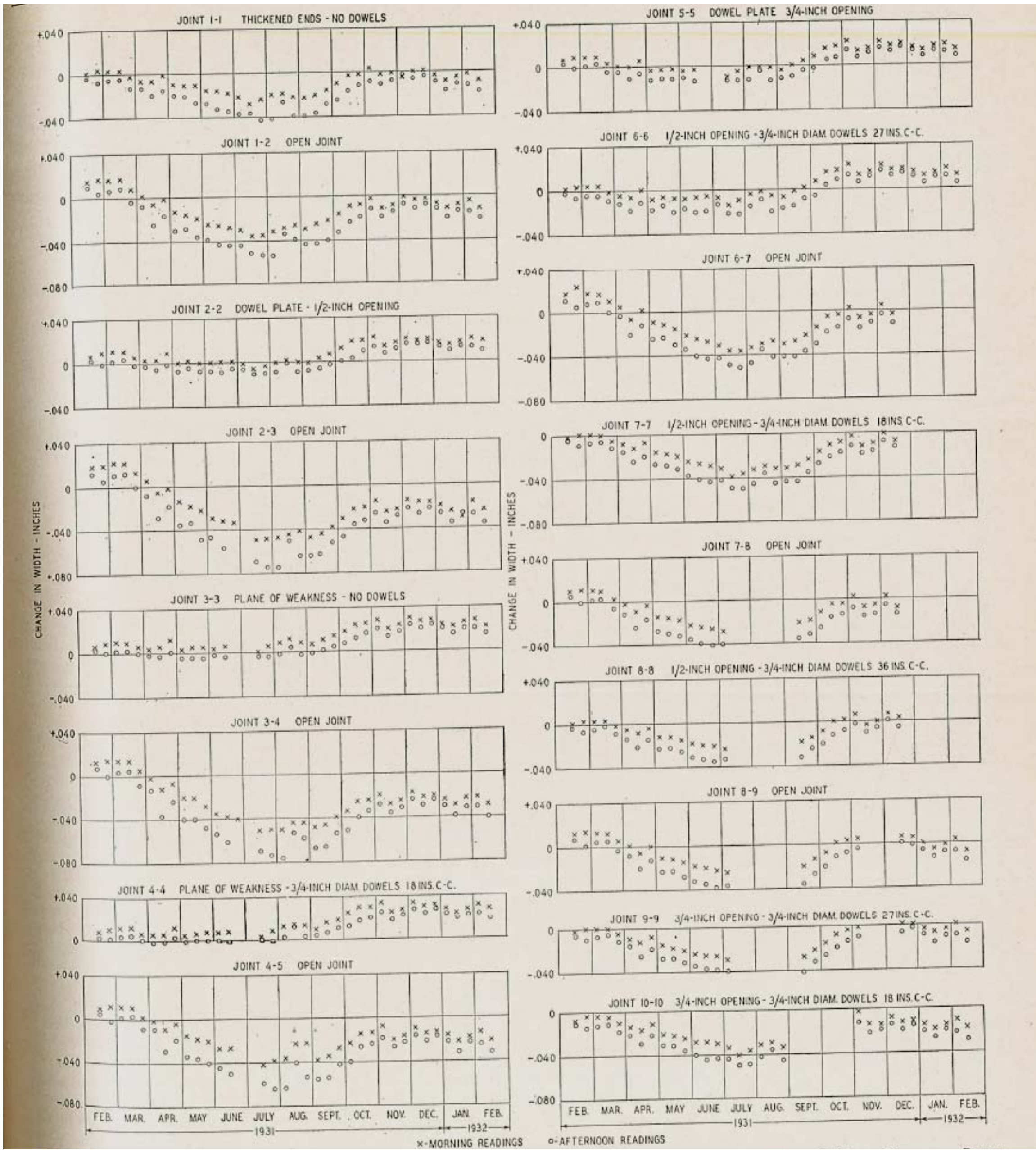

FIGURE 6.29. ANNUAL CHANGES IN JOINT OPENINGS OBSERVED BY TELLER AND SUTHERLAND (1936).

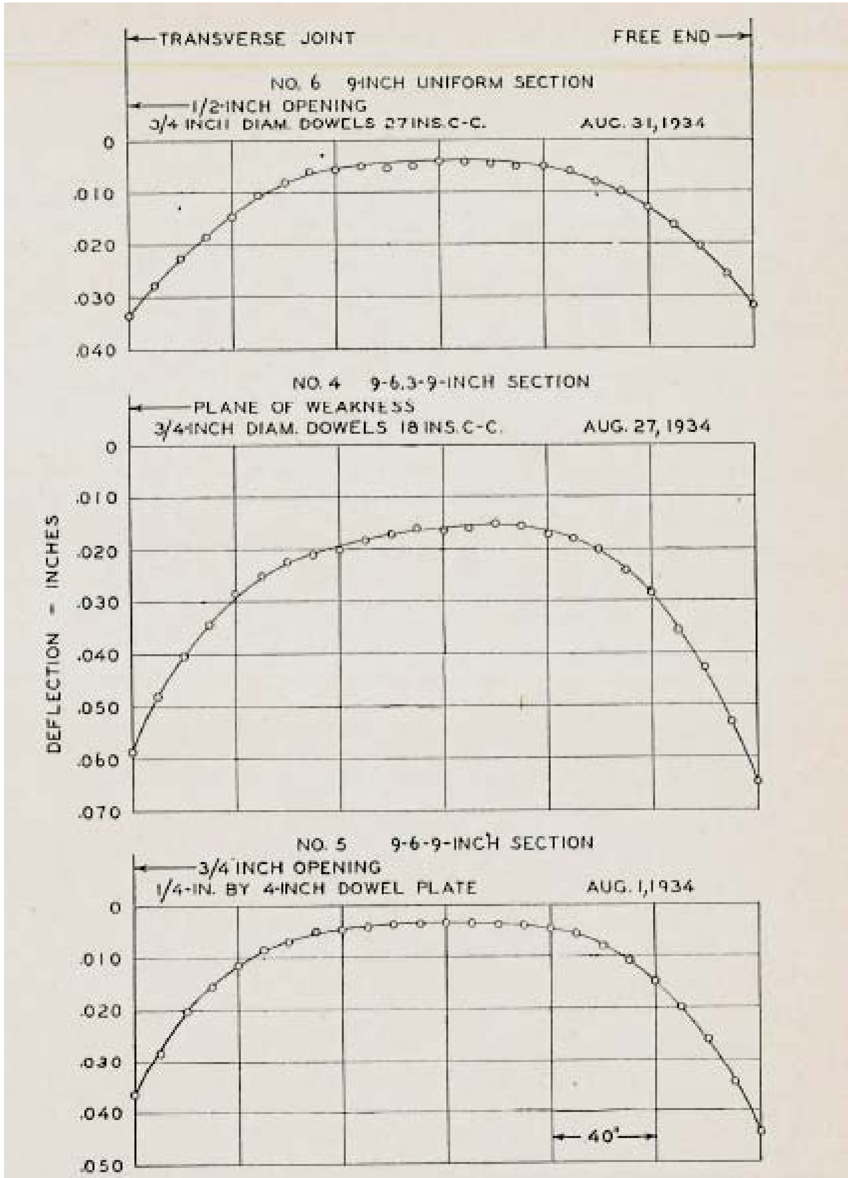

FIGURE 6.30. DAILY MAXIMUM DAY-TIME THERMAL CURLING DEFLECTIONS OBSERVED BY TELLER AND SUTHERLAND (1936).

6.5 JAPANESE STUDY

Perhaps the most interesting recent study regarding climate effects on thick slabs versus thin slabs was a study performed by Nishizawa et al. (2009). Nishizawa presented a new method for predicting thermal gradients in slabs of various thicknesses and used FE modeling and a field test site to evaluate and verify the new model. He was using a new tool to evaluate the long standing assumption in Japan that the non-linear thermal gradient effect causes a 30% reduction in edge stress that was established by Iwama (1966) based on Timoshenko's model for gradients. The non-linear gradient affect was recognized early by airfield pavement researchers (Pringle 1950). This Nishizawa et al. (2009) model is perhaps the most capable model for predicting temperature gradients in PCC pavements that has been developed to date

Figures 6.31 shows the test layout used by Nishizawa et al. (2009) and also shows an overall view of the test site.

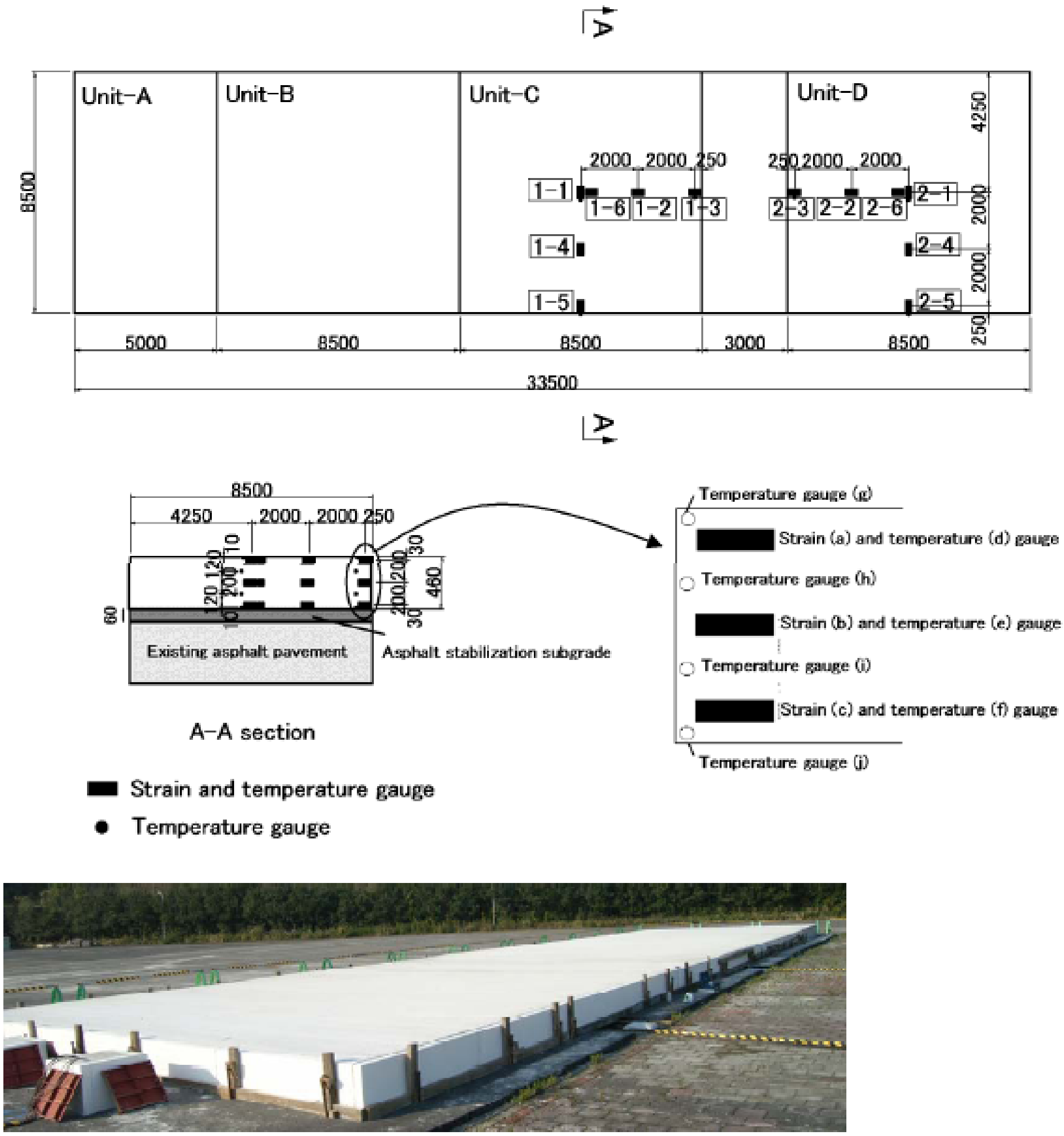

FIGURE 6.31. TEST SITE LAYOUT (NISHIZAWA ET AL 2009).

Figure 6.32 shows a key finding from the study. It shows the apparent effects of combined thermal stress and subgrade drag on the total tensile stress. During the heat of the day, there was significant internal subgrade drag compression in the slab that was counteracting the tension at bottom of slab caused by curling stress. Using strain gages, Nishizawa showed that the subgrade drag effect tended to pull the peak tensile stress multiplier to be out later in the afternoon relative to the time of peak thermal gradient.

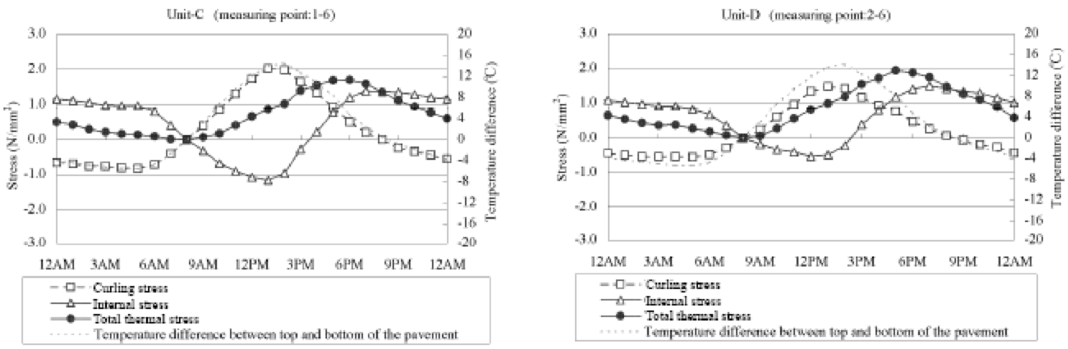

FIGURE 6.32. THERMAL STRESSES MEASURED FOR THICK (RIGHT) VERSUS THIN (LEFT) SLABS (NISHIZAWA ET AL. 2009).

Figure 6.33 shows their thermal gradient model predictions as a function of slab thickness for the same thermal input at the top of slabs. Clearly the upper 300 mm shows a large change in the thermal gradients for all slab thicknesses. Figure 6.34 shows measured versus predicted restraint strain gradients.

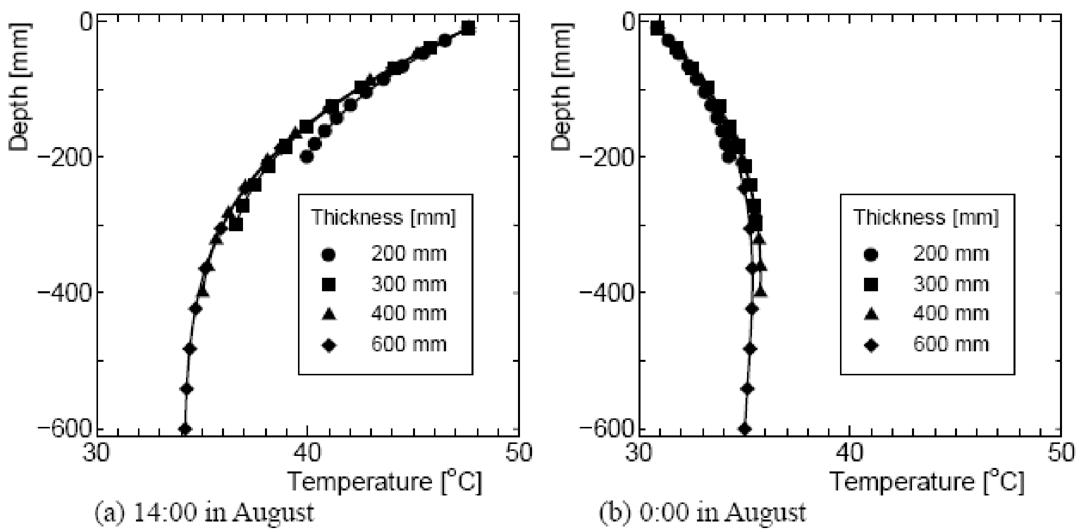

FIGURE 6.33. THERMAL GRADIENT SHAPES FOR THIN VERSUS THICK SLABS (NISHIZAWA ET AL 2009).

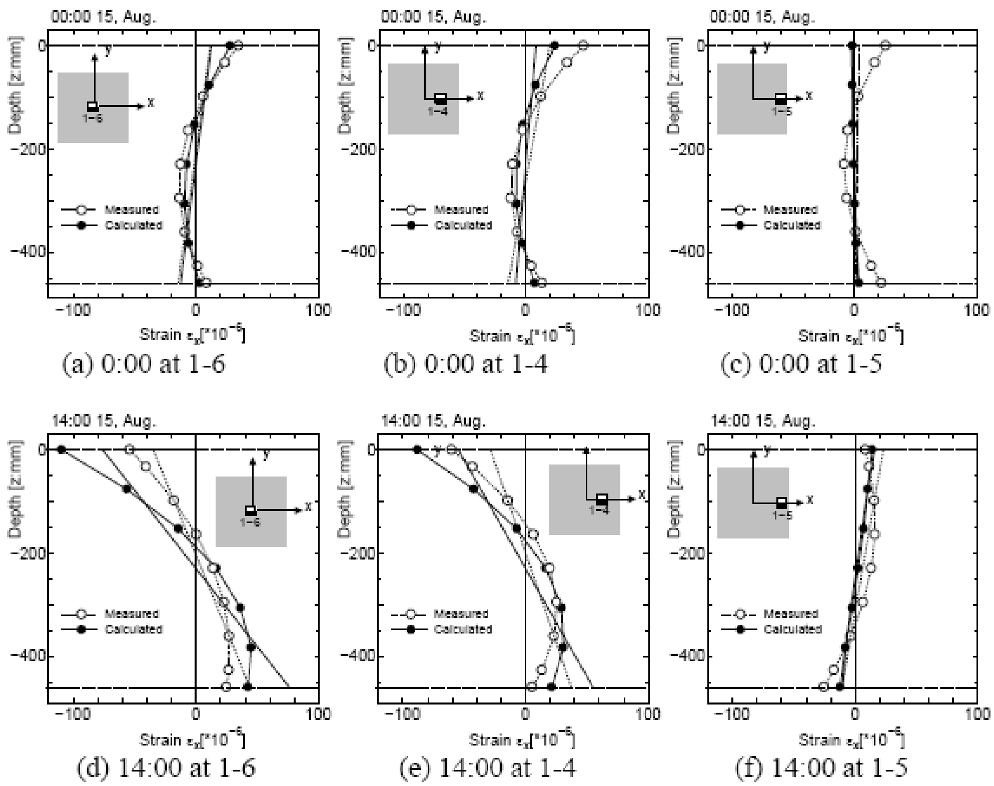

FIGURE 6.34. COMPARISON OF MEASURED AND CALCULATED RESTRAINT STRAIN (INTERNAL STRESS) AT DIFFERENT POSITIONS IN THE SLABS (NISHIZAWA ET AL 2009).

Figures 6.35 to 6.37 show perhaps the most interesting plots from Nishizawa et al. (2009). Figure 6.35 shows how a linear and a non-linear temperature distribution affect the total tensile stress at the outer bottom edge of a slab for various slab thicknesses. Figure 6.36 shows the effect of slab thickness on thermal stress distribution. This figure shows in general the effective linear portion of the thermal gradient is significantly larger in magnitude for thinner slabs, given the same thermal input at the top of slab. Figure 6.37 shows the effect of slab thickness on the daily maximum thermal stress. This figure shows that slabs having a thickness of about 400 mm are most sensitive to thermal gradient related stresses, when compared to slabs thicker or thinner than this value.

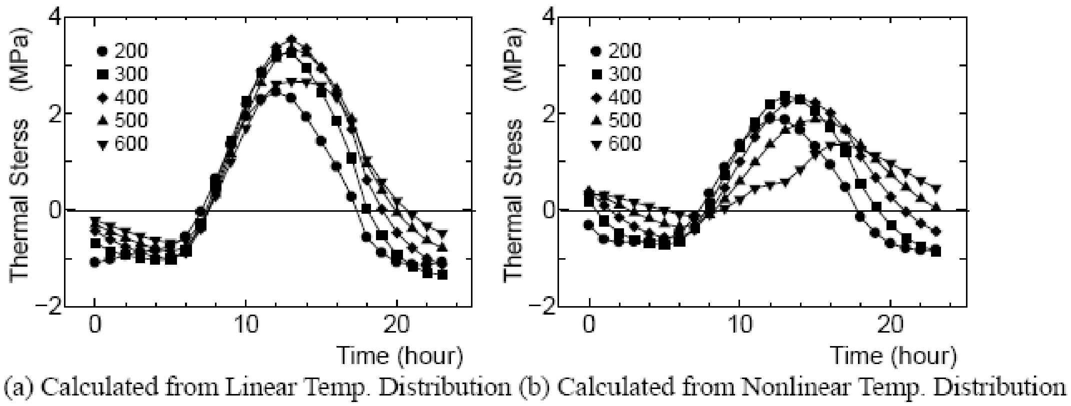

FIGURE 6.35. THERMAL STRESS MAGNITUDES FOR VARIOUS SLAB THICKNESSES PREDICTED FROM LINEAR THERMAL GRADIENTS (LEFT) AND NON-LINEAR THERMAL GRADIENTS (RIGHT), NISHIZAWA ET AL. (2009).

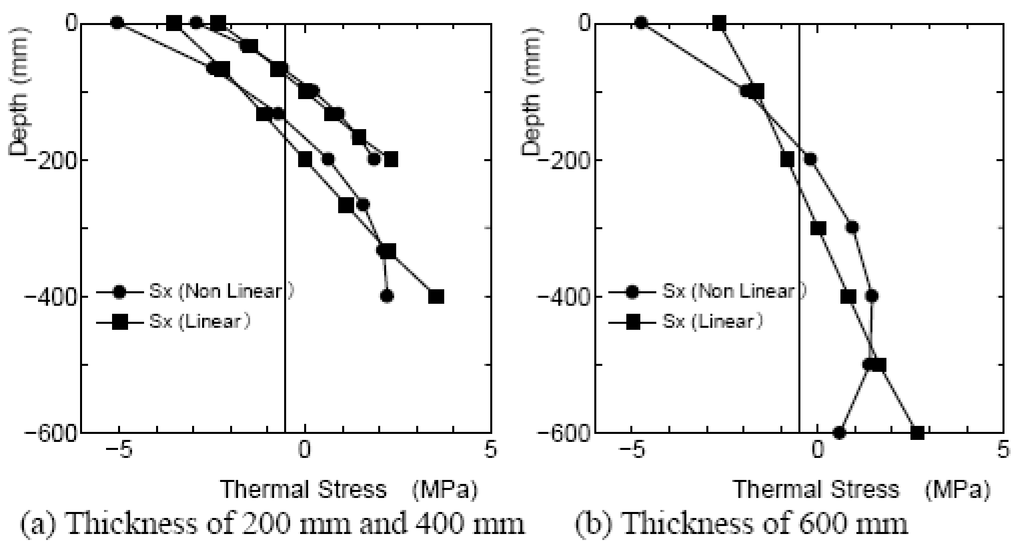

FIGURE 6.36. EFFECT OF SLAB THICKNESS ON THERMAL STRESS DISTRIBUTION FOR LINEAR AND NON-LINEAR THERMAL GRADIENT MODELS, NISHIZAWA ET AL. (2009).

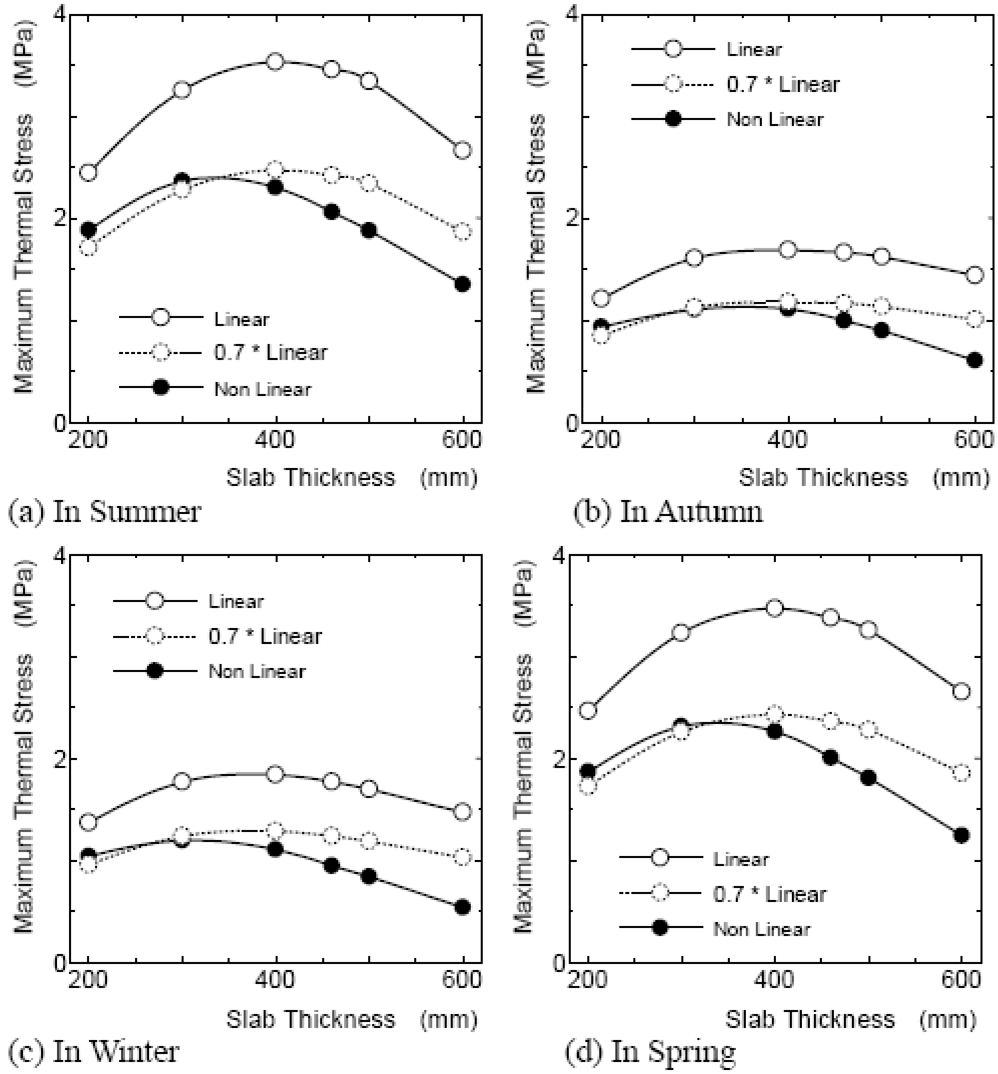

FIGURE 6.37. EFFECT OF SLAB THICKNESS ON DAILY MAXIMUM THERMAL STRESS, NISHIZAWA ET AL. (2009).

CHAPTER 7: SUMMARY OF KEY VARIABLES AFFECTING LOAD TRANSFER

Based on an extensive literature review and considering FWD analyses and available instrumentation data, the following list of variables are the key variables related to the load transfer characteristics of joints and cracks. The list is divided into two sections. The first section contains the key primary variables that control the load transfer value from a mechanistic perspective. The second part of the list includes important secondary variables that in a sense cause variation of the key primary mechanistic variables.

7.1 PRIMARY VARIABLES AFFECTING LOAD TRANSFER AT JOINTS IN PCC PAVEMENTS

1. ***Joint Opening:*** This is the primary factor controlling the joint stiffness for aggregate interlock joints that do not have dowels for transferring the load. At temperatures significantly below the casting temperatures of the PCC panels, the joints will open significantly and lose the ability to transfer loads. As pavements age and go through repeated summer thermal expansion cycles, the slabs will physically push themselves apart over time, causing a progressive opening of some joints. A proper jointing pattern can reduce progressive opening of joints. In general, over time, the contraction joints will progressively open, and the expansion joint areas will progressively close, and outer edges of the pavement system will be pushed further outward.

2. ***Joint Shear Face Roughness:*** The nature of the toughness and irregularity of the crack that forms through the sawcut joints will control how the joint responds to changes in joint opening. For example, a PCC mixture with soft aggregates may tend to crack through aggregates, rather than around aggregates, developing a smoother crack surface and resulting in greater sensitivity of the joint to loss of load transfer capability as a result of increases in joint opening.

3. ***Reinforcement Across the Joint***: Reinforcement provided across the joint (e.g., dowels) can resist the loss of load transfer during cold weather that results from opening of the joints related to thermal contraction of the slab. Deformed bar type reinforcement (i.e., tie bars) can prevent joints from opening during winter months and during contraction of the joints that occur during the early morning hours. Reinforcement provided across the joint works in combination with joint shear face roughness in the overall total joint stiffness response. When joint opening becomes large enough to eliminate joint face roughness contribution, the reinforcement and its embedment zone support condition are the only shear load transfer mechanism. The shear transfer mechanisms associated with the dowel or tie bar interaction with the concrete are complex. In general if the reinforcement across the joint is spaced too far apart or has too small of a diameter for the type of loads at a site, the stress levels between the reinforcement and the PCC will be larger and some crushing and permanent deformation of the embedment interaction zone will occur, resulting in looseness around the reinforcements. This looseness will show up as reduced stiffness or non-linear stiffness having some apparent slack, reducing the ability of the joint to transfer stress and reduce bending stress levels in the loaded slab.

4. ***Slab Thickness:*** There appears to be a general trend of lower achievable stress load transfer between slabs as the slab thickness increases. This may be related to the fact that flexural rigidity of slabs increases in proportion with the slab thickness cubed, while the available joint shear area only increases in proportion to slab thickness, to the power of one.

5. ***Slab Curvature***: Slab curvature caused by thermal gradient related expansion and contraction of the PCC is defined as curling. Slab curvature caused by any other mechanisms such as moisture gradient, curing, construction temperatures, cumulative slab moment creep, base moisture supply is defined as warpin***g***. Curling is well understood and can be reliably modeled. Warping remains a mystery and is one of the largest gaps of knowledge between real slab behavior and our ability to model slab behavior. In general, warping can become extreme in PCC slabs. In dry climates slabs may develop an up-warp condition that far exceeds afternoon down-curl magnitudes, resulting in slabs that never actually have any downward curvature during the most extreme of daytime thermal gradient conditions. Curling can have a large effect on load transfer for highway slabs, especially slabs that have significant up-warp and joint lift-off from the foundation during the early morning pre-sunrise hours when thermal gradients are most extreme.

6. ***Load Magnitude***: Load magnitude can significantly affect the load transfer value, with load transfer generally increasing with FWD load magnitude. This is explained by the presence of some slack in the joints.

7. ***Base and Foundation Type:*** Significant difference in joint behavior will exist for bound versus unbound bases, especially during the early life of the pavement before fatigue affects the base at the joints. For strong bound bases such as lean concrete or cement treated aggregate bases that may act as a buried cracked slab, the base may act with the slab in load transfer shear area for quite some time effectively increasing the top slab effective thickness value. For softer bound bases such as asphalt treated aggregates, the effect may not be similar to having additional slab thickness, but the effect may be more like a subgrade change to an elastic solid type subgrade.

7.2 SECONDARY VARIABLES (SIGNIFICANT CAUSE FACTORS FOR PRIMARY VARIABLES)

1. ***Air Temperature:*** The ambient air temperature, or typical daily change in air temperature, is the primary cause for changes in the joint opening size and the slab curvature changes from curling caused by thermal gradients.

2. ***Annual Precipitation:*** In highway slabs, the average warping was found to be related to annual precipitation. Flatter slabs and smaller joint openings are associated with higher and more uniform precipitation rates. The average warp magnitude at sites having 45 inches of annual precipitation develop slab curvature equal to that caused by a 2°F/inch thermal gradient. Dry climate sites with 5 to 10 inches of annual precipitation are likely

to have panels that are up-warped possibly lifting joints off of the foundation with equivalent thermal gradient shapes corresponding to about a 3.5°F/inch thermal gradient. Annual precipitation may also be related to joint opening sizes where a trend of slightly larger joint openings in drier climates would be expected.

3. ***Slab Length Relative to Thickness***: At the same given slab thickness, longer panels in general will develop larger joint openings and have greater deflections in response to daily curling temperature gradients. In the context of slab modeling, the dimensionless ratio of the slab length to the radius of relative stiffness value *(L/ι)* is often used to describe slab geometry. There is a critical slab length for a given combination of radius of relative stiffness and slab length values. When slab length is about 8.5 times the radius of relative stiffness, the joint movement response and the mid slab stress levels will be a maximum for thermal responses. Slabs shorter than this will have reduced joint movements and reduced internal stresses for a given thermal gradient magnitude.

4. ***Load Positions/Configuration***: Included in this consideration would be top-down versus bottom-up fatigue crack analyses and consideration of slab curvature from curling and warping. An important concept frequently overlooked for top versus bottom of slab stress, is that for top of slab stress fatigue accumulation, there are two maximum top of slab stress spikes at roughly the mid slab position for the passing of one wheel load across a slab, each time the heavy wheel crosses the joints at each end of the slab. Only one maximum bottom of slab tensile stress occurs and it is beneath the wheel load.

5. ***Joint Age/Traffic:*** The joint will experience progressive loosening and gap development over its life, resulting in a loss of stiffness and non-linear stiffness, where little to no stiffness may be present for smaller loads near the end of the service life. There is some data from highway slabs indicating that PCC mixtures having relatively high stiffness or modulus, while having relatively low tensile strength (i.e. low strain capacity PCC) compared to average PCC strength to stiffness ratios can lose aggregate interlock more quickly and fault more quickly over time that average pavements. Durability related distress is almost certainly correlated to more rapid loss of load transfer toughness and interlock along joint and crack faces.

8. BIBLIOGRAPHY

Advisory Circular AC 150/5320-6D (1995), with four official changes. Federal Aviation Administration.

Advisory Circular AC 150/5320-6E (2010). Federal Aviation Administration.

Ahlvin, R. G. (1991). "Origin of Developments for Structural Design of Pavements", Technical Report GL-91-1, USAE Waterways Experiment Station, Vicksburg, MS.

Ahlvin, R. G. et al. (1971). "Multiple-Wheel, Heavy Gear Load Pavement Tests", Technical Report No. S-71-1, 5 volumes, USAE Waterways Experiment Station, Vicksburg, MS.

Armaghani J.M., Lybas J.M., Tia M., Ruth B.E., (1986). "Concrete Pavement Joint Stiffness Evaluation". *Transportation Research Record 1099*, TRB.

Barenberg E. J. and R. E. Smith. (1979). "Longitudinal Joint Systems in Slip-Formed Rigid Pavements, Vol. I: Literature Survey and Field Inspection" Report No. FAA-RD-79-4-I, Federal Aviation Administration, Washington, D.C.

Barenberg, E.J. Arntzen, D.M. (1981). "Design of Airport Pavement as Affected by Load Transfer and Support Conditions". Proceedings of the Second International Conference on Concrete Pavements. Purdue University.

Barker W.R. (1981). "Introduction to a Rigid Pavement Design Procedure". Proceedings of the Second International Conference on Concrete Pavements. Purdue University.

Bradbury, R.D. (1938). "Reinforced Concrete Pavements", Wire Reinforcement Institute, Washington, DC.

Brill, D.R. (1998). "Development of Advanced Computational Models for Airport Pavement Design". DOT/FAA/AR-97/47. US DOT Office of Aviation Research.

Brill, D.R. (2010). "Calibration of FAARFIELD Rigid Pavement Design Procedure". DOT/FAA/AR-09/57. Office of Research and Technology Development, Washington, DC 20591.

Bush III, A.J. Hall, J.W. (1981). "Experience with Nondestructive Structural Evaluation of Airport Pavements". Proceedings of the Second International Conference on Concrete Pavements. Purdue University.

Bush III, A.J., Alexander, D.R., Hall, J.W. (1985). "Nondestructive Airfield Rigid Pavement Evaluation". Proceedings of the Third International Conference on Concrete Pavements. Purdue University.

Bush III, A.J., Brown, W.R., Bailey, C.E. (1989). "An Evaluation Procedure for Rigid Airfield Pavements". Proceedings of the Fourth International Conference on Concrete Pavements. Purdue University.

Byrum, C.R., Hansen W., Kohn S.D. (1997) "The Effects of Strength and Other Properties on the Performance of PCC Pavements". Proceedings of the Sixth International Conference on Concrete Pavements Design and Materials for High Performance. Purdue University, Nov. 18-21, 1997.

Byrum, C.R. (2009) "Measuring Curvature in Concrete Slabs and Connecting the Data to Slab Modeling Theory". *Transportation Research Record 2094*, Transportation Research Board, National Academy Press, Washington DC.

Byrum, C.R. (2007) "Evaluation of Pavement Slab Rocking and Pumping using Elevation Profile Data". *Transportation Research Record 1947*, Transportation Research Board, National Academy Press, Washington DC.

Byrum, C.R. (2000). "A High Speed Profiler Based Slab Curvature Index for Jointed Concrete Pavement Curling and Warping Analyses". Ph.D. Dissertation, University of Michigan, 2001.

Byrum, C.R. (2001). "The Effect of Locked-in Curvature on Pavement Performance". Published in a book titled, "Long-Term Pavement Performance: Making Something of It". Edited by R.G. Hicks and J. B. Sorenson. American Society of Civil Engineers, 2001.

Byrum C.R., and Hansen, W. (1994) *An Influence Function Approach to Analysis of Jointed Concrete Pavement.* Transportation Research Record, No. 1449, Transportation Research Board, National Research Council.

Crovetti, J.A. (1994). "Design and Evaluation of Jointed Concrete Pavement Systems Incorporating Open-Graded Permeable Bases". PhD Dissertation, University of Illinois at Urbana-Champaign

Department of Defense. (2001). "Pavement Design for Airfields" UFC 3-260-02, Washington, DC.

Fine, Lenore and Remington (1972). "The US Army in WWII: The Corps of Engineers: Construction in the United States", Office of the Chief of Military History, US Army, Washington, D.C.

Finney, E., Oehler, L. (1959). "Final Report- Design Project Michigan Test Road". Michigan State Highway Department Report No. 302, Project No 39 F-7(2).

Gillespie, T. D. et al. (1993). "Effects of Heavy-Vehicle Characteristics on Pavement Response and Performance". NCHRP Report 353, TRB National Research Council. Washington D. C.

Grau, R. W. (1972). "Strengthening of Keyed Longitudinal Construction Joints in Rigid

Pavements" Miscellaneous Paper S-72-43. US Army Engineer Waterways Experiment Station, Vicksburg, MS.

Guo, H., Larson, R.M., Snyder, M.B. (1993). "A Non-Linear Mechanistic Model for Dowel Looseness in PCC Pavements". Proceedings of the Fifth International Conference on Concrete Pavements. Purdue University.

Hammons, M., D. Pittman, and D. Mathews. (1995). "Effectiveness of Load Transfer Devices" DOT/FAA/AR-95/80, Federal Aviation Administration, Washington, D.C.

Hammons, M. I (1998). "Advanced Pavement Design: Finite Element Modeling for Rigid Pavement Joints, Report II: Model Development". DOT/FAA/AR-97/7. US DOT Office of Aviation Research.

Hansen, W. et al. (1996). "The Effect of Higher Strength and Associated Concrete Properties on Pavement Performance (Interim Report)". FHWA DTFH61-95-R-00108.

Hutchinson, R. L. and P. Vedros (1977). "Performance of Heavy-Load Portland Cement Concrete (Rigid) Airfield Pavements" Proceedings of the 1st International Conference on Concrete Pavements, Purdue University, West Lafayette, IN.

Hutchinson, R. L. (1966). "Basis for Rigid Pavement Design for Military Airfields", Miscellaneous Paper No. 5-7, USAE Ohio River Division Laboratory, Cincinnati, OH.

Ioannides, A. M. and M. I. Hammons. (1996). "Westergaard-Type Solution for Edge Load Transfer Problem" *Transportation Research Record 1525*, Transportation Research Board, Washington, D.C.

Ioannides, A.M. and Khazanovich, L., "Nonlinear Temperature Effects on Multi-Layered Concrete Pavements," *Journal of Transportation Engineering*, ASCE, 124, 2, (Mar./Apr., 1998): 128-136.

Jensen, E.A., Hansen, W. (2001). "Mechanism of Load Transfer Crack Width Relation in JPCP: Influence of Coarse Aggregate Properties". Proceedings of the Seventh International Conference on Concrete Pavements. Purdue University.

Jun, D.X., Ming, H.X., Jun, Z.J., (1997). "The Loss of Load Transfer Capacity at Joints of Airfield Concrete Pavements Under Repetitive Loads". Proceedings of the Sixth International Conference on Concrete Pavements. Purdue University.

Kawa, I. et al. (2002) "Implementation of Rigid Pavement Thickness Design for New Pavements" Proceedings of the 2002 Airport Technology Transfer Conference. Federal Aviation Administration. May, 2002.

Kazuyuki, K., Nakagawa, S., Nishizawa, T., Kasahara, A. (1993). "Evaluation Method for Joint Load Transfer Efficiency in Concrete Pavements". Proceedings of the Fifth International Conference on Concrete Pavements. Purdue University.

Khazanovich L. Gotlif, A. (2003) "Evaluation of Joint and Crack Load Transfer- Final Report". FHWA-RD-02-088. National Technical Information Services, 2003.

Kohn, S.D. (1985). "Evaluation of the FAA Design Procedure for High Traffic Volume Rigid Pavements". Proceedings of the Third International Conference on Concrete Pavements. Purdue University.

Kohn, S.D., Gemayel, C.A., Alexander, D.R. Tons, E. (1989). "Development of a Thickness Design Procedure for Stabilized Layers under Rigid Airfield Pavements". Proceedings of the Fourth International Conference on Concrete Pavements. Purdue University.

Marsey, W., Dong, M. (2004) "Profile Measurements of Portland Cement Concrete Test Slab at the National Airport Test Facility". Proceedings of the 2004 FAA Worldwide Airport Technology Transfer Conference.

Mellinger, F. and P. Carlton. (1955). "Application of Models to Design Studies of Concrete Airfield Pavements" Proceedings of the 34th Annual Meeting, Highway Research Board, Washington, D.C.

Nishizawa, T., Koyanagawa, M., Takeuchi, Y., Kimura, M. (2001). "Study on Mechanical Behavior of Dowel Bar in Transverse Joint of Concrete Pavement". Proceedings of the Seventh International Conference on Concrete Pavements. Purdue University.

Nishizawa, T., Fukuda, T., Matsuno, S., (1989). "A Refined Model of Doweled Joints for Concrete Pavement using FEM Analysis". Proceedings of the Fourth International Conference on Concrete Pavements. Purdue University.

Nishizawa, T., Ozeki, T., Katoh, K., Matsui, K., (2009). "FEM Analysis of Thermal Stresses in Thick Airfield Concrete Slabs". Proceedings of the 88th Annual Meeting of the Transportation Research Board, pre-print CD ROM. The National Academies.

Owusu-Antwi, EB., Meyer, A.H., Hudson, W.R., (1989). "Preliminary Evaluation of Procedures for the Assessment of Load Transfer Across Joints and Cracks in Rigid Pavements using the Falling Weight Deflectometer". Proceedings of the Fourth International Conference on Concrete Pavements. Purdue University.

Parker Jr., F., Barker, W., Gunkel, R., Odom, E. (1979) Development of a Structural Design Procedure for Rigid Airport Pavements. FAA-RD-77-81. U.S.D.O.T. 1979.

Pringle, T. (1950). "Structural Design of Joints for Airport Pavements" American Concrete Institute Title No. 46-59

Prozzi, J., Balmaceda, P., De Beer, M. (1993). "Nondestructive Tests Procedure for Field Evaluation of Transverse Joints in Concrete Pavements". Proceedings of the Fifth International Conference on Concrete Pavements. Purdue University.

Ricalde, L (2007). Analysis of HWD Data from CC2 Traffic Tests at the National Airport Pavement Test Facility. Proceedings of the 2007 FAA Worldwide Airport Technology Transfer Conference.

Roesler, J.R., Hiller, J.E., Littleton, P.C. (2005). "Large Scale Airfield Concrete Slab Fatigue Tests". Proceedings of the Eighth International Conference on Concrete Pavements. Purdue University.

Roesler, J., Evangelista, F., Domingues, M. (2007). "Effect of gear positions on airfield rigid pavement critical stress locations". Proceedings of the 2007 FAA Worldwide Airport Technology Transfer Conference. Atlantic City, NJ. 2007.

Rollings, R. S. (2003). "Evolution of Airfield Design Philosophies" *Proceedings*, XXII World Road Congress, Permanent International Association of Road Congresses, Durban, South Africa.

Rollings, R. S. (2001). "Concrete Pavement Design: Its More than a Thickness Design Chart" Proceedings, 7th International Conference on Concrete Pavements, Orlando, Florida.

Rollings, R. S. and D. W. Pittman. (1992). "Application of Field Instrumentation and Performance Monitoring of Rigid Pavements,"ASCE *Journal of Transportation Engineering*, Vol. 118, No. 3.

Rollings, R. S. and M. P. Rollings. (1991). "Pavement Failures: Oversights, Omissions, and Wishful Thinking," ASCE *Journal of Performance of Constructed Facilities*, Vol. 5, No. 4.

Rollings, R. S. (1987). "Design of Rigid Overlays for Airfield Pavements," doctoral dissertation, University of Maryland, (UMI Dissertation Information Services, No. 8808598).

Rollings, R. S. (1989). "Developments in the Corps of Engineers Rigid Airfield Pavement Design," Proceedings, 4th International Conference on Concrete Pavements, Purdue University, West Lafayette, IN.

Rollings, R. S. (1981). "Corps of Engineers Design Procedures for Rigid Airfield Pavements," Proceedings, 2nd International Conference on Concrete Pavements, Purdue University, West Lafayette, IN.

Rufino, D.M., Roesler, J. Berenberg, E., Tutumuler, E. (2001). "Analysis of Pavement Responses to Aircraft and Environmental Loading at Denver International Airport". Proceedings of the Seventh International Conference on Concrete Pavements. Purdue University.

Rufino, D.M. (2003). "Mechanistic Analysis of In-Service Airfield Concrete Pavement Responses". PhD Dissertation, University of Illinois at Urbana-Champaign.

Rufino, D.M., Roesler, J. Berenberg, E (2004). "Mechanistic Analysis of Pavement Responses From Denver International Airport". FAA Center of Excellence for Airport Technology. C.O.E. Report No. 26.

Rufino, D., Roesler, J. (2004) "Effect of pavement temperature on concrete pavement joint responses" Proceedings of the 2004 FAA Worldwide Airport Technology Transfer Conference. Atlantic City, NJ. 2004.

Sale, J.P. (1977). "Rigid Pavement Design for Airfields". Proceedings of the First International Conference on Concrete Pavements. Purdue University.

Sale, J. P. and R. L. Hutchinson. (1959). "Design of Rigid Pavement Design Criteria for Military Airfields" *Journal of the Air Transport Division*, Vol. 85, No. 3, ASCE.

Skarlatos, M.S. and Ioannides A.M. (1998). "The Theory of Concrete Pavement Joints" Proceedings, Fourth International Workshop on design theories and their verification of concrete slabs for pavements and railroads, 10-11 September, Bussaco, Portugal, pp. 187-208.

Skarlatos, M. S. (1949). "Deflections and Stresses in Concrete Pavements of Airfields with Continuous Elastic Joints" Report AD 628501, US Army Engineer Ohio River Division Laboratories.

Strauss, P.J., Perrie, B.D., du Plessis, L., Rossmann, D. (2005). "Load Transfer through Aggregate Interlock: Crack Width, Aggregate Type, and Performance". Proceedings of the Eighth International Conference on Concrete Pavements. Purdue University.

Tabatabaie, A.M. et al (1979). "Longitudinal Joint Systems in Slip-Formed Rigid Pavements, Vol. II: Analysis of Load Transfer Systems for Concrete Pavements" Report No. FAA-RD-79-4-I, Federal Aviation Administration, Washington, D.C.

Teller, L.W., Sutherland E.C. (1936). "The Structural Design of Concrete Pavements Part 2- Observed Effects of Variations in Temperature and Moisture on Size Shape and Stress Resistance of Concrete Pavements". *Public Roads* Journal of Highway Research, USDA Vol 16., No. 9.

Teller, L.W., Sutherland E.C. (1936). "The Structural Design of Concrete Pavements Part 3- A Study of Concrete Pavement Cross Sections". *Public Roads* Journal of Highway Research, USDA Vol 16., No. 10.

Teller, L.W., Sutherland E.C. (1936). "The Structural Design of Concrete Pavements Part 4- A Study of the Structural Action of Several Types of Transverse and Longitudinal Joint Designs". *Public Roads* Journal of Highway Research, USDA Vol 17., No. 7 and No. 8

Teller, L.W., Cashell, H.D. (1958). "Performance of Dowelled Joints under Repetitive Loading". *Public Roads*, Volume 30, No. 1. US Department of Commerce.

US Army Corps of Engineers. (1950a). "Lockbourne No. 2 - Experimental Mat," Rigid Pavement Laboratory.

US Army Corps of Engineers. (1950b). "Lockbourne No. 2 - Modification, Multiple-Wheel Study," Rigid Pavement Laboratory.

US Army Corps of Engineers. (1946). "Lockbourne No. 1 Test Track, Final Report," Rigid Pavement Laboratory.

Van Breemen, W., Finney, E. (1950). "Design and Construction of Joints in Concrete Pavements". *American Concrete Institute* Title No. 46-59.

Westergaard, H. M., (1948). "New Formulas for Stresses in Concrete Pavements of Airfields," *Transactions*, ASCE, Vol. 113, pp. 425-444.

Westergaard, H.M. (1927). "Analysis of Stresses in Concrete Roads Caused by Temperature". *Public Roads* Journal of Highway Research, USDA Vol 8., No. 3.

Westergaard, H.M. (1926). "Stresses in Concrete Pavements Computed by Theoretical Analysis". *Public Roads* Journal of Highway Research, USDA, Vol. 7., No. 2.

Zollinger, D.G., Soares, J. (1999) "Performance of Continuously Reinforced Concrete Pavements: Volume VII: Summary". FHWA-RD-98-102. Federal Highway Administration.